POLITECNICO DI TORINO

Master degree in Mechanical Engineering

MASTER DEGREE THESIS

Energy Performance Evaluation of Fuel Cell Heavy-Duty Vehicles for Long Haul Applications: A Study of the European Fleet through VECTO Simulations

Supervisors:

Prof. Luciano ROLANDO

Prof. Federico MILLO

Company tutors:

Eng. Evangelos BITSANIS

Eng. Stijn BROEKAERT

Candidate:

Simone DE VIVO

April 2024

Sommario

Il settore del trasporto merci su strada è un pilastro importante dell'economia europea, interessando il 75% della movimentazione complessiva [27]. Tuttavia, è anche una fonte significativa di CO_2, rappresentando circa il 5% delle emissioni totali di gas serra dell'Unione Europea [1]. Di conseguenza, la decarbonizzazione di questo settore risulta essere di estrema rilevanza ma allo stesso tempo particolarmente ardua, non solo per l'intrinseca dipendenza di detto settore dai combustibili fossili, ma anche per la costante crescita della sua attività anno dopo anno. Per decenni, l'impatto ambientale di questo campo è stato ampiamente trascurato. Solo nel 2019 si è verificato un importante cambiamento con l'adozione dei primi standard di emissione di CO_2 per i nuovi veicoli pesanti immatricolati all'interno dell'UE, collocando il trasporto merci su strada su un percorso verso la neutralità delle emissioni di carbonio. Dall'introduzione di queste norme, il panorama industriale ha subito profonde trasformazioni. L'attenzione della ricerca e dei costruttori si è concentrata sullo studio di veicoli pesanti a zero emissioni, sollecitata dalla necessità di allinearsi agli ambiziosi obiettivi stabiliti dalle normative europee. Tra le varie innovazioni che stanno emergendo, i veicoli elettrici alimentati da celle a combustibile ad idrogeno hanno raccolto un'attenzione particolare. Questi veicoli sono visti con sempre più entusiasmo come una soluzione valida e promettente per raggiungere gli obiettivi di decarbonizzazione, rendendoli una componente di rilievo nel futuro del trasporto ecologico.

La ricerca svolta in questa tesi è contestualizzata all'interno del rappresentato panorama di trasformazione ed è stata condotta in collaborazione con la "Sustainable Transport unit" del Joint Research Centre della Commissione Europea. L'obiettivo centrale di questo studio è condurre una valutazione completa delle prestazioni energetiche dei veicoli pesanti impegnati in operazioni a lungo raggio, comprendendo un'ampia gamma di casi d'uso e concentrandosi in particolare sul consumo di idrogeno, un aspetto di fondamentale importanza per i veicoli a celle a combustibile. Per effettuare le simulazioni dei veicoli è stato utilizzato il Vehicle Energy Consumption Calculation Tool (VECTO), il software ufficiale della Commissione Europea per il calcolo del consumo di carburante e di energia dei veicoli pesanti. Per delineare lo stato attuale della tecnologia delle celle a combustibile e delle sue applicazioni in questo campo, è stata intrapresa un'ampia analisi della letteratura scientifica, che ha contribuito a fornire una base strutturata per l'intero lavoro. La fase iniziale dello studio ha previsto lo sviluppo di un modello VECTO per un veicolo generico a celle a combustibile, rappresentativo del segmento dei veicoli pesanti per il trasporto merci a lungo raggio. È stato riprodotto un autoarticolato appartenente al gruppo 5, riconosciuto come la configurazione più diffusa in Europa. Dopo la validazione del modello effettuata mediante un confronto con dati di letteratura, il suo powertrain ibrido-FC è stato integrato con le caratteristiche medie dei veicoli convenzionali che costituiscono la flotta europea HDV di riferimento, per ricreare suddetta flotta in versione ibrida-FC mediante VECTO. Otto veicoli sono stati riprodotti e simulati per diversi profili di missione, quest'ultimi progettati per rispecchiare i diversi scenari operativi della vita reale. I risultati delle simulazioni, che forniscono un quadro di riferimento del comportamento energetico di questi veicoli innovativi, sono stati commentati ed analizzati. Infine, sono state valutate potenziali strategie di miglioramento dell'efficienza energetica e dell'adattabilità operativa della flotta. Ciò è stato ottenuto agendo sul grado di ibridazione dei veicoli, cambiando la taglia del sistema di celle a combustibile insieme alle dimensioni del pacco batteria.

Abstract

The road freight sector is an important pillar of the European economy as 75% of goods are transported on wheels [27], but it is also a significant source of CO_2 emissions, accounting for about 5% of the EU's total greenhouse gas (GHG) emissions [1]. The challenge of decarbonising this branch is particularly arduous, not only because of its inherent dependence on fossil fuels, but also because of the substantial increase in road freight activities year after year. For decades, the environmental impact of this sector, particularly in terms of GHG emissions, was largely overlooked. It was only in 2019 that a pivotal shift occurred with the adoption of the first CO_2 emission standards for new heavy-duty vehicles (HDVs) within the EU, moving road freight transport towards carbon neutrality. Since the introduction of these regulations, the industry landscape has undergone profound transformations. The focus of research has pivoted towards Zero Emission Heavy-Duty Vehicles (ZE-HDVs), propelled by the need to align with the ambitious objectives established by European regulations. Among the various innovations emerging in this space, hydrogen fuel cell-powered electric vehicles have garnered particular attention. These vehicles are increasingly viewed as a viable and promising solution for achieving the decarbonization goals of the road freight sector, making them a critical component of the future of green transport.

The research performed in this thesis is contextualized within this transformation landscape, and it was carried out in collaboration with the Sustainable Transport unit of the European Commission's Joint Research Centre (JRC).

The central aim of this study was to conduct a comprehensive evaluation of the energy performance of HDVs engaged in long-haul operations, encompassing a broad range of use cases, and with a particular focus on hydrogen consumption, an aspect of paramount importance for fuel cell (FC) vehicles. The Vehicle Energy Consumption Calculation Tool (VECTO), the official European Commission's software for calculating the fuel and energy consumption of heavy-duty vehicles was employed to perform the vehicle simulations.

An extensive literature review was undertaken to delineate the contemporary landscape of fuel cell technology and its application to this field, thereby providing a structured foundation for the entire work.

The initial phase of the study involved the development of a VECTO model for a generic FC vehicle, representative of the heavy long-haul freight vehicle segment. A 4x2 tractor-trailer (Group 5), recognised as the most prevalent configuration across Europe, was reproduced. Following the model's validation against established literature data, its FC hybrid powertrain was integrated with the average characteristics of the conventional vehicles constituting the European reference HDV fleet, to recreate this fleet in FC-hybrid version through VECTO. A total of eight vehicles were reproduced and simulated for different mission profiles, designed to mirror the different real-life operational scenarios. The results of these simulations, which provide a framework for the energy behaviour of these innovative vehicles, were commented on and analysed. Finally, potential strategies to improve the energy efficiency and operational adaptability of the fleet were assessed. This was achieved by acting on the degree of hybridisation of vehicles, by varying the size of the FCS together with the capacity of the battery pack.

Table of contents

List of Tables

List of Figures

Acronyms

ADAS	Advanced driver assistance systems
ASM	Asynchronous induction motor
BEV	Battery electric vehicle
CCH2	Cryo-Compressed hydrogen
CFCS	Composite fuel cell system
CNG	Compressed natural gas
CH_2	Compressed hydrogen
CO_2	Carbon dioxide
CS	Charge sustaining
DC	Direct current
EC	Energy consumption
eDrive	Electric drive
EM	Electric motor
EMS	Energy management system
ESS	Energy storage system
EU	European Union
FC	Fuel cell
FCEV	Fuel cell electric vehicle
FCS	Fuel cell system
GHG	Greenhouse gas
GVW	Gross vehicle weight
H_2	Hydrogen
HD	Heavy duty
HRS	Hydrogen refuelling station
HSS	Hydrogen storage system
HV	High voltage
HVAC	Heating, ventilation, air conditioning
ICCT	International Council on Clean Transportation
ICE	Internal combustion engine
ICEV	Internal combustion engine vehicle
IWM	In-wheel motor
JRC	Joint Research Centre
LFP	Lithium iron phosphate
LH_2	Liquid hydrogen
LH	Long haul
LNG	Liquefied natural gas
LV	Low voltage
MEA	Membrane electrode assembly
MGVW	Maximum gross vehicle weight
NCA	Nickel cobalt aluminium oxide
NMC	Nickel manganese cobalt oxide
NO_x	Nitrogen oxides
NOVC-HEVs	Not Off-Vehicle Charging hybrid electric vehicles

OEM	Original equipment manufacturer
OP	Operating point
PEMFC	Proton-exchange membrane fuel cell
PEV	Pure electric vehicle
PM-SM	Permanent magnet synchronous motor
PTO	Power take-off
RD	Regional delivery
REESS	Rechargeable energy storage system
RRC	Rolling resistance coefficient.
RUL	Remaining useful life
SOC	Battery state of charge
TPMLM	Technically permissible maximum laden mass
TTW	Tank to wheel
VECTO	Vehicle energy consumption calculation tool
WTW	Well to wheel
ZE	Zero emissions

1. Introduction

In recent decades, the concerns related to greenhouse gases and pollutant emissions from human activities and their varied repercussions have garnered increasing attention from civil society and major political institutions. Following the Paris Agreement of 2015, the European Union (EU) has united around the ambitious goal of fighting climate change through the usage of clean technologies and sustainable energy sources. This shared commitment is decisively focused on the pursuit of decarbonisation in various sectors, among which mobility is of particular relevance. The transport sector remains a significant contributor to greenhouse gas emissions, responsible for nearly a quarter of the total emissions within the European Union in 2021 and is the only field that has never reduced its carbon footprint with respect to the 1990 level [2], on the contrary recording a 25% increase in 2016. This trend is illustrated in Figure 1.1, which also presents projections for future emissions alongside those of the entire transport sector, all related to the emission values of 1990. These projections indicate that, in the absence of further CO_2 mitigation measures, the percentage attributable to the road transport sector, for which the HDV segment is a significant contributor, is set to grow steadily [1].

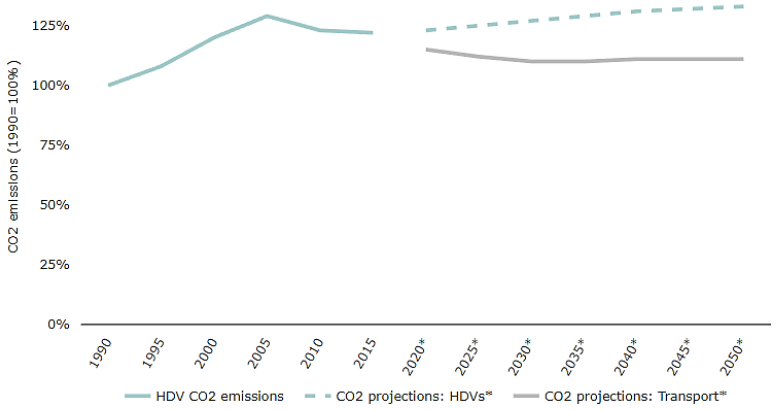

Figure 1.1: Reported and projected CO_2 emissions from HDV in the EU.

Road transport accounts for 72% of total GHG emissions in the transport field, with passenger cars and heavy-duty vehicles being the biggest emitters, as depicted in Figure 1.2 [3].

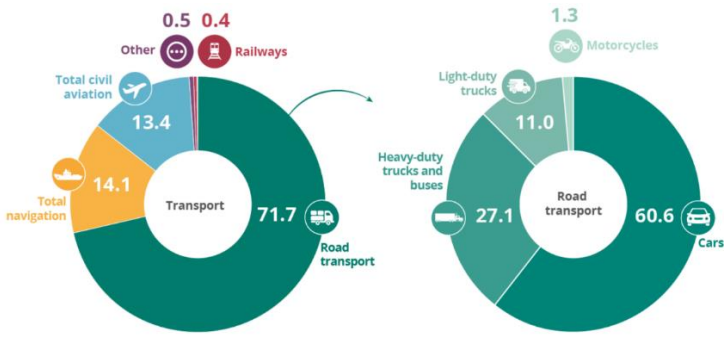

Figure 1.2: Greenhouse gas emissions shares from transport in the EU.

Therefore, the transition of the road freight sector towards sustainability is a crucial aspect of the European Union's strategy to reduce greenhouse gas emissions and achieve carbon neutrality targets outlined in the European Green Deal of 2019. The challenge of decarbonising the heavy-duty transport sector is very demanding, both because of its high dependence on fossil fuels and the steady growth of road freight transport activities over the years. Moreover, this task has been made even more difficult by the fact that the study of the environmental impact of this sector has been historically neglected. The absence of a standardized regulatory framework for accurately monitoring the CO2 emissions of heavy-duty vehicles has obscured our comprehension of their impact, thereby hindering the formulation of efficient policies.
A breakthrough came in 2017 by establishing a methodology for emissions calculation based on simulations and embedded within a broad regulatory framework. To this purpose, the Vehicle Energy Consumption Calculation TOol (VECTO) was created, as the official European Commission software for calculating fuel consumption and CO2 emissions through detailed vehicle modelling. This made it possible to quickly create a baseline against which to set emission reduction targets for the sector, placing it for the first time on a path towards decarbonisation. In their current form, the standards mandate a 15% reduction in CO2 emissions from newly registered heavy-duty vehicles in the EU by 2025, relative to the baseline year of 2019, with this target escalating to 30% by the year 2030.
Their introduction has brought about a profound change in the industrial landscape, accelerating the adoption of energy-efficient technologies in HDVs, and the market introduction of zero-emission vehicles. This change is manifested not only in the growing and more ambitious goals of manufacturers to convert their fleets to environmentally friendly vehicles but also in the burgeoning market share of ZE-HDVs, which has increased sharply in recent years. Among the various innovations emerging in this field, hydrogen fuel cell-powered electric vehicles have attracted particular attention from research and manufacturers. These vehicles are increasingly viewed as a viable and promising solution for achieving the decarbonization goal of the road freight sector, positioning them as an essential element in the evolution of sustainable transportation.

The research performed in this thesis is contextualized within this transformation landscape, and it was carried out in collaboration with the Sustainable Transport unit of the European Commission’s Joint Research Centre (JRC).
The primary aim of this study is to conduct a comprehensive evaluation of the energy performance, with a particular focus on the hydrogen consumption, of fuel cell HDVs engaged in long-haul operations, encompassing a broad range of use cases. To this purpose, vehicle simulations were performed employing the VECTO software, carefully observing the conditions required by the regulations and the annexes of the tool.
In order to understand the contemporary landscape of fuel cell technology and its applications in this field, an extensive literature review was conducted. The main findings that are useful for the integration of this study have been reported in the initial chapters. The research also helped to outline the methodology used for the analysis undertaken.
By creating a generic and representative VECTO heavy vehicle model tailored for long-haul freight applications, a reference FC hybrid powertrain was defined. Following the model's

validation, this FC hybrid powertrain was integrated with the average characteristics of the conventional vehicles that formed the European reference HDV fleet for the years 2019 and 2020, in order to recreate it in the FC-hybrid version. The entire fleet was then reproduced and simulated across different mission profiles, designed to mirror the different real-life operational scenarios. The results were commented on and assessed. Subsequently, further analysis explored potential strategies for improving fuel efficiency and operational adaptability of specific configurations. This was achieved by adjusting the vehicle's degree of hybridization, by varying the size of the FCS together with the capacity of the battery pack.

The relevance of this study lies in two fundamental aspects. Firstly, in the use of the VECTO software. This tool represents a novelty in the scenario of modelling these alternative vehicles, in fact, the version employed has only been available since November 2023, marking an important step in establishing a comprehensive environment for the development and regulation of these vehicles. Secondly, in the breadth of the case studies examined. The study helped to create a framework for the energy behaviour of this type of vehicle by covering all the main configurations found on European roads, according to the precise modalities and conditions prescribed by the EU regulations.

2. Fuel cell system functioning

Fuel cells are devices that produce electricity from the chemical energy of reactants through an electrochemical reaction, promising highly efficient and environmentally friendly power generation. Compared to an internal combustion engine (ICE), fuel cell systems have the advantage of higher efficiency, zero exhaust emissions since no combustion takes place, and reduced operating noise. These main factors make this technology suitable to replace the tested and economical internal combustion engines, making them the preferred choice for future hydrogen HD mobility. At first, this section provides an overview of existing FC types. Specifically, the study focuses on those using hydrogen as a fuel, identifying PEM cells as the most suitable solution for vehicular use. Consequently, their operation and integration within a complex set of subsystems, necessary for the correct operation of the converter, is explained in detail. Finally, the main methods of on-board vehicle hydrogen storage are presented. In particular, the latter represents an issue of crucial importance and complexity that must be addressed if a wide deployment in the long-haul freight sector is to be achieved.

2.1 Fuel cell types overview and technology advantages

The main FC functional mechanisms are ensured by two electrodes, anode and cathode, where the chemical reactions occur that allow controlled oxidation of the fuel, and by an electrolyte between them with the function of transporting ions from one electrode to the other. Fuel cells are distinguished by the electrolyte that is used and the operating temperature. There are six principal types of fuel cell, namely [4]:

- Low temperature (50–150°C): alkaline electrolyte (AFC), proton-exchange membrane (PEMFC), direct methanol (DMFC).
- Medium temperature (around 200°C): phosphoric acid (PAFC).
- High temperature (600–1000°C): molten carbonate (MCFC) and solid oxide (SOFC).

Low-temperature cells pose fewer technological problems, favouring the use of less costly materials, and thus their cost is reduced. However, they are characterised by lower efficiencies and noble metal-based catalysts must be used to achieve acceptable reaction kinetics. In contrast, high-temperature fuel cells require complex systems to control the heat released, but at the same time, they can be well integrated into combined-type cycles, allowing the global efficiency to be further increased. Each type has different application fields depending on its features (fuel, range of operating temperature, poisoning sensitivity, start-up time, power density, etc). Table 2.1 shows the main fuel cell branches, highlighting the main characteristics.

Table 2.1: Main types of fuel cells with their characteristics of operation [5].

Fuel cell type	Fuel	Mobile ion	Operating temperature [°C]	Electrical Efficiency [%]	Power density [mW/cm^2] [12]
Alkaline (AFC)	Pure H_2	OH^-	60 ÷ 100	60	300 ÷ 500
Proton exchange membrane (PEMFC)	Pure H_2	H^+	80 ÷ 120	60	300 ÷ 900
Direct Methanol (DMFC)	Methanol	H^+	20 ÷ 90	-	-
Phosphoric acid (PAFC)	H_2	H^+	180 ÷ 200	40	150 ÷ 300
Molten carbonate (MCFC)	H_2, various hydrocarbon fuels	CO_3^{2-}	630 ÷ 670	50	150
Solid oxide (SOFC)	H_2, various hydrocarbon fuels	O^{2-}	800 ÷ 1000	60	150 ÷ 270

For all fuel cell types, at present, a significant barrier to commercialization is the capital cost. However, several advantages characterize the different classes to varying degrees, making fuel cells interesting for several applications. These include the following:

1. High efficiency (up to ≈ 0.6), considerably better than that of internal combustion engines.
2. Wide operating range with a high level of efficiency.
3. Some classes can use several types of fuel as reactants such as hydrogen, methanol and methane.
4. The essentials of a fuel cell involve few, if any, moving parts. This can lead to highly reliable and long-lasting systems.
5. Their environmental impact is limited. When hydrogen is the fuel, pure water is the by-product of the main reaction of the fuel cell. Consequently, this power source is “zero emission”.
6. The heat produced during operation can be used with co-generation.
7. Since small fuel-cell systems can be just as efficient as large ones, a notable feature of the technology is the very wide range of sizes (from a few W up to several MW).

To have no CO_2 emissions, a carbon-free fuel must be used. Consequently, for automotive applications, the primary focus is on hydrogen-fuelled cells, with particular attention given to

Proton Exchange Membrane cells for several reasons. PEMFCs boast a superior power density compared to other fuel cell types, reaching up to 1 W/cm^2. Notably, their operation at relatively low temperatures (typically 70-85°C) not only results in a compact footprint, eliminating the need for heat dissipation systems or component insulation, but also facilitates a quicker start-up time. A significant advantage of PEMFCs lies in their flexibility regarding reagent gases, eliminating the need for pure gases, an aspect challenging and costly to achieve in a vehicular context. However, they do necessitate an effective filtering system, particularly for atmospheric air intake.

2.2 Hydrogen fuel cell and working principles

The ensuing discussion will concentrate on fuel cells using hydrogen and an acid electrolyte, given their prominence in automotive applications, as previously mentioned. Specifically, PEMFCs fall into this category, employing a solid membrane composed of perfluoro-sulfonic acid, commonly known by the brand name "Nafion", as the electrolyte.

A fuel cell operates as an open electrochemical cell, demanding a continuous supply of hydrogen and oxygen at regulated pressure, temperature, and humidity to ensure efficient operation. Fuel cell units consist of key components, including the electrolyte, anodic and cathodic catalytic layers, gas diffusion layer, and bipolar plates. Connectors are placed at the ends of the cell for electrical connection to the load, and finally, end plates maintain the entire structure and ensure gas impermeability. Figure 2.1 shows a schematic of a fuel cell unit, highlighting the aforementioned components and their sequential arrangement.

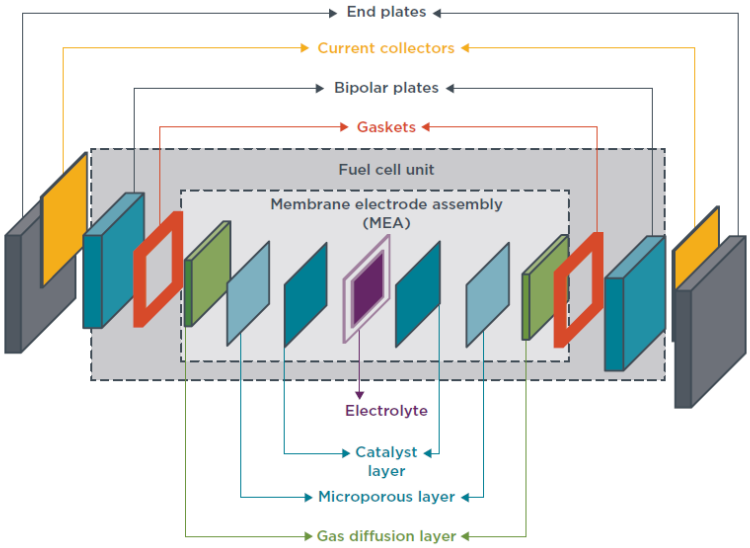

Figure 2.1: Schematic of a fuel cell unit.

The membrane electrode assembly (MEA) is the core component of a fuel cell unit where the oxidation-reduction reactions occur. It consists of the union of the gas diffusion layer, electrode, and electrolyte. The former consists of porous carbon and has the function of allowing reactant gases to permeate the catalytic layers with direct and uniform access. Adjacent to the gas diffusion layer lies the electrode, a thin film typically ranging from 5 to 50 µm in thickness [4], containing the catalyst of platinum particles supported by carbon powder. The primary function of the latter is to accelerate the reaction speed, thereby enhancing overall system efficiency. Platinum is the most used metal due to its high catalytic activity and stability; however, its cost, scarcity, and sensitivity to carbon monoxide poisoning limit its potential. For these reasons, several other technologies based on other precious metals such as ruthenium and palladium are being investigated [6]. The electrolyte membrane plays a crucial role in both separating reactant gases and facilitating the transport of electric charges between the anode and cathode. Specifically, the membrane must function as both an electronic insulator and an effective ionic conductor. The "Nafion" electrolyte, used in PEMFCs, exhibits excellent performance in terms of durability, chemical stability, and conductivity. Nevertheless, its production is characterized by high costs, and, moreover, it demands meticulous and complex control to ensure proper functioning, particularly in terms of hydration and operating temperature.

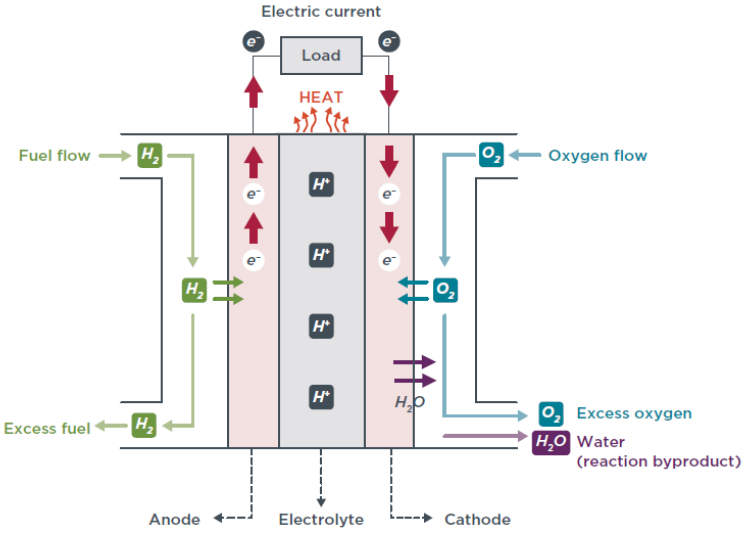

Figure 2.2: Fuel cell working principle scheme.

Throughout the operation of the fuel cell, hydrogen is introduced into the anode-side feed channel. It subsequently passes through the gas diffusion layer and reaches the catalyst layer. Here, the oxidation reaction takes place leading to the dissociation of the gas molecules and the release of electrons and protons (H^+ ions):

$$H_2 \longrightarrow 2H^+ + 2e^-;$$

(Eq. 2.1)

This reaction not only releases energy in the form of heat but also initiates a flow of electrons through the external circuit connected to the electrodes, and therefore, an electric current to

power the load. Simultaneously, there is a flow of H^+ ions through the electrolyte, directed towards the cathode. On the cathode side, oxygen from atmospheric air is reduced combining with electrons from the external circuit and H^+ ions from the electrolyte to form water, as indicated by the reduction semi-reaction:

$$\frac{1}{2}O_2 + 2H^+ + 2e^- \longrightarrow H_2O;$$

(Eq. 2.2)

The overall reaction is:

$$\frac{1}{2}O_2 + H_2 \longrightarrow H_2O + heat.$$

(Eq. 2.3)

The only products of the overall reaction are water and heat, which must be extracted from the fuel cell assembly for its proper functioning. Furthermore, it is important to note that the reactions mentioned are global reactions, and in both anodic and cathodic catalyst layers many intermediate reactions, now omitted, occur.

In a fuel cell, the electrical energy released is generated by the change in the Gibbs free energy of formation, which corresponds to the difference between the Gibbs free energy of formation of the products and that of the reactants. In fact, assuming a thermodynamically reversible chemical system, the Gibbs free energy released by the reaction coincides with the maximum amount of electrical work that can be generated. From this consideration, with simple steps, it is possible to univocally calculate the ideal open-circuit voltage (also called Nerst voltage) for a hydrogen-fuelled cell under standard ambient conditions (298.15 K and 1 bar), which is equal to 1.23 V [4]. However, real fuel cells deviate from ideal and reversible behaviour due to kinetic phenomena, leading to a reduction in the just-mentioned output voltage. These losses, also known as “polarizations”, can be attributed to four main causes:

1. Activation losses: These occur because part of the cell's energy must be expended to overcome the activation energy barrier of the half-reactions at the electrodes.
2. Ohmic losses: These losses arise from the resistance to the flow of electrons through the material of the electrodes and the various interconnections, as well as the resistance to the flow of ions through the electrolyte.
3. Concentration losses: Stemming from changes in reactant concentration at the electrode surface as fuel is consumed, resulting in a voltage drop due to insufficient transport of reactants to the electrode.
4. Fuel crossover losses: Present because a portion of hydrogen and electrons can cross the electrolyte membrane, though they are generally negligible compared to other losses.

By accounting for these losses and subtracting them from the theoretical fuel cell open-circuit voltage, a “polarization curve”, reported in Figure 2.3, is obtained. This curve illustrates the relationship between the DC voltage at the cell terminals and the current density (current per unit membrane area) drawn by the external load. From this trend, it can be observed that for

small values of current density, concentration and ohmic losses are negligible, but as the current density increases, they become preponderant.

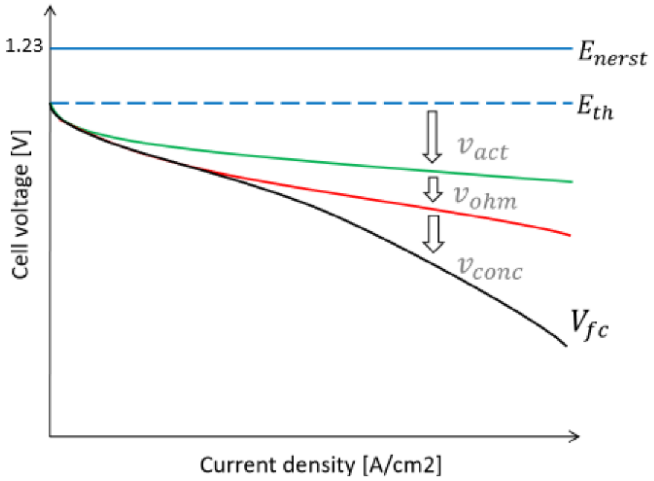

Figure 2.3: PEM-FC polarization curve and related voltage drops.

2.3 Fuel cell system and balance of plant

A single cell can produce a maximum voltage in the range of 0.6-0.8 V. Therefore, to achieve the voltage needed for a specific application, it becomes imperative to connect numerous units in series, creating what is referred to as a "stack" of fuel cells. Multiple fuel cell stacks can also be run in parallel to increase the power output to the desired level by increasing the effective active surface area while respecting FC current density limits. Moreover, such multi-stack assemblies could also be arranged sequentially, improving the efficiency of the FCS at part load while satisfying peak power demands.

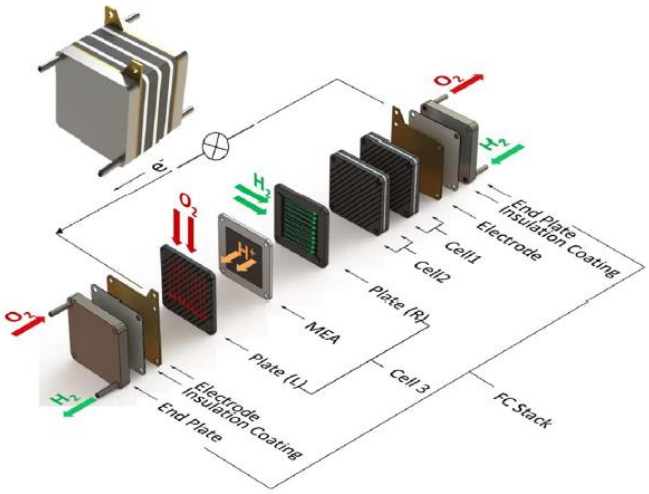

Figure 2.4: Fuel cell stack schematization.

The individual FC units are enclosed by the bipolar plates, which serve as electrically conducting interfaces contacting the positive electrode of one cell and the negative electrode of the adjacent one. Consequently, these plates form the structural backbone of a fuel cell stack, facilitating the flow of electric current produced by the interconnected cells in series. Simultaneously, the bipolar plates play a crucial role in distributing reactant gases across cell surfaces, evacuating reaction products, and efficiently cooling individual membrane assemblies. This functionality is accomplished through an intricate network of channels machined or moulded on either side of the plate, providing pathways for fluid flows. The geometric design of these channels significantly influences stack performance, and various designs have been proposed to optimize this aspect. Beyond their electric current and fluid management role, bipolar plates also fulfil a structural function within the stack, ensuring the overall compactness of the structure. The materials used for these plates must possess not only low electrical resistance but also high corrosion resistance, given that each plate is in contact with both electrodes. Furthermore, they must exhibit good mechanical strength to withstand the compression required for maintaining the stack's integrity, even at elevated temperatures. For these reasons, bipolar plates for low-temperature FCs are typically made of graphite or metal. Historically, graphite has been used, although naturally brittle and complex to process. Consequently, there has recently been a gradual transition towards metallic bipolar plates, which include materials such as aluminium, titanium and stainless steel. Metal plates are preferred for their ease of production, robust mechanical properties, and high conductivity. However, they require anti-corrosion coatings, which can introduce surface defects and potentially lead to a shorter service life.

Nevertheless, for the proper functioning of the fuel cell stack, several auxiliary subsystems are indispensable, and their assembly is referred to as the “balance of plant” (BOP). Together, the fuel cell stack and the balance of plant constitute a “fuel cell system” (FCS). A schematic of the latter is shown in Figure 2.5.

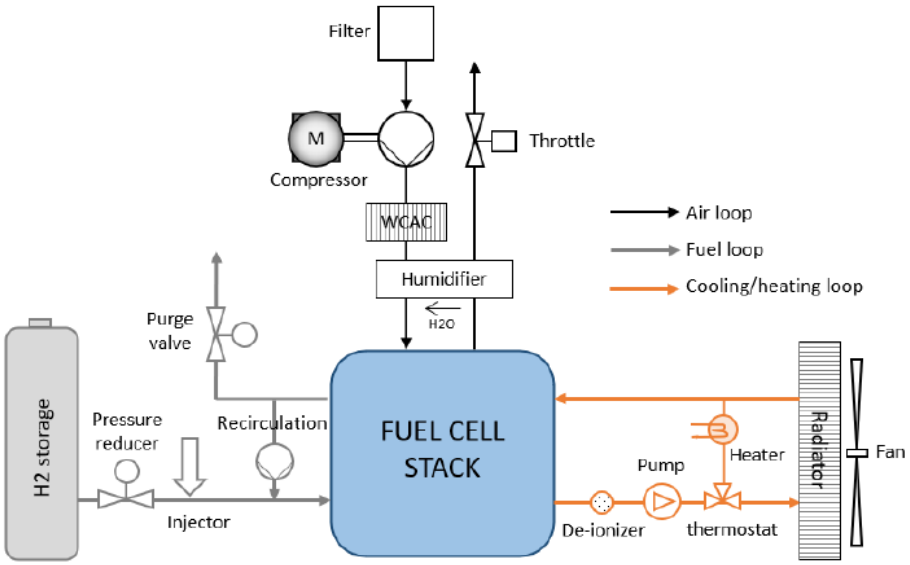

Figure 2.5: Fuel cell balance of plant.

The BOP is fundamental for ensuring the proper management of the inputs and outputs of the fuel cell stack, consequently, it includes air, fuel and thermal management systems:

- The main task of the "air loop" is to supply sufficient oxygen to the cathode as a function of the required load. For a pressurized system, the air is supplied by a compressor which controls the intake air pressure. The air is heated by the compression; therefore a downstream cooler manages its temperature to prevent dehumidification and degradation of the fuel cell membrane. Additionally, a humidifier is integrated into the air loop to prevent the drying out of the membrane and ensure optimal proton conductivity. It is noteworthy that the air loop constitutes the most energy-intensive auxiliary subsystem, potentially consuming more than 15% of the fuel cell stack power [6].

- The "fuel loop" is responsible for supplying hydrogen to the anode. A pressure-reducing valve is required to meet the low pressure of the hydrogen supply to the anode, typically between 1 and 4 bar [6]. The hydrogen flow rate is then regulated using an injector. The agglomeration in the anode of water and nitrogen gas from the cathode reduces the hydrogen pressure, resulting in stratification and forming inert hydrogen zones affecting the fuel cell stack performance. For this reason, hydrogen and water are frequently removed using a purge valve. A recirculation pump injects the hydrogen back into the fuel line to minimise the loss of unreacted fuel.

- The "cooling loop" is needed for FC thermal management, extracting waste heat from the stack to maintain its operating temperature, preventing degradation and efficiency deterioration. Furthermore, in cold start conditions, an electric resistance heater is required to facilitate the initiation of the fuel cell system. Liquid cooling is the predominant method in FC electric vehicles due to its high heat removal capacity: a high-voltage pump facilitates the circulation of coolant, ensuring a substantial mass flow across the heat exchanger. The heat exchanger, in turn, undergoes cooling through the operation of a fan [7].

The "FC control subsystem" is responsible for overseeing and coordinating all components of the BOP. This system monitors the condition of the FCS and autonomously adjusts to meet the power requirements of the vehicle, ensuring safety by preventing hazardous conditions, and safeguarding the fuel cell system from damage.

Each of these subsystems necessitates a portion of the power generated by the fuel cell stack, resulting in a systematic reduction of the overall efficiency of the FCS compared to that of the stack alone. Figure 2.6 shows the schematic definition of the boundaries for the FC stack and the system.

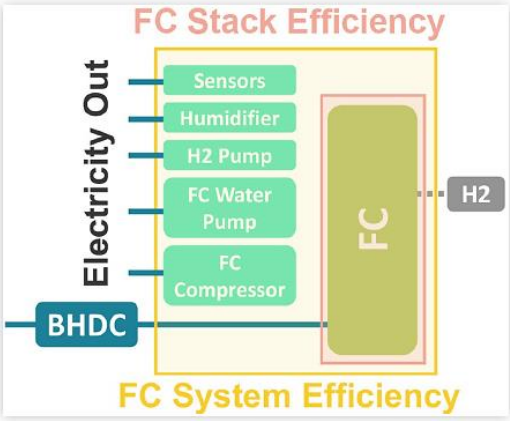

Figure 2.6: Schematic definition of boundaries for FC stack and system.

The efficiency of the FC stack can be quantified as the ratio of electrical output power to the power supplied into the system by the fuel:

$$\eta_{stack} = \frac{P_{out,el}}{\dot{m}_{H_2} * H_i},$$

(Eq. 2.4)

while the efficiency of the FC system also considers the power consumption of the auxiliaries:

$$\eta_{system} = \frac{P_{out,el} - P_{aux}}{\dot{m}_{H_2} * H_i} = \frac{P_{out,net}}{\dot{m}_{H_2} * H_i}.$$

(Eq. 2.5)

This leads to different efficiency trends as a function of the load, as depicted in Figure 2.7 [8]: the FC stack efficiency curve is highest at part load operation (very low electrical currents) and decreases linearly at high loads due to raised losses. In contrast, the FC system efficiency curve is lowest at the beginning of the FC load range due to predominant auxiliary consumption. It reaches its maximum at an intermediate net power before slightly falling again due to a possible increase in the auxiliary consumption (mainly air compressor). This graph shows that the average FCS efficiency on a mission profile is reduced by periods of low or very high load operation. From this observation, important basic considerations can be made regarding the design of both the stack and the hybrid vehicle architecture, topics that will be explored in the subsequent chapter.

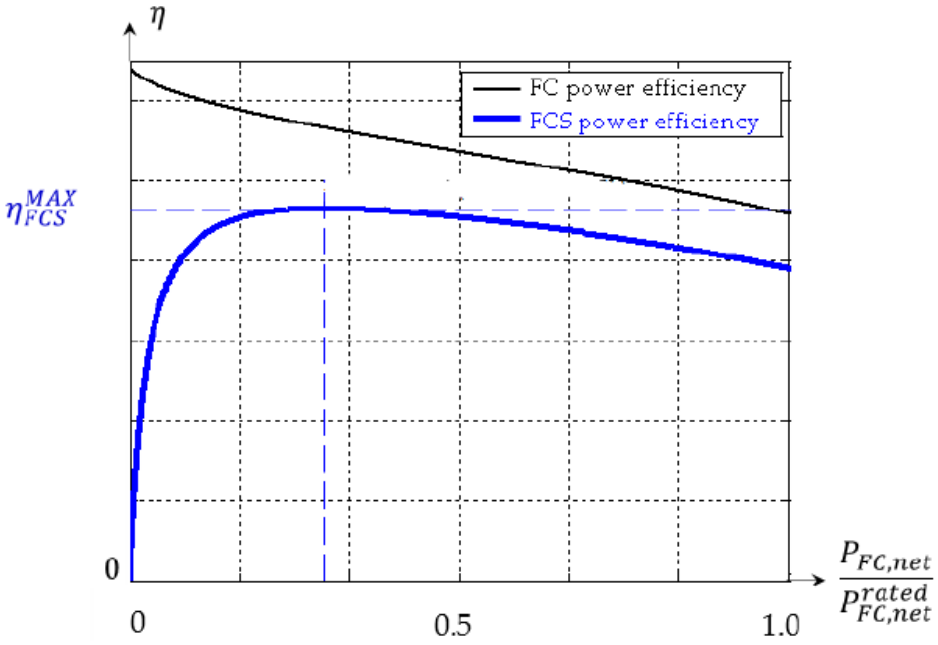

Figure 2.7: FC and FCS efficiency curves.

2.4 On-Board H_2 storage

Hydrogen fuel features high specific energy, but low volumetric density as compared to conventional liquid fuels (Figure 2.8) and even electrochemical batteries, making their onboard storage an important challenge to address.

Parameter	Unit	Gasoline	Diesel	Hydrogen
Chemical formula		C4 - C12	C8 – C25	H2
Composition (C, H, O)	Mass-%	86, 14, 0	87, 13, 0	0, 100, 0
Lower heating value	MJ/kg	42.7	42.78	120
Density	kg/m^3	720 - 780	848	0.089
Stoichiometric air/fuel ratio	kg/kg	14.7	14.5	34.3
Flammability limits	Vol-% ϕ	1.0-7.6 0.7-2.5	1.0-6 0.7-2.1	4-75 0.1-5
Laminar flame speed	cm/s	35-50	na	210
Auto-ignition temperature	°C	approx. 350	approx. 265	585

Properties given at standard temperature (273.15 K) and pressure (101325 Pa).

Figure 2.8: Hydrogen and conventional liquid fuels characteristics.

The research objective is to minimise the storage volume, respecting technological, safety and cost constraints, while guaranteeing a hydrogen vehicle range at least comparable to that of current conventional vehicles. To achieve this goal, solutions must be sought that allow for

achieving high storage densities. There are several hydrogen storage methods, but automotive research is mainly focusing on the following:

1. compressed hydrogen (CH_2).
2. liquid hydrogen at cryogenic temperatures (LH_2).
3. cryo-compressed hydrogen (CCH_2).
4. storage in metal hydrides.

The first two have already been tested and are used in real vehicles, while others, which are very promising, are still in the experimental phase and currently still do not find application in prototypes. The prevailing method for hydrogen storage in heavy-duty vehicle applications is the use of compressed gas stored at either 350 bar or 700 bar, typically in multiple tanks constructed from composite materials. These tanks are commonly positioned behind the driver's cab or between the axles. However, the 350-bar solution, owing to its relatively low volumetric density of approximately 16 gH_2 per litre of Hydrogen Storage System (HSS) [9], presents a drawback in terms of driving range. Indeed, manufacturers utilizing this approach indicate a limited range of about 400 km for their trucks. Conversely, the 700-bar compressed hydrogen solution offers a more promising prospect for extended driving range. This is attributable to its higher volumetric density, measuring at 27 gH_2 per litre of HSS [10]. To further enhance the onboard volumetric storage capacity over pressurised tanks, hydrogen may be liquefied in a highly cooled cryogenic form, requiring a temperature of up to -253°C. This HSS technology significantly boosts volumetric density, surpassing 36 gH_2 per litre [9]. The objective of this technology is to extend the driving range of hydrogen trucks to 1000 km, with a reduced refuelling time. However, this approach confronts various technical and logistical challenges, including hydrogen tank boil-off losses and the necessity for hydrogen liquefaction.

Cryo-compressed hydrogen (CCH_2) is a hybrid method combining compressed gas and liquid hydrogen where H_2 is compressed at 300 bar and stored at -150°C to -240°C. The use of compressed hydrogen at low temperatures rather than ambient temperatures provides the highest system storage density (it is expected to achieve volumetric density exceeding 72 gH_2 per litre of HSS), in addition to fundamental weight, cost and safety advantages. However, CCH_2 tanks are complex systems, with performance that continuously varies depending on use patterns, insulation performance and vessel characteristics [11]. For these reasons, the management of on-board hydrogen mass is tricky, and this storage technology is still under development.

Metal hydrides are solid compounds formed as a result of the diffusion of hydrogen in the metal's crystal lattice by occupying the interstitial space; thus, they are characterised by the ability to perform hydrogen charge-release cycles reversibly, under well-defined pressure and temperature conditions. In on-board vehicle applications, the absorbent alloy can be housed in the form of compressed powder within stainless steel tubes, integrated by a specific thermal control system. Indeed, due to the exothermic hydrogenation and endothermic dehydrogenation reactions, a complex thermal management strategy is needed, and moreover, this oscillating operation makes the system inefficient and with slow dynamics. These complexities contribute

to the fact that this technology is currently still in the research phase, with no applications in the heavy-duty sector yet. However, metal hydride storage is estimated to offer a much higher volumetric energy density than compressed H_2.
The details of various current onboard H_2 storage techniques for long haul HDVs have been listed in Table 2.2.

Table 2.2: Hydrogen storage methods characteristics.

Storage method	Volumetric density [gH_2/l]	Pressure [bar]	Temperature [°C]
Compressed 350 bar	16	350	Ambient
Compressed 700 bar	27	700	Ambient
Liquid	36	1 ÷ 70	-253 ÷ -244
Cryo-compressed	72	300	-150 ÷ -240
Metal hydride ($NaAlH_4$)	70	20	260 ÷ 425
Metal hydride ($LiBH+MgH_2$)	80	-	-

The overall environmental impact of vehicles utilizing hydrogen as an energy source, as per the "well-to-wheel" (WTW) approach, depends significantly on the method of hydrogen production. Hydrogen is termed "green" when produced from water through electrolysis using electricity sourced from renewable resources. Conversely, the most cost-effective method of hydrogen production is "grey" hydrogen [13], derived from steam reforming of natural gas. However, if this process incorporates carbon capture technology, it leads to the production of "blue" hydrogen, thereby mitigating CO_2 emissions. As the nomenclature implies, the preference is for green hydrogen, ensuring that the shift in technology results in a tangible reduction in CO_2 emissions. Nevertheless, the quantities of green hydrogen produced currently are relatively small, and its cost remains prohibitively high.

3. FC propulsion for the long-haul freight sector decarbonisation

The current section aims to provide a detailed review of the heavy-duty fuel cell propulsion technology, which stands as a pivotal solution for the future decarbonization of the long-haul freight vehicle sector. The main objective is to identify and present the current state of technology while highlighting its main challenges and recent development trends. However, before delving into these aspects, a comparison of this technology with other competing low and zero-carbon solutions will be provided in order to argue why the use of an FC-powered architecture is particularly suitable and more advantageous than alternatives for applications of this nature. For these purposes, a comprehensive analysis of the available literature has been conducted.

3.1 Fuel cell powertrain in heavy-duty vehicles

3.1.1 Alternative powertrains for HDVs

The current technological landscape for HDV powertrains is characterized by a diverse array of options, spanning from traditional internal combustion engines to innovative zero-emission alternatives. Among these, battery electric vehicles, vehicles powered by lower-carbon or synthetic fuels (E-fuels), and catenary trucks represent significant contenders alongside fuel cell electric vehicles. Nowadays, these technologies are being explored and tested concurrently, reflecting a multifaceted approach to the decarbonization of the long-haul freight sector. It is anticipated that a combination of these technologies, rather than a singular solution, will be adopted to meet the varied demands of different applications, use cases, and geographical regions. This stems from the understanding that no single technology holds a definitive edge in CO_2 reduction across all scenarios, with each presenting its unique set of challenges and limitations. BEVs, FCVs, and not-hybrid catenary systems fall within the category of zero-emission vehicles (ZEVs). Theoretically, the focus should be on their utilization to meet emission regulation standards and achieve CO_2 reduction targets. Considering the technology readiness level, also derived from the experience in the passenger car industry, the availability of recharging infrastructure, and the emissions reduction potential, BEVs seem to be the zero-emission technology most prepared for widespread commercialization in the long-haul freight sector as well, standing out as a primary alternative to FCVs. Indeed, not-hybrid catenary trucks are a very promising solution in terms of CO_2 reducing emissions, with savings comparable to BEV if no auxiliary combustion engines are installed. As catenary trucks are charged through the overhead pantograph connection to the electricity grid, they do not require a battery charging process, so they offer a potentially high range. However, these trucks are highly dependent on

the roll-out of a comprehensive infrastructure network which also limits the flexibility of routes. For this reason, the development of this solution is viewed as a long-term goal and, currently, feasibility is still being assessed including through experimental tests.

FCVs, as well as BEVs, offer fundamental advantages over their diesel counterparts. Firstly, the electric driveline exhibits higher energy efficiency than internal combustion engine powertrains. Indeed, fuel cell hybrid powertrain efficiency is approximately 16% higher compared to that of a diesel, while for battery-electric vehicles it reaches an impressive 45% [14]. The electric driveline is much simpler than that of a conventional diesel truck as there are not as many mechanical moving parts. This also results in significantly lower malfunctions and maintenance costs compared to conventional vehicles. Additionally, they are characterized by regenerative braking capabilities. Capturing kinetic energy during vehicle deceleration, it contributes to an overall reduction in energy consumption, increased driving range, and reduced wear on conventional brake pads. From the environmental point of view, both BEVs and FCVs do not produce emissions during their operation other than those related to wear (e.g. from tires and brakes), and fuel cell vehicles only emit water at the tailpipe. Nevertheless, for such an assessment it is essential to consider the overall energy consumption and emissions, also taking into account electricity and battery production, as well as the hydrogen supply chain, following more complex approaches such as the WTW. This consideration becomes particularly critical when dealing with grey or blue hydrogen, where the environmental impact is associated with the methods of hydrogen production, which are heavily based on fossil fuel consumption.

However, the widespread adoption of electric propulsion for long-haul applications is currently hindered by various technical and practical constraints. Particularly relevant among these are limitations in vehicle range and extended charging times that impact delivery schedules and vehicle uptime. Furthermore, the increase in vehicle size and the reduction in payload capacity due to the additional weight of batteries further hampers the economic feasibility of BEVs for the commercial market. In fact, several studies have demonstrated that BEVs are more suitable in passenger and light transport contexts. For instance, the research by Forrest et al. [15] indicated that BEVs could potentially replace 62 to 76% of light-duty commercial trucks in California. Yet, when it comes to heavy-duty trucks, FCVs emerge as a more viable option due to their range and refuelling capabilities. A similar conclusion was reached also by Ribberink et al. [16] in their study assessing the feasibility of BEVs and FCVs for replacing medium and heavy-duty buses and trucks in Canada.

On the other hand, technologies that maintain the internal combustion engine as the primary energy converter, such as vehicles powered by lower-carbon or synthetic fuels, are also under evaluation. Their technical design and integration into the market are relatively straightforward compared to the aforementioned alternatives, making them viable short-term solutions. Nevertheless, they still inherit the drawbacks associated with engine utilization. Lower-carbon fuel trucks, for example, powered by LNG or CNG, have limited reduction potential of CO_2 (from 3% to 14% less CO_2 emissions than diesel [14]), pollutants, and particle emissions. Yet these trucks have already found a market in Europe and are employed as an alternative to diesel trucks, highlighting their advanced technology readiness. Nevertheless, CNG and LNG also see

limited refuelling infrastructure. Another alternative for diesel combustion engines are heavy-duty trucks fuelled by E-fuels, a CO_2-neutral alternative. Two E-fuels could be used with existing engine technology: e-DME (synthetic dimethyl ether) and e-Diesel, where the latter could directly be used in existing drop-in fuel infrastructure. In this case, the emission reduction potential is limited and strongly depends on the origin of the electricity used for their production. Several E-fuel projects have shown technological readiness, but fuel production cost and NO_x emission remain substantial hurdles for commercialization. Figure 3.1 summarises the current level of technological readiness for each of the alternatives discussed.

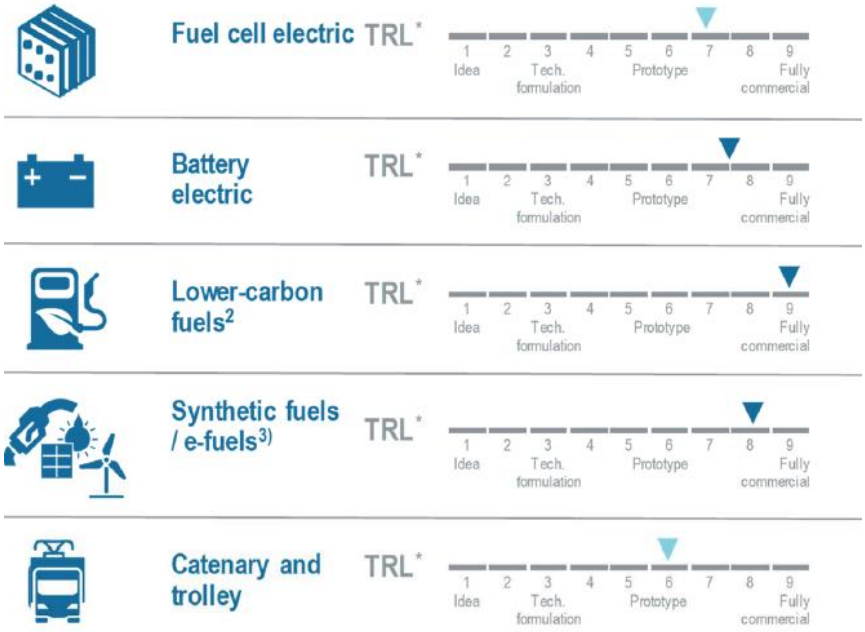

Figure 3.1: Technological readiness level for alternative powertrains.

3.1.2 FC technology strengths and challenges to deployment

Fuel cell systems present a unique advantage over traditional electrochemical batteries by decoupling the power generation mechanism from the energy storage component. This separation allows for greater flexibility and efficiency in the design and operation of such systems, by minimizing their interdependencies. The ability to store energy in tanks becomes particularly relevant when considering the high specific energy density of hydrogen and the advantages that this brings. Hydrogen tanks, being both space-efficient and lighter than batteries, contribute to a reduced powertrain weight, facilitating increased payload capacity. This weight reduction not only offers economic advantages, overcoming a critical issue for battery electric vehicles but also enhances the practicality and handling of the vehicle. Furthermore, from which it follows that FCVs offer a greater driving range and shorter refuelling times when compared to BEVs. The autonomy of a fuel cell heavy-duty vehicle is influenced by both the payload it carries and the amount of hydrogen stored in the vehicle. As

detailed in the following chapter, manufacturers claim that a typical fuel cell HDV can achieve a range of 350 to 400 km with a single refuelling session when using the simplest storage method of compressed hydrogen at 350 bar. This range is already notably higher than that of a typical battery-powered freight vehicle, which typically falls between 150 and 400 km on a single charge [17], [14]. In addition, it's worth noting that the FCV range can significantly increase with the adoption of higher energy density technologies. As far as refuelling time is concerned, it depends on various factors, including the type of hydrogen storage system employed, the storage capacity of the vehicle, and the technology of the refuelling station. Currently, the state-of-the-art refuelling flow rate is approximately 120 g/s, as stipulated by the SAE J2601-2 standard, one of the initial protocols for gaseous hydrogen refuelling of HDVs [10]. This results in times on the order of magnitude of minutes. Overall, the refuelling session of an FC-HDV is considerably shorter than the several hours required for a full battery recharge even with high-speed charging infrastructure. These factors collectively establish the FC solution as a more favourable pathway for the future decarbonization and electrification of the heavy-duty transport sector, where minimizing downtime and maximizing operational efficiency is essential.

Nevertheless, it is crucial to acknowledge that impediments to the commercialization of fuel cell electric vehicles persist, mainly associated with economic challenges. The current cost of the powertrain for FC trucks is considerably higher when compared to the well-established diesel engine technology, and at the same time energy and fuel costs, especially for green hydrogen, remain elevated. Economic barriers concern the lack of funding and incentive schemes, such as financial support to mitigate the cost of FC technology to make it cost-competitive for truck operators. Therefore, given the uncertain future cost trajectory of green hydrogen and the absence of definitive decisions on support mechanisms for the mid-to-long term, alternative powertrain options may be favoured in the meantime. Furthermore, technical hurdles in the development and deployment of heavy-duty FCVs encompass various aspects. These include challenges in product design, integrating the FC powertrain into existing truck chassis while optimizing weight and dimensions, ensuring optimal performance, and seamlessly integrating different systems. Other critical considerations involve the lifetime and the thermodynamic optimization of the fuel cell stack, limitations in the mass of hydrogen that can be stored on board, as well as the establishment of efficient refuelling networks with standardized protocols. Overall, in the context of the current technological and non-technological barriers identified, none are insurmountable for the successful commercialization of FC-HDVs. However, large-scale deployment of FCV technology in the long-haul freight sector can be sped up in the upcoming years. In the short term, dedicated research and innovation projects are necessary to continue the development of FC components and applications for trucks, and the European Union is actively moving towards this goal.

3.2 FC-hybrid vehicle powertrain topology

Fuel cell electric trucks operate as series-hybrid vehicles, wherein the fuel converter (the FCS) and the REESS lines are linked through an electrical link and the electric motor is the only source of power to the wheels. Depending on the expected usage, the FCV powertrain could be implemented in several ways by changing the size and proportion of the fuel cell system, as an electric generation unit, and the energy storage system to fulfil the performance requirement [10]. This observation leads to the introduction of a key parameter known as the "hybridization factor". This metric plays an essential role in classifying hybrid vehicles, aligning with the relative sizes of the on-board energy sources. It can be expressed as:

$$R_{h,series} = \frac{P_{el,gen}}{P_{em}} \in [0,1],$$

(Eq. 3.1)

where:

- $P_{el,gen}$ is the power provided by the electric generation unit (FCS or ICE in conventional-hybrid vehicles).
- P_{em} is the electric motor power.

Based on the hybridization factor's value, it becomes feasible to categorize various configurations of a series-hybrid vehicle, and identify two pure configurations at the extremes of its existence field:

- If $R_{h,series} = 0$, the vehicle does not have any secondary power source and it means that all the requested power is drawn by the battery pack. Therefore, this is a pure BEV.
- If $R_{h,series} = 1$, all the power required by the electric motor is produced solely by electric generation without any contribution from the ESS. This kind of architecture is called "Electric transmission". When contemplating the utilization of FCS as electrical generation units, this solution becomes hardly feasible. The FCS should be designed to provide the maximum power request expected by the vehicle and operate under highly dynamic conditions, which in turn results in decreased operational efficiency and accelerated device degradation. Furthermore, the powertrain would lack regeneration capability.
- When $R_{h,series} \in (0,1)$, both power sources are present and work in synergy, and the architecture can effectively be called "hybrid". With the increase in the size of the FCS, the hybridization factor likewise rises, while the capacity of the auxiliary energy device exhibits the opposite trend. These relative features lead to the classification of hybrid vehicles into categories as illustrated in Figure 3.2. FC-

hybrid architectures are particularly advantageous, especially since the integration of a battery solves several critical challenges inherent to fuel cells. These issues include irreversibility, the slow dynamic response to fluctuations in power demand, and the complexities associated with starting and warming up to the optimal operating temperature. Furthermore, by managing power flows, it becomes possible to optimize both fuel consumption and powertrain efficiency.

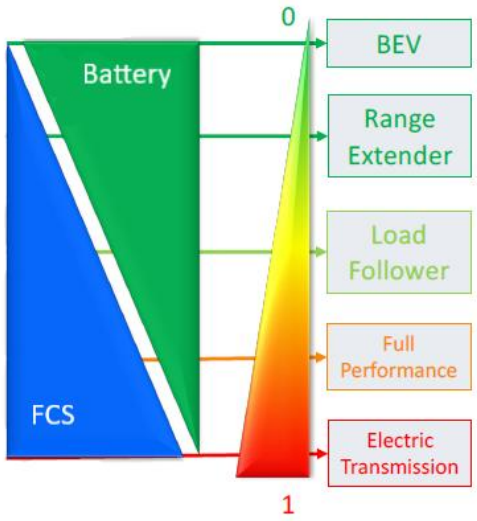

Figure 3.2: Vehicle configurations according to hybridization factor.

For HD long-haul applications, a load follower or full performance hybridization factor is preferable, where a powerful FCS takes primary responsibility for covering traction and auxiliaries power requirements, while the ESS (usually an electrochemical battery pack or supercapacitor) is used under cold start, very low load, boosting, and for storing and reusing energy from regenerative braking. Thus, a much smaller ESS size than heavy-duty plug-in HEVs and BEVs is chosen for such applications, reducing related costs and weight, while maintaining a good payload capacity. On the other hand, a range-extended powertrain relies mainly on a battery as the energy source, with a smaller fuel cell unit providing additional extended driving. FCS range extenders, as well as plug-in battery charging, are uncommon for long-haul operations due to the requirements of long-distance freight applications to minimize vehicle costs and battery weight. A compact FCS range extender presents a viable solution for HD-BEV applications in regional delivery scenarios where the daily mileage is relatively limited. This approach enables the utilization of grid electricity for most daily trips while retaining the capability to undertake occasional long-distance journeys [10].

The powertrain topology for a generic fuel cell hybrid vehicle suited for long-haul heavy-duty applications is schematized in Figure 3.3. The actual energy carriers are the hydrogen tank and the battery pack. The former is connected with a feed circuit to the FCS, which is properly an energy conversion device. Both the battery and the FCS are electrically connected to the high-voltage DC-link through electronic converters. Within the vehicle electronic control unit (ECU), an energy management system employs a sophisticated control strategy to define the

distribution of electrical power between sources and the operation of actuators, based on information such as the driver commands and the current state of the vehicle. Then, the inverter modulates the electrical power supplied to the electric motor, which converts it into mechanical power. This is transferred to the vehicle's drive wheels through the transmission and axle.

The following sections will individually present the operation and characteristics of the main subsystems mentioned, focusing on the requirements for long-haul freight applications.

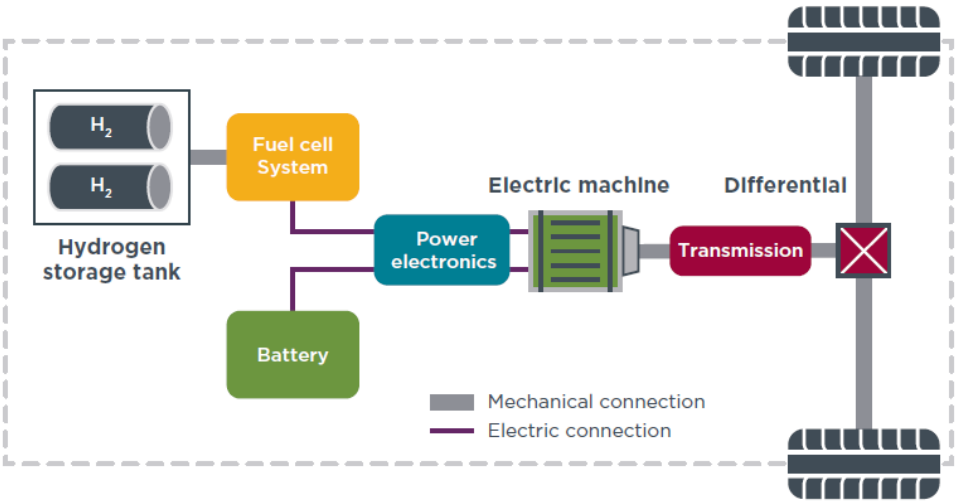

Figure 3.3: Fuel cell vehicle powertrain architecture.

3.2.1 Power sources

In FC-HDVs, the power required for propulsion and auxiliary loads can be sourced from a combination of FCS and one or more onboard energy storage systems such as electrochemical batteries and supercapacitors. This hybrid approach aims to improve overall powertrain efficiency, support FCS functionality, ensure vehicle drivability, and provide optimal cold start characteristics. Depending on the vehicle hybridization factor, we may have different sizes of fuel cell systems. While traditionally it was sized to efficiently meet the vehicle's slightly above-average power requirements, recent applications exhibit a trend toward oversizing. In these cases, the fuel cell system is designed with a maximum power capacity significantly higher than the expected average power required for the specific application. This design choice allows the FCS to frequently operate in the low-power region, where its efficiency remains close to the maximum value, contributing to an overall improvement in the driveline's efficiency, however at the expense of cost.

The presence of a secondary ESS is crucial for these applications for optimizing the FCS operation and managing the vehicle's energy efficiently. Although supercapacitors, as well as flywheel systems, offer higher specific power (as shown in Figure 3.4), and could efficiently handle high transient load demands, electrochemical batteries are currently the most preferred solution due to their suitability for matching HDV specific energy, robustness, and reliability

requirements. Specifically, Li-ion cells offer the highest overall performance, the widest choice of specific power to specific energy balance and are the current preference from a price-performance perspective. Typically, a slightly larger battery pack is used for this type of vehicle, featuring higher current and energy capacity compared to ICE-hybrid drive concepts.

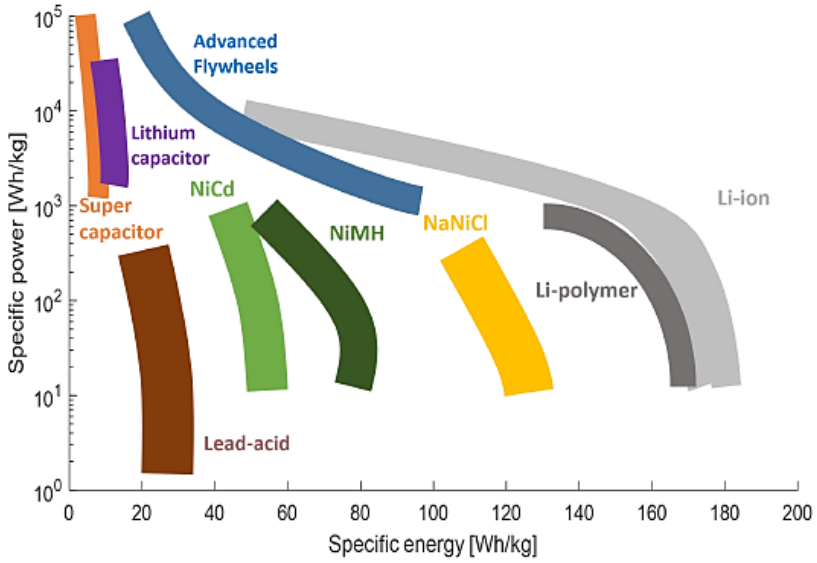

Figure 3.4: Comparison of specific power and specific energy for different energy storage systems.

In freight vehicles, the battery's energy density stands out as one of the most important parameters, directly impacting the maximum payload and volume that the vehicle can transport over a given distance. However, there are other critical parameters, such as battery durability, that play an important role in battery selection. The cathode chemistry of the Li-ion battery remains the most critical design element to achieve high performance and durability. The three most important Li-ion cathode chemistries are NMC, NCA, and LFP.

Lithium nickel manganese cobalt oxide (NMC) is a leading Li-ion cathode chemistry, prevalent in over 28% of global electric vehicles in 2020, including electric heavy-duty vehicles [17]. The performance of NMC batteries depends on the relative ratios of nickel, manganese, and cobalt oxide. Most commonly, NMC batteries use equal parts of these elements (NMC-111). This cathode type, combined with a graphite anode, allows Li-ion cells to achieve energy densities of up to 350 Wh/kg. In the coming years, significant progress is expected considering that a further increase in energy density of up to 400 Wh/kg can be achieved by improvements to the anode, such as the addition of silicon or the use of lithium metal [18]. Furthermore, NMC cells demonstrate a robust cycle life, exceeding 2000 cycles before a 20% loss of their original capacity. Lithium nickel cobalt aluminium oxide (NCA) is similar to NMC cells in terms of energy density and durability, but it is slightly costlier, making it less employed. Lithium iron phosphate (LFP) represents another widely adopted Li-ion cathode chemistry for electric vehicles. Although batteries with LFP chemistry offer lower energy density compared to NMC and NCA chemistries, they compensate with a higher cycle life, exceeding 2500 cycles.

3.2.2 Electric motor and transmission

The fuel cell powertrain is propelled by one or more electric drives (eDrive), comprising an electric machine equipped with power electronics and a controller. This electric drive, functioning as a reversible machine, not only provides traction efforts but also can recuperate kinetic and potential energy from the moving vehicle during braking and downhill descents, offering significant advantages.

Two predominant types of electric machines, namely asynchronous induction machines (ASM) and permanent magnet synchronous machines (PM-SM), have emerged as the preferred choices for modern road vehicle applications. Both electric motor (EM) types operate on alternating current, necessitating the use of an inverter for their functioning. In the case of ASM, a rotating field is generated by alternating current in the stator, which in turn creates a magnetic field in a rotor through electromagnetic induction. To induce an electromotive force, the rotor's magnetic field trails that of the stator resulting in a relative motion referred to as "slip". ASMs have a simple rotor construction, which can result in lower manufacturing costs compared to synchronous motors. However, the motor control is more complex, requiring careful control of the variable frequency in the magnetic field of the stator and the resulting slip. Typically, ASM machines feature a slightly lower efficiency than synchronous motors. In PM-SM machines the rotor's magnetic field relies on permanent magnets, and the rotating magnetic fields in the stator and the rotor move synchronously, eliminating losses associated with slip. However, higher manufacturing costs are encountered due to the rare-earth metals used in the permanent magnets. Compared to the ASMs, the PM-SMs offer higher power density, a more compact mechanical structure, higher efficiency, and greater torque capacity.

In terms of innovative electric propulsion systems suitable for heavy-duty vehicles, the hub-mounted eDrive emerges as a standout option. As demonstrated by Jiayi et al. [19], this powertrain configuration is well-suited for heavy and multi-axle vehicles, delivering excellent vehicle dynamic performance and effective on-board energy management, including fuel cell vehicles. The primary advantage of the hub motor, also known as the "in-wheel motor (IWM)", lies in its ability to streamline drivetrain packaging through transmission integration. Furthermore, since the torque of each IWM can be independently controlled, this solution advances electronic control and vehicle dynamics management, resulting in enhanced vehicle performance and safety. However, the widespread adoption of this technology is constrained by limited regenerative braking capabilities due to size and cost constraints.

Certainly, linking the motor to the wheels necessitates the use of a transmission. For medium and heavy-duty applications, a multi-speed transmission is preferred over single-gear reduction to satisfy the weight-critical vehicle key performance requirements of high gradability, acceleration, and speed. The use of multiple, predominantly automatic, reductions is well suited to the advanced control strategies of electric vehicles, promoting efficient operation and downsizing of the electric drive. This, in turn, leads to a reduction in weight, energy consumption, cost, and overall environmental impact of the powertrain. Finally, it is noteworthy that for an electric powertrain, the number of employed ratios is significantly lower than those

utilized in heavy vehicles with a combustion engine. In electric powertrains, typically between 2 and 6 gear ratios are utilized, in contrast to the more common use of 12-speed transmissions in ICEVs.

3.2.3 DC-link and converters

The various power sources and loads including the electric motor, auxiliaries, and power take-off, are typically interconnected through a common high-voltage DC bus, the voltage level of which is regulated by a DC-bus controller, to facilitate efficient powertrain functioning in all conditions and vehicle operations. In heavy-duty applications, a DC bus voltage level between 350 V and 800 V must be guaranteed [20]. The trend, as in all electric vehicles, is to use a very high voltage to reduce the size of cables, and thus their weight and cost. Achieving the desired degrees of freedom in bus voltage regulation involves employing various power converter configurations between power sources, loads, and the DC bus. On the other hand, if there is no DC-DC conversion between the power sources and the eDrive, the efficiency and performance of the electric motor can be significantly impacted during high load demands or low battery state of charge (SOC) due to a reduction in DC-bus voltage [10]. With the FC being an irreversible device operating at a largely varying load-dependent terminal voltage, and generally designed for a lower stack voltage level due to mechanical construction limitations, a unidirectional HV DC/DC boost converter is required to interface it with the DC bus. Instead, a bidirectional HV DC/DC converter is employed to connect the on-board energy storage with the DC-link to maintain its desired voltage level and efficient eDrive operation irrespective of the varying ESS states.

The electrified nature of the FCV powertrain facilitates the incorporation of electrically operated auxiliary loads. These include cooling pumps and fans, the HVAC compressor and heater, power steering, and pneumatic systems, along with motorized power take-off and lighting systems. HDVs use either 24 V or 48 V bus voltage, which is higher than the 12 V employed in light duty vehicles. As a result, an LV DC/DC converter is required to step down the voltage from the HV DC-link to 24 V, supplying auxiliary loads and electronic control units. Alternatively, for higher power auxiliary loads such as PTO, power steering, and air compressors, a 48 V DC/DC conversion may be more appropriate [20].

3.2.4 Energy management system

FC-HDVs are equipped with intricate powertrains featuring multiple power sources and loads. Achieving efficient and robust management of these diverse subsystems is crucial to minimizing overall hydrogen fuel consumption. Energy management system (EMS) plays a key role in the operation of a hybrid vehicle by enabling the optimal distribution of energy from available sources, including the fuel cell system and high-voltage battery. When integrated with

eco-driving, eco-comfort strategies, or electrically operated auxiliaries, this management extends to power users, such as the electric actuators, cooling systems, and auxiliary loads. The goal is to operate these subsystems with overall high efficiency, aligning with the aforementioned fuel economy objectives while ensuring functional safety. During this operation, constraints related to the physical limits of the actuators, the limitation of energy stored in the REESS, and the obligation to maintain the battery SOC within prescribed limits must always be observed. In addition, powertrain management allows to address of other significant objectives, such as extending the remaining useful life (RUL) of key components like the FCS and the HV battery, which is essential to meet the demanding mileage requirements expected for heavy-duty vehicles, and sustaining the end-of-cycle battery state of charge at or around its initial mission value. In the specific context of Not Off-Vehicle Charging hybrid electric vehicles (NOVC-HEVs), where the fuel cell serves as the primary energy source and the battery external recharging via an electrical grid connection is not possible, the EMS enables the "Charge Sustaining (CS) mode" thanks to an accurate power distribution between energy sources, as the net energy variation of the battery should be zero between the beginning and end of a driving mission. From a practical point of view, it is sufficient to keep the SOC between two limit values, a maximum, and a minimum, as a certain difference between the SOC values is acceptable and does not affect the functionality of the vehicle. This operational approach ensures repeatability in vehicle operation across successive journeys, as long as there is still fuel in the tank. Instead, from an energy analysis perspective, it permits an accurate estimation of fuel consumption during a mission without having to consider the impact of deviations in the energy storage of the ESS.

Implementation of powertrain control in an integrated multi-level framework can facilitate the application of complex optimization-based strategies onto real-time vehicle controllers. In the context of hybrid vehicle energy management systems, a hierarchical control structure is typically employed. Figure 3.5 provides a schematic representation of its structure and functioning in relation to the other vehicle components. At the highest level, a "supervisory control" operates. Below this, there is a lower-level controller referred to as the "energy management controller". Further down the hierarchy, we encounter the low-level controls governing individual components, including the motor, inverter, or clutches. The supervisory controller determines the current optimal operating mode of the vehicle by evaluating factors such as driver demand and the operating conditions of various components. Additionally, it states when to implement the power distribution algorithm embedded within the energy management controller. The output variables of the latter are the setpoints for the low-level control units of the various components.

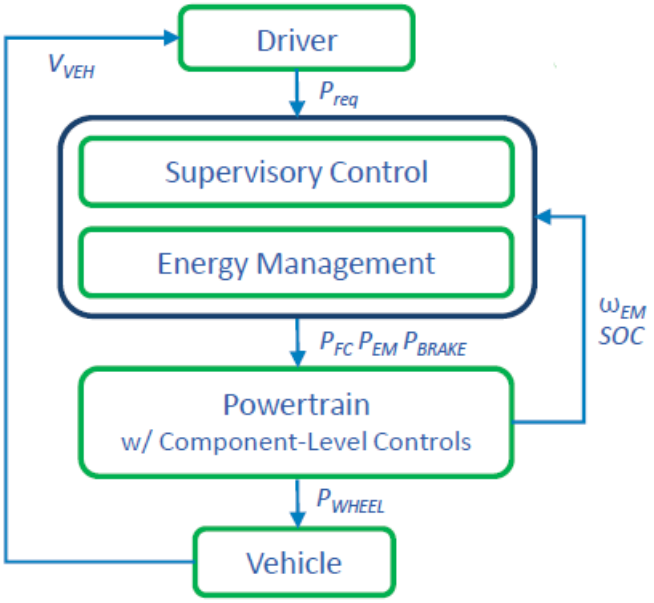

Figure 3.5: Hierarchical control structure of the vehicle energy management system.

Energy management strategies, that operate with minimal or no prior route information and are suitable for real-time implementation given limited on-board calculation power, are referred to as "online strategies". Strategies that are non-causal, globally optimal, requiring detailed a priori route and vehicle state information, and too calculation intensive for their on-board implementation are known as "offline strategies". They are instead used to represent the optimal system behaviour as benchmarks for developing online strategies, assessing their quality, or generating predictive optimal powertrain state trajectories for the EMS. Considering that both are hybrid vehicles with multiple power sources the control approach used in well-established HD powertrains with ICE and battery can serve as a reference framework for the development of effective energy management strategies in FC-HDVs. The only difference between the two vehicle configurations is the on-board fuel energy conversion device, therefore the many strategies that can be used are essentially the same.

4. Market development and products actual state

The road freight sector is an important pillar of the European economy as 75% of goods are transported on wheels, but also a significant source of CO_2 emissions [14]. As a zero-emission (ZE) solution with a similar performance as conventional diesel-powered heavy-duty vehicles, FC trucks have substantial market potential, but their current adoption remains severely constrained. This section offers a concise overview of the European ZE-HDVs market in recent years to delineate the potential for further growth in the deployment of fuel cell technology for heavy transport. Subsequently, a brief introduction to several FC vehicles, for which production has been announced by leading manufacturers worldwide, is provided, also highlighting the declared characteristics of the powertrain. Finally, it introduces the most relevant and recent research projects focused on FCHDVs in Europe.

4.1 ZE-HDVs market in Europe

In the global market for zero-emission heavy-duty vehicles, Europe stands as the second-largest region, with China leading the pack and responsible for a staggering 89% of global sales in 2022. Out of the 127,000 ZE-HDVs sold worldwide in the same year, Europe accounted for 4.1%, reflecting a notable increase from the previous year's share of 3.1% [21].
As reported by the ICCT study "Zero-emission bus and truck market in Europe: A 2022 update" [21], the sales of ZE-HDVs (including battery and fuel cell electric buses, light and medium trucks, and heavy long-haul freight vehicles) experienced a robust 23% growth in 2022 compared to 2021, surpassing the 5,000 units for the first time, as Figure 4.1 shows. The main driver for this growth was from heavy truck sales, soaring from 300 units the previous year to over 800. Indeed, it is important to note that, despite this growth, ZE-HDVs still represent a fraction of the overall market. In 2022, a total of 265,000 conventional diesel heavy trucks were sold in Europe, overshadowing zero-emission heavy vehicles with a mere 0.3% share of total sales.

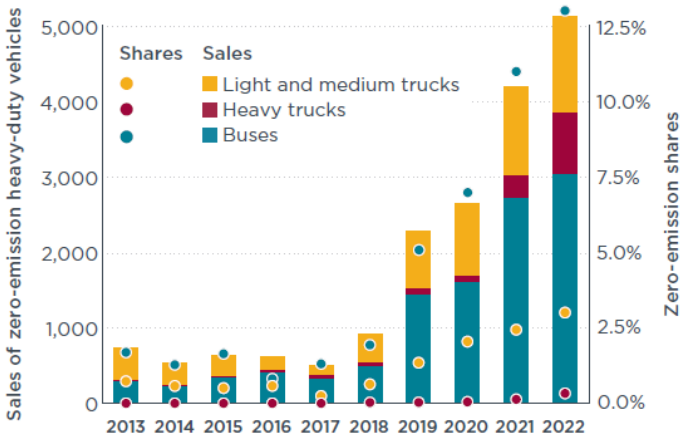

Figure 4.1: Sales and shares ZE-HDVs by vehicle type.

Within ZE-HDVs sales, battery electric vehicles emerged as the dominant category. Conversely, hydrogen fuel cell vehicles claimed only a small share, with FC heavy trucks representing a modest 3% of total sales. Notably, the majority of fuel cell HDVs were sold in Germany and the Netherlands, emphasizing regional variations in the adoption of zero-emission technologies within the European market.

In the landscape of HDV sales (both conventional and zero-emission) in 2022, schematised in Figure 4.2, heavy trucks for long-haul freight transport constituted a substantial 80%. This category encompasses trucks with a gross vehicle weight above 16 tonnes, spanning various axle configurations such as 4x2, 6x4, 6x6, 8x2, and 8x4, encompassing both rigid and tractor trucks. Notably, most of these heavy trucks adopted the tractor-trailer configuration, amounting to around 175,000 units and representing 52% of the total sales.

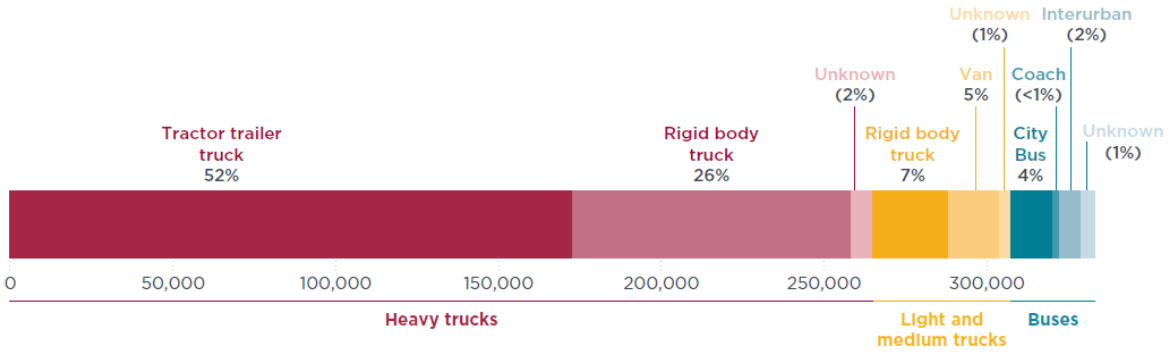

Figure 4.2: New heavy-duty vehicle registrations in Europe by vehicle category in 2022.

4.2 Market-launched and upcoming FC-HDVs

Several heavy-duty original equipment manufacturers (OEMs) are actively advocating for the development and market implementation of FC electric vehicles to bridge the gap towards the economic feasibility of fuel cell propulsion and future sustainable mobility. While FC technology for heavy-duty vehicles is currently undergoing initial stages of demonstration and prototyping, the growing availability of ZE-HDVs, driven by the EU's HDV CO_2 standards, has prompted several OEMs to outline targets for the market penetration of ZE-HDV for the coming years, together with announcements of new industry ventures and models development [22]. The subsequent overview provides insight into the primary fuel cell vehicles designated for the European market. Other manufacturers, including DAF, VDL, and Scania, are also progressing in this direction, conducting prototype testing in controlled environments. However, these initiatives are still at an experimental stage and not yet oriented toward the consumer market, as will be explained in the next section.

Hyundai XCIENT [23]

The Hyundai XCIENT stands out as a hydrogen fuel cell-powered heavy-duty rigid truck specifically crafted for long distance freight operations. To meet the different European customer needs, the vehicle is available in two distinct configurations:

- Rigid truck 4x2 with a maximum gross combination weight (MGCW) of 38 tons.
- Rigid truck 6x2 with an increased MGCW of 42 tons, providing an optimal choice for those requiring enhanced load capacity.

Both configurations share the same powertrain, featuring a 180 kW hydrogen fuel cell system comprised of two 90 kW stacks running in parallel. The accompanying battery pack has a total capacity of 72 kWh, operating at a nominal voltage of 630 V and consisting of three 24 kWh Li-ion batteries connected in parallel. The electric motor is equipped with a rated power of 350 kW and a torque of 2,237 Nm. Positioned behind the driver's cab, the hydrogen tanks offer a storage capacity of approximately 31 kg, compressed to 350 bar. Hyundai claims a driving range of about 400 km on a single fill-up, a figure validated through real driving operations.

Figure 4.3: Hyundai XCIENT, 6x2 rigid truck.

Moreover, the Hyundai Motor Company has entered a strategic partnership with hydrogen infrastructure provider H2Energy, known as Hyundai Hydrogen Mobility. This collaboration was launched in Switzerland in 2020, with the objective of introducing 1,600 XCIENTs, which include articulated trucks, along with the essential hydrogen infrastructure, to the Swiss market by 2025. The joint venture also seeks to assess the performance, reliability, and safety of these new vehicles during actual operations. The outcomes of this evaluation have proven promising: up to March 2022, the XCIENT has covered more than 3 million kilometres without a single accident.

Daimler Truck GenH2 [24]

Daimler has articulated an ambitious vision for its new HDV registrations, with a target of potentially achieving 60% ZE status by 2030 and a more robust 100% target for ZE-HDV market penetration by 2039 [22]. To achieve this goal, Daimler has developed the GenH2, a 4x2 hydrogen fuel cell electric tractor designed for long-haul transport, utilizing the chassis of the conventional Actros truck. The model is currently undergoing trials, with series production anticipated to commence by 2027.
The GenH2 is equipped with two cryogenic liquid hydrogen tanks operating at -253 °C, boasting a storage capacity of 80 kilograms (40 kg each), specifically tailored for covering extensive distances, up to 1000 km declared. The hydrogen fuel cell system, rated at 300 kW (2x 150 kW), is complemented by a 70 kWh battery pack delivering a power output of up to 400 kW. This setup supports two electric motors, each capable of sustaining 230 kW continuous power.

Figure 4.4: Daimler Truck GenH2, 4x2 tractor.

Nikola Tre [25, 26]

The Nikola Tre is the result of a collaboration between the American Nikola Motor Company and Iveco. This vehicle is available in both battery and fuel cell configurations, thanks to a versatile platform designed for heavy articulated tractors that can accommodate both propulsion technologies. The Nikola Tre platform is based on the IVECO S-Way truck chassis, while the Nikola Motor's technologies are used both for the electric powertrain and the infotainment. In its fuel cell version, the Nikola Tre is a 6x2 tractor equipped with a 120 kW FCS and a continuous power electric motor boasting 480 kW. With a compressed hydrogen storage capacity of approximately 70 kilograms at 700 bar pressure, coupled with a rapid refuelling time of just under 20 minutes, this variant offers a range of up to 800 km. Nikola estimates that it will enter the European market in 2024.

Figure 4.5: Nikola Tre, 6x2 tractor.

Table 4.1: FC truck technical specifications summary.

FC vehicle	FCS	Battery	EM Power	H_2 storage	Declared range
Hyundai XCIENT	180 kW	72 kWh	350 kW	31 kg CH_2 (350 bar)	400 km
Daimler GenH2	300 kW	70 kWh	460 kW (2 x 230 kW)	80 kg LH_2	1000 km
Nikola Tre	120 kW	70 kWh	480 kW	70 kg CH_2 (700 bar)	800 km

4.3 Research projects

Trial and demonstration activities play a crucial role in paving the way for the commercialization of FC heavy-duty trucks, addressing challenges related to technological development, implementation, and cost competitiveness. There is a rising level of interest and engagement in this technology, evident in the increasing number of projects worldwide that effectively showcase the viability of these trucks. In Europe, diverse demonstration initiatives, spanning various vehicle types and operational scenarios, are being conducted through collaborative efforts involving multi-partner coalitions. These collaborations extend beyond OEMs and component manufacturers to include active participation from infrastructure providers. Overall, several noteworthy European projects have been identified and will be presented.

- ***"H2-Share" project*** [27, 28]

The "H2-Share" project was conducted between 2017 and 2020 across Belgium, France, Germany, and the Netherlands in collaboration with the Dutch company VDL. It was the first FC heavy vehicle test project in Europe, with its main objectives focused on the development of the first hydrogen-powered truck in Europe, and the demonstration of the functionality of this technology under real conditions in different regions. A 27-ton (MGVW) 6x2 rigid truck, designed by VDL, was employed and tested in each region for three months.

- ***"H2-Haul" project*** [29]

The "H2-Haul" project, undertaken by a collaboration between IVECO, FPT Industrial, and VDL, spans the duration of 2019-2024 and operates in Belgium, France, Germany, and Switzerland. The initiative involves the testing of 16 heavy-duty hydrogen fuel cell trucks in commercial and logistics operations across designated sites in the aforementioned countries. The specific goals encompass the design of three different types of long-haul FC-HD trucks, ranging from rigid to articulated vehicles (from 26 to 44 tonnes) to meet customer requirements across different operating environments, their certification for safe use on European roads, and the establishment of new high-capacity hydrogen refuelling stations with low environmental impact. To validate the viability of the technology, the project aims to drive the trucks for over one million kilometres during normal commercial operations.

- ***"Hydrogen region 2.0" project*** [27]

VDL and DAF are jointly engaged in the "Hydrogen Region 2.0" project, which takes place in the Flanders region of Belgium. The project involves the development and demonstration of a 44-ton hydrogen tractor-trailer manufactured by VDL, along with a focus on establishing multiple filling stations. This collaborative effort receives support from companies and organizations specializing in hydrogen infrastructure and zero-emission applications, contributing significantly to the ongoing efforts in advancing sustainable transportation solutions.

Table 4.2 - Technical specifications summary of project vehicles.

Project	FC vehicle	FCS	Battery	H_2 storage	Declare range
H2-Share	Rigid truck (6x2)	88 kW	84 kWh	30 kg CH_2 (350 bar)	400 km
H2-Haul	Rigid truck	-	-	-	-
	Tractor-trailer	-	-	-	-
Hydrogen region 2.0	Tractor-trailer (4x2)	88 kW	72 kWh	30 kg CH_2 (350 bar)	350 km

5. VECTO

5.1 Regulation context and VECTO introduction

The first regulations addressing CO_2 emissions from vehicles in Europe were outlined in Regulation (EC) 443/2009 and Regulation (EU) 510/2011, which set mandatory emission targets for new passenger cars and light commercial vehicle fleets respectively. Nevertheless, extending similar CO_2 emission standards to heavy commercial vehicles proved unfeasible until 2017, primarily due to two main problems. At first, in contrast to light-duty vehicles, HDVs present a large variety of configurations that are tailored to the needs of the desired application and the final user. It is therefore complex to use the results obtained from dynamometer measurements to create general criteria for assessing and monitoring the compliance of the entire heavy vehicle fleet with CO_2 emissions, also considering that the size of vehicles requires equally large and expensive benches, which are consequently not widely widespread. Furthermore, the implementation of various CO_2-reducing technologies in the future will make the evaluation even more complex. expanding the number of possible configurations. Secondly, there was a lack of agreed-upon recording and monitoring methodologies for evaluating these emissions. This absence of a monitoring mechanism has contributed to a limited understanding of the precise CO_2 emissions of HDVs, impeding the development of effective policies.

To address these issues, the European Commission has developed the Vehicle Energy Consumption Calculation TOol. This tool utilizes a vehicle simulation approach to calculate energy and fuel consumption and CO_2 emissions for heavy-duty vehicles, aiming to encompass all possible vehicle configurations effectively. The main objective is to provide a controlled and regulated means of calculating fuel consumption and CO_2 emissions by modelling vehicle operation over realistic driving cycles, ensuring repeatability, reliability, and flexibility, and eliminating the need for testing the entire vehicle while still meeting regulatory requirements. Nevertheless, the realization of this ambitious objective demanded the prior establishment of a standardized regulation governing the determination and certification of CO_2 emissions at the vehicle level for HDVs, creating the legal framework within which VECTO and stakeholders must operate. In December 2017, Commission Regulation (EU) 2017/2400 was officially published, providing the necessary regulatory structure [30]. This regulation has adopted a methodology that integrates physical tests and VECTO simulations to accurately calculate the above-mentioned fundamental parameters of new heavy-duty vehicles placed on the EU market, laying down the rules for using the simulation tool and for the official declaration of the values thus determined.

Detailed procedures for physical tests, whether at the component or vehicle level, have been established to generate certified input data for the VECTO tool. In instances where conducting experimental tests proves impractical, the regulation has introduced “standard values” as representative, verified reference points for specific components, thereby offering alternative input data. Moreover, Regulation (EU) 2017/2400 provides the European classification of freight vehicles (vehicle category “N”), which is of fundamental importance for navigating this

wide field. As Figure 5.1 shows, vehicles are categorized into numbered "Groups" based on three elements:

1. Axle configuration. This is represented by figures such as "4×2", where the first number is associated with the total number of vehicle axles and the second with the number of driving axles.
2. Chassis configuration (rigid lorry or tractor). A "rigid lorry" refers to a type of truck that consists of a single rigid chassis, without a detachable trailer. The "tractor" refers to a powerful motor vehicle designed to tow heavy trailers. It comprises the engine and the powertrain, while the external trailer is attached for the transport of goods.
3. Technically permissible maximum laden mass (TPMLM), in tons, denotes the maximum gross vehicle weight, encompassing the trailer and its cargo.

VECTO group	Axle type	Chassis configuration	Gross vehicle weight (tonnes)
0	4x2	Rigid	< 7.5
1	4x2	Rigid/Tractor	7.5 - 10
2	4x2	Rigid/Tractor	10 - 12
3	4x2	Rigid/Tractor	12 - 16
4	4x2	Rigid	> 16
5	4x2	Tractor	> 16
9	6x2	Rigid	All weights
10	6x2	Tractor	All weights
11	6x4	Rigid	All weights
12	6x4	Tractor	All weights
16	8x4	Rigid	All weights

Figure 5.1: Heavy-duty vehicle segmentation in the European Union.

The CO_2 emissions and fuel consumption certification procedure for HDVs forms a fundamental basis for the recently adopted CO_2 standards outlined in Regulation (EU) 2019/1242. These standards mandate a 15% reduction in the average CO_2 emissions of the new HDV fleet by 2025 and a 30% reduction by 2030 [31]. The reduction targets do not apply to each vehicle sold but rather to the average, sales-weighed CO_2 emissions of each manufacturer, which must reduce the average emissions of all vehicles falling under each group by the target, relative to the reference CO_2 emissions. The latter is defined as the fleet-average CO_2 emissions of newly registered HDVs in the reference period from July 1^{st,} 2019 to June 30^{th,} 2020 [32]. However, the current CO_2 standards apply to only a fraction of new trucks, targeting the groups responsible for 69% of HDV CO_2 emissions and 59% of HDV sales in 2023 [33]. These vehicle classes (specifically Groups 4, 5, 9, and 10) include heavy lorries with a technically permissible maximum laden mass above 16 tons and equipped with a 4×2 or 6×2 axle configuration. In February 2023, the European Commission proposed a revision of these standards [34], aiming to broaden their scope to encompass buses, coaches, trailers, and several new types of trucks

(Figure 5.2) covering vehicles responsible for 91% of heavy-duty CO_2 emissions and 83% of sales [33].

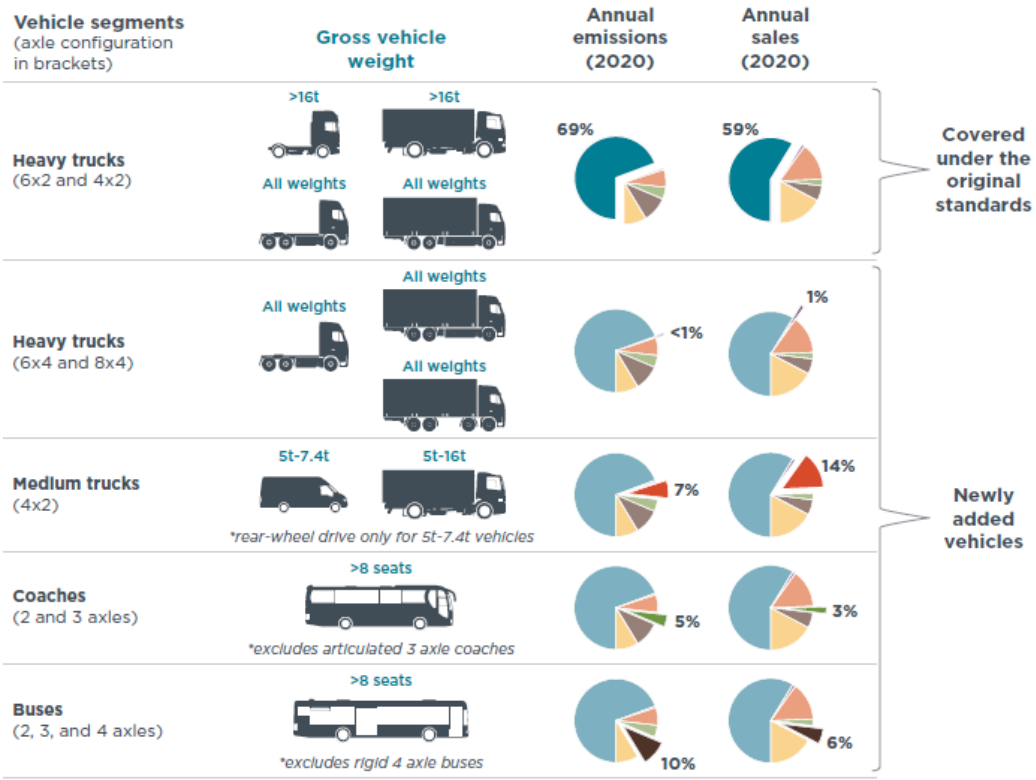

Figure 5.2: Scope of vehicles covered under the CO_2 standards and their annual emissions relative to all HDVs.

Compliance with CO_2 emissions targets is determined using the certification data produced by the VECTO simulation tool, as articulated by Regulation (EU) 2018/956. This regulation mandates HDV manufacturers to certify the emissions of all vehicles registered as of 1st January 2019 (in accordance with the provisions of (EU) 2017/2400) through modelling and simulation in VECTO of each of them, and report annually to the European Environment Agency. Conformity is measured at the fleet level, giving manufacturers the freedom to manage emissions among the vehicles in their fleet, achieving higher performance in one group and lower performance in another at their convenience.

The first version of VECTO was developed in 2012 through a collaboration between Graz University of Technology and the European Commission's Joint Research Centre, with significant contributions from various European OEMs and component manufacturers. Several tests, conducted on trucks between 2012-2014, demonstrated VECTO accuracy and reliability [35]. Since its inception, VECTO has undergone multiple updates and enhancements, solidifying its status as the official tool for certifying CO_2 emissions from HDVs within the European Union. The software evolution has been marked by continuous monitoring of emerging technologies, coupled with ongoing improvements aimed at expanding its capabilities to encompass new technologies and vehicle categories. Originally designed for modelling a

limited range of conventional trucks, the software has since been expanded to encompass buses and coaches, which can also be modelled with alternative powertrains including hybrid, electric, and fuel cell, in different architectures. However, VECTO is currently only used for certification purposes for vehicles with an internal combustion engine and belonging to the groups covered by the regulations [36].

5.2 VECTO operation

5.2.1 Software overview

VECTO is a simulation tool designed for the calculation of vehicle fuel consumption, CO_2 emissions, and energy consumption (EC), thanks to its capacity to accurately capture energy flows within HDV powertrains. It employs a backward-looking simulation approach, where the speed information is used as input to resolve the vehicle longitudinal dynamics, in combination with some forward-looking control modules for the modelling of those functionalities that would not be possible with the purely backward approach such as target speed cycles, driver operation, and simulation of common driver aid technologies (eco roll, look-ahead coasting, overspeeding) [37]. The simulation of the vehicle's longitudinal dynamics over the mission profile is achieved by considering driving resistances, given vehicle speed and acceleration. This process yields outputs such as power requested at the wheels, traction forces, and torques. The driving resistances considered, as illustrated in Figure 5.3, include rolling resistance, air resistance, gradient, and acceleration resistance, which also incorporates the effect of rotational inertia in the transmission. Then driveline component losses and the power demand of the auxiliaries are taken into consideration to evaluate the instantaneous engine power. The engine speed is determined by the engaged gear, the powertrain gear ratios, and the dynamic tyre radius.

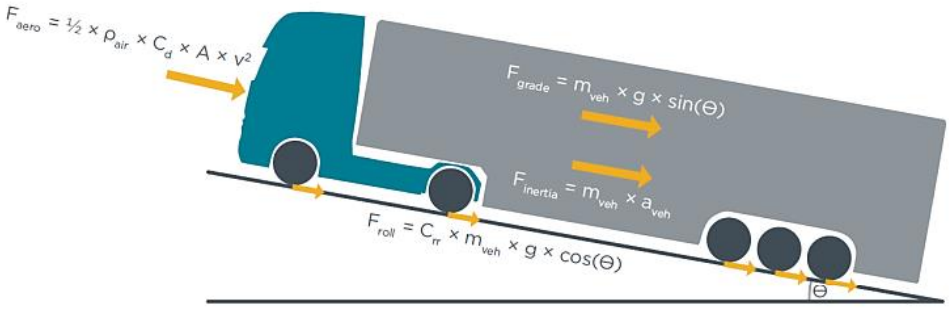

Figure 5.3: Vehicle driving resistances.

The calculation procedure outlined thus far, and depicted schematically in Figure 5.4, is applicable universally, regardless of the vehicle architecture. For a conventional vehicle, the final step involves obtaining instantaneous fuel consumption and CO_2 emissions through interpolation, discerning the operating point on the engine fuel/ CO_2 map. However, for hybrid

or electric architecture, additional considerations regarding powertrain operation are necessary. Knowing the mechanical power demand of the traction electric motor, one must calculate the electrical power required for its correct supply, tracing back through the DC-link to the energy sources. Now, the total electric power required is processed by the vehicle supervisory controller. Here, the specific energy management algorithm plays a crucial role in the model, exerting influence on the final energy consumption outcome.

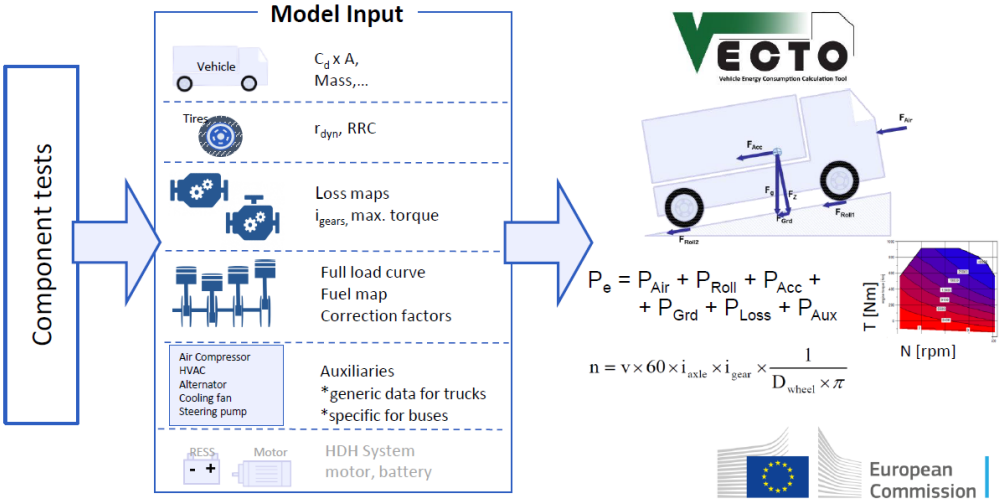

Figure 5.4: Schematisation of the VECTO simulation approach.

In cooperation with vehicle manufacturers, a set of operational cycles has been developed to reflect the different real-world uses of vehicles in Europe. These are known as “mission profiles”, each outlining a relevant and representative driving scenario, referred to as a “driving cycle” and articulated in terms of target speed and road gradient over the driving distance, together with a specific load condition. The driving cycles available in VECTO and suitable for representing the potential operating conditions of heavy long-haul transport vehicles include the following [38], also shown in Figure 5.5:

1. The "Long Haul" (LH) cycle depicts a transport scenario covering extended distances, primarily comprising highway driving. Characterized by an average speed of 80 km/h and a minimal share of stop time, this cycle stands out for its low transience, featuring the least amount of acceleration time.
2. The “Regional Delivery” (RD) cycle is representative of extra-urban driving conditions, with portions of urban and highway driving. The cycle is highly dynamic due to the many accelerations and decelerations and has an average speed of about 60 km/h.
3. The “Urban Delivery” cycle represents an urban route characterized by a low average speed, increased number of stop events, and stop time share. It is generally applied to the simulation of light rigid trucks (up to Group 4), which mainly operate in urban contexts, but may sometimes perform long-range missions.

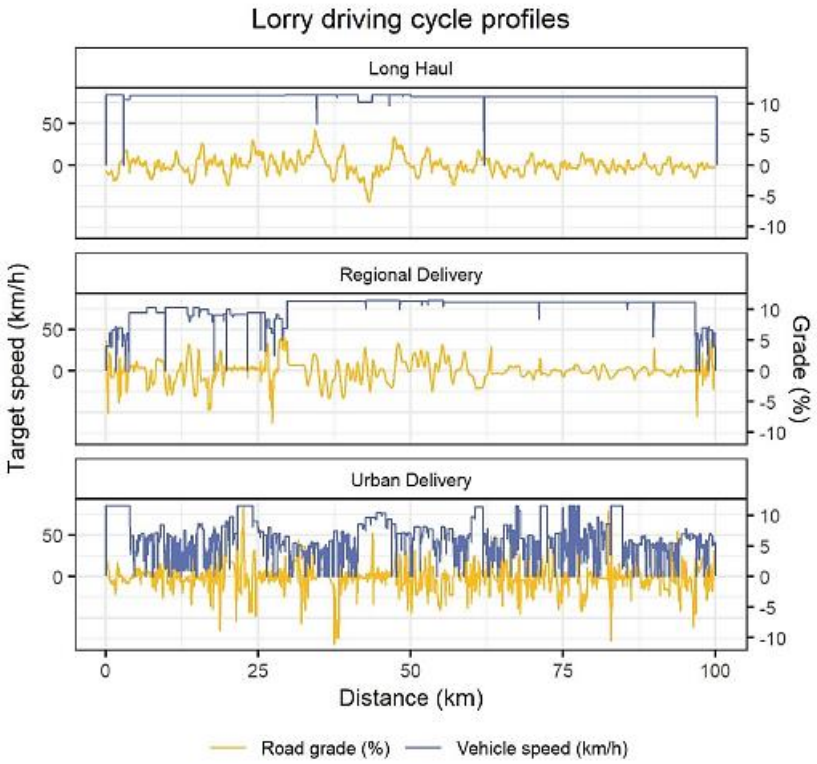

Figure 5.5: VECTO driving cycles.

The tool provides two simulation modes: Declaration and Engineering mode. In the Declaration mode a vehicle configuration is selected, and consequently, the software automatically sets a number of predefined vehicle parameters in accordance with the technical specifications outlined by European legislation. It also applies a series of predefined driving profiles that include fixed parameters such as the driving cycle and payload. This mode facilitates the declaration of a vehicle by OEMs for official certification purposes. Conversely, in Engineering mode, users have the flexibility to adjust all parameters, allowing for experimentation and validation of their vehicle models.

In both scenarios, initiating a simulation requires the loading of a "Job File" into the main form, the graphical interface that becomes accessible upon launching the VECTO software, as reported in Figure 5.6.

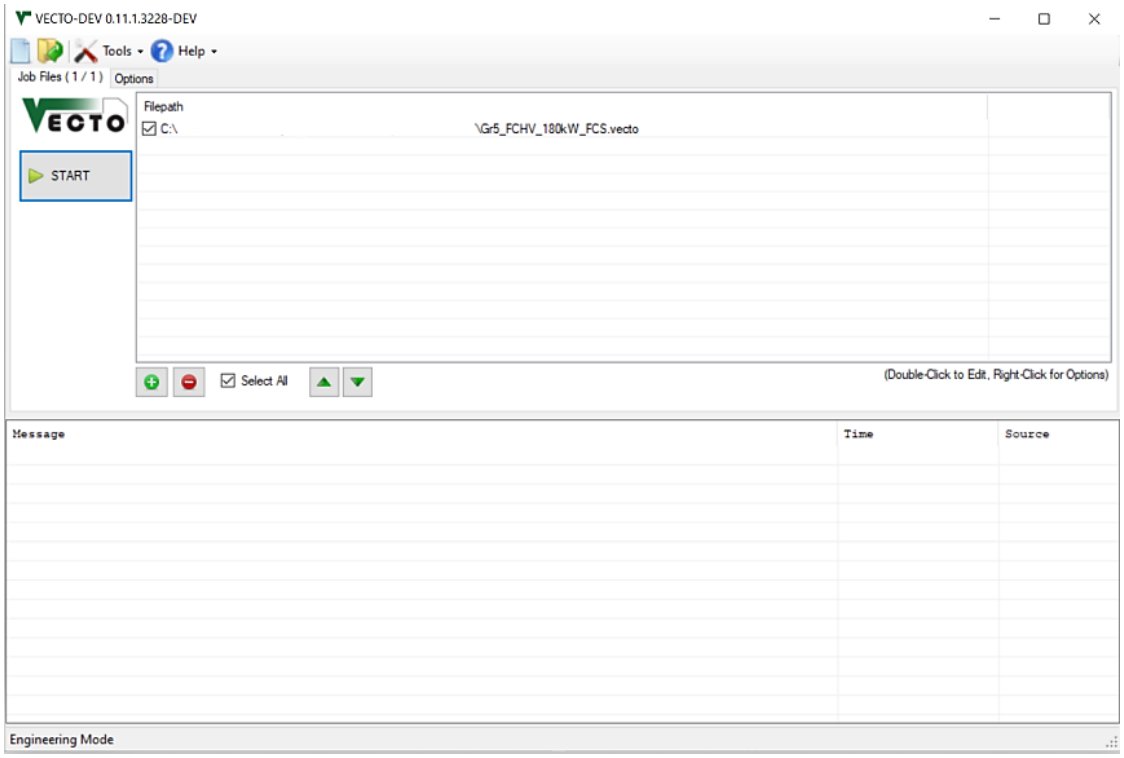

Figure 5.6: VECTO graphical interface.

The Job File (.vecto), whose graphical interface is shown in Figure 5.7, encompasses all the necessary information for executing a VECTO calculation. It outlines the vehicle specifications and the driving cycles that will be simulated. In summary, it includes [39]:

- File-path to the Vehicle File defining not-engine/gearbox-related vehicle parameters.
- File-path to the Engine File, which includes the full load curve and the fuel consumption map. This window is disabled if there is no ICE in the vehicle architecture.
- File-path to the Gearbox File specifying gear ratios and transmission losses.
- File-path to the Gearshift Parameters File allowing the override of parameters within the gearshift strategy.
- File-path to the Hybrid Strategy Parameters File, which defines all parameters employed by the Parallel/Serial hybrid control strategy to optimize torque distribution between the electric motor and combustion engine. This window is enabled only for conventional hybrid vehicles.
- Auxiliaries power consumption.
- Advanced Driver Assistance Systems (ADAS) parameters.
- Parameters for the driver model.
- Driving Cycles.

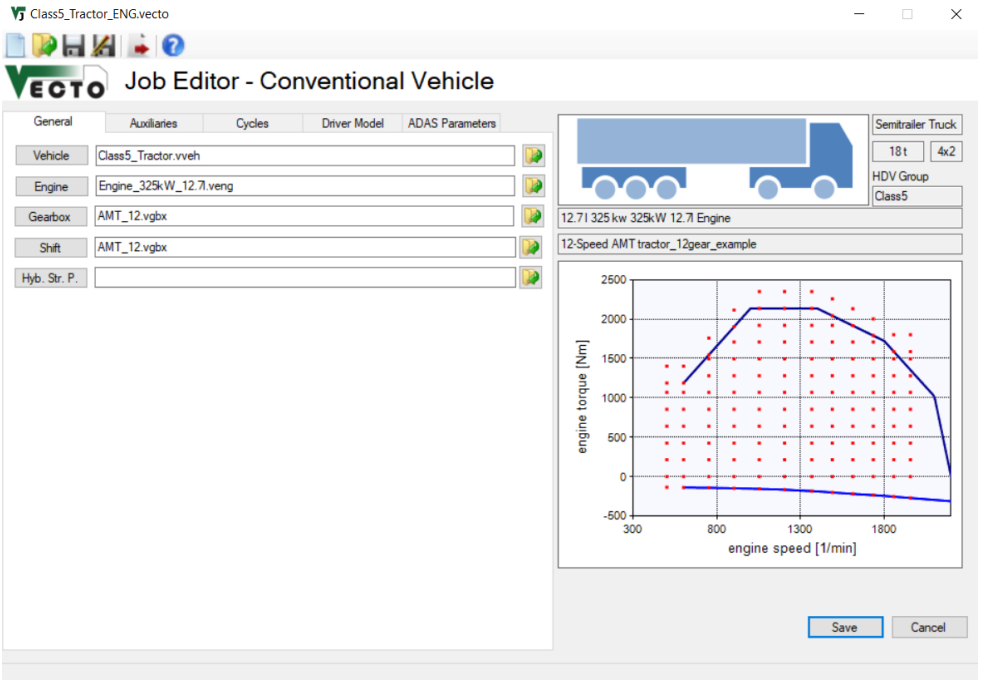

Figure 5.7: VECTO Job File example.

5.2.2 Model Input

For VECTO to effectively solve the vehicle longitudinal dynamics and perform its comprehensive energy analysis, it is necessary to reproduce the entire powertrain and chassis configuration of the subject vehicle. For this purpose, a large amount of input data must be provided, presenting either tabulated in the form of maps (e.g. engine fuel maps, transmission torque loss maps) or scalar values (e.g. rolling resistance, vehicle curb mass). The detailed procedures for measuring and declaring these VECTO inputs are described in the technical annexes of Regulation (EU) 2017/2400. Outlined below is a concise overview of the essential inputs required for VECTO, specifically in the context of an FC-powered electric powertrain. Other parameters are used in the simulation, but they are present in separate fields from the categories that will be mentioned. Most of these latter inputs could retain the software's default values, as they are validated data representative of the average driving conditions in Europe, such as the saturation curve of the vehicle's maximum acceleration.

Vehicle File (.vveh)

A vehicle file is created by compiling up to 8 tabs, depending on powertrain architecture and simulation mode, to customize all parameters associated with the vehicle. The most relevant ones are presented below.

- General Tab

This tab, shown in Figure 5.8, defines the main vehicle and chassis parameters, encompassing axles configuration and RRC values, air resistance, masses and payload, and dynamic tyre radius.

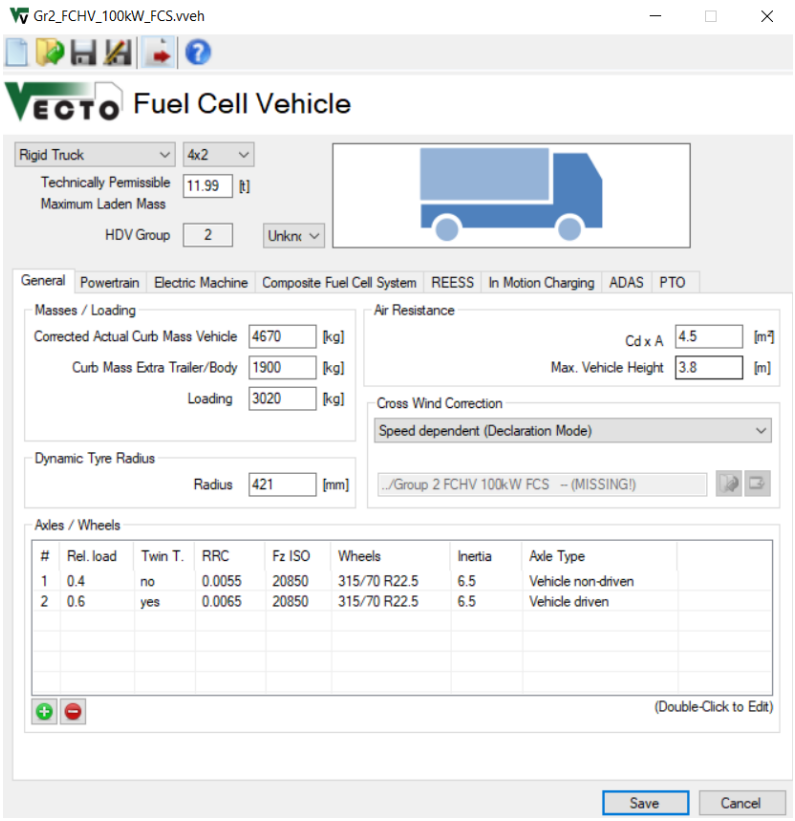

Figure 5.8: Vehicle File - General Tab.

The mass input consists of three values: curb weight, extra curb weight, and payload. The curb weight pertains to the mass of the chassis and cabin, while the extra curb weight corresponds to the mass of the truck body and/or the trailer. Payload specifies the load for both the vehicle and, if available, the trailer. Regarding the aerodynamic characteristics, the input is set as the product between the drag coefficient and the vehicle's frontal area (C_dA), since the regulation provides an experimental procedure for its direct estimation through constant vehicle speed tests. Additionally, VECTO offers the possibility also to consider the influence of crosswind for air resistance calculation: in Declaration mode, a generic crosswind correction, which assumes that a certain average wind speed happens uniformly distributed from all directions, is applied by default [37]. Rolling resistance, representing energy losses due to tire deformation from road contact, is expressed by the rolling resistance coefficient (RRC). For each axle, parameters like relative axle load, tyre RRC_{ISO} and F_{zISO} values must be provided to calculate the total rolling resistance coefficient, representative of the vehicle-loading-tyres combination efficiency and evaluable by the following equation [39]:

$$RRC = \sum_{i=1}^{N} s_i * RRC_{ISO,i} * \left(\frac{s_i * m * g}{w_i * F_{zISO,i}}\right)^{-0.1}$$

(Eq. 5.1)

where:

- RRC is the total rolling resistance coefficient used for longitudinal dynamics calculations.
- s_i is the weight share for axle i, suggested by VECTO annex according to vehicle type and driving cycle.
- $RRC_{ISO,i}$ is the tyre RRC determined with a standardized test.
- w_i is the number of tyres on the axle.
- $F_{zISO,i}$ is the tyre test load used to determine the RRC_{ISO} (or the 85% of its maximum load capacity).
- m is the total vehicle mass.
- $g = 9.80665\ m/s^2$ is the gravitational constant.
- N is the total number of axles, considering both the tractor and any trailer.

Completing the axle configuration involves specifying whether it is a drive axle, the presence of twin wheels, wheel inertia values, and the adopted tyre marking.

- Electric Machine Tab

The "Electric Machine" tab (Figure 5.9) is specifically designed for all electric components employed in propelling the vehicle, particularly in the context of hybrid electric and pure electric vehicles.

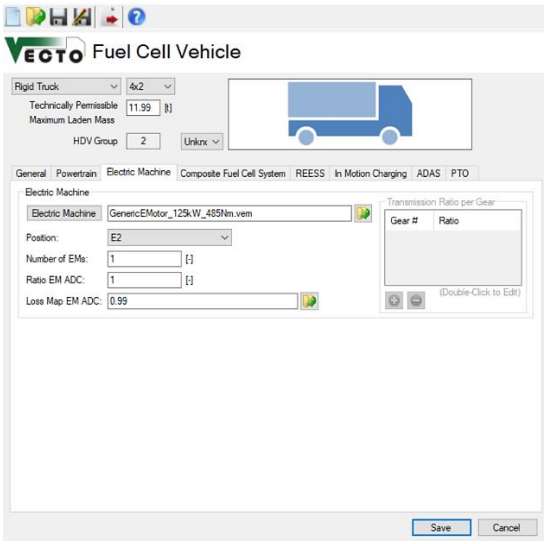

Figure 5.9: Vehicle File – Electric Motor Tab.

The position where the electric machine is allocated in the powertrain is customizable. It may be connected to the powertrain via a fixed gear ratio, with the option to set this ratio alongside the transmission step loss map. Utilizing the Electric Motor Editor, as reported in Figure 5.10, facilitates the creation of the electric motor model. This involves specifying the type of EM, key parameters, and maps, such as the motor's maximum drive and recuperation torque, the drag torque as well as the electric power consumption map. The latter map consists of a grid of operating points within a Cartesian system of motor speed and torque in which each point is associated with an electrical power consumption value. Consequently, the efficiency indication is provided indirectly, and for a particular motor operating point, it is computed through linear interpolation. These maps can be viewed from the graph area on the right, as soon as they are loaded into the software.

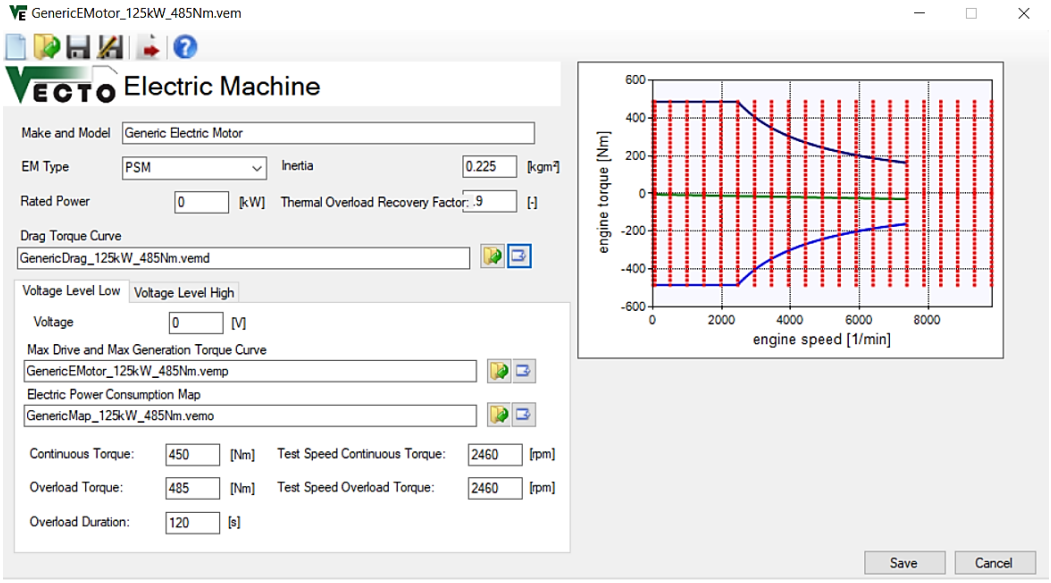

Figure 5.10: Electric Motor Editor.

- Composite Fuel Cell System Tab

For fuel cell hybrid vehicles, the input element on the “Composite Fuel Cell System Tab” is enabled (Figure 5.11). Here, users can load or create the FCS file and specify the configuration in which multiple systems are arranged. VECTO allows the creation of a Composite-FCS (CFCS) comprising a maximum of two strings connected in parallel, each with a maximum of three systems connected in series.

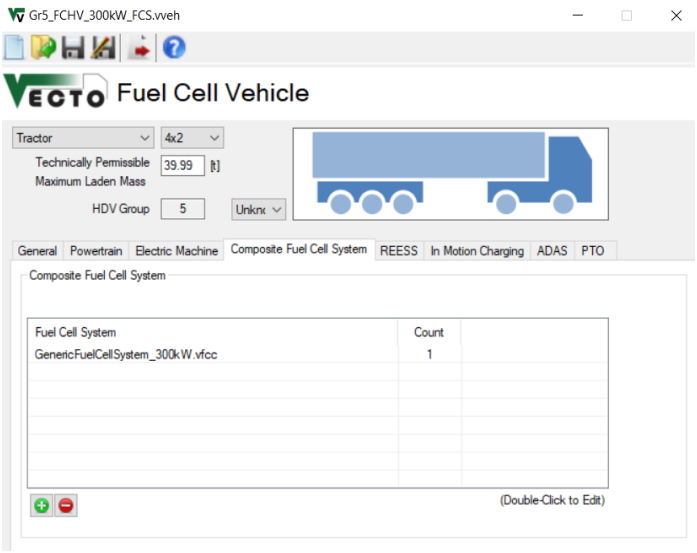

Figure 5.11: Vehicle File – Composite Fuel Cell System Tab.

Figure 5.12 shows the graphical interface of the fuel cell system editor. For its modelling, the essential inputs include the hydrogen consumption map as a function of the power delivered by the system, and the minimum/maximum power that it can provide. The use of this map, extracted through a specific experimental procedure defined by the Regulation (EU) 2017/2400 and detailed below, allows a quick and straightforward calculation of hydrogen consumption, including the comprehensive impact of system losses and the operating conditions of the stack.

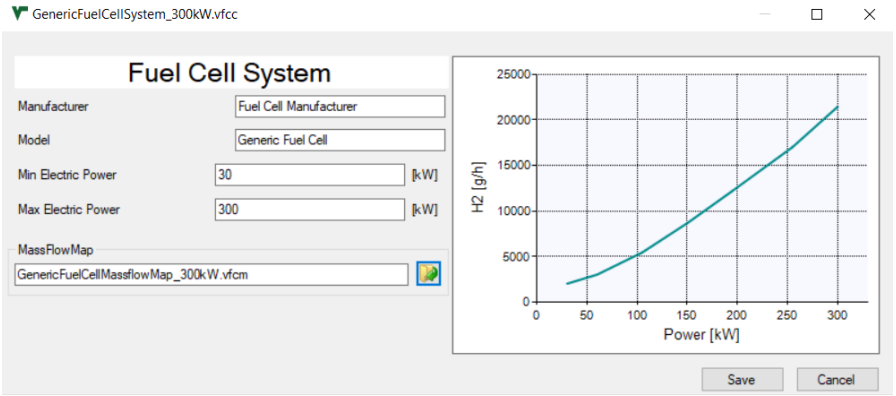

Figure 5.12: Fuel Cell System Editor.

- REESS Tab

The "REESS Tab", enabled for hybrid vehicles and pure electric vehicles, covers all inputs related to the rechargeable electric energy storage system. Within the REESS Dialog, depicted in Figure 5.13, modifications can be made to the battery file and its integration with the electric system. Notably, multiple battery packs can be configured, either in series or in parallel, and the initial state of charge for the entire system can be defined.

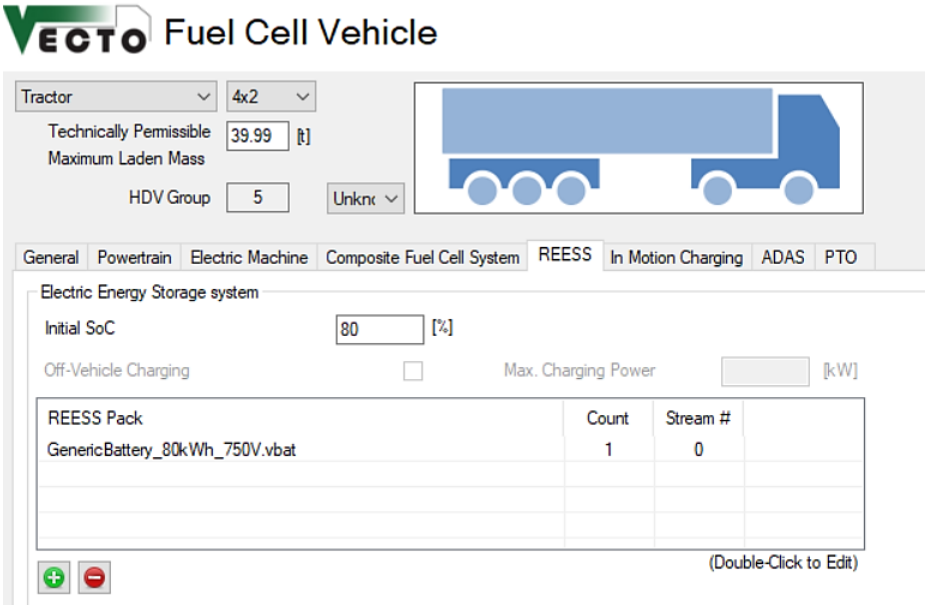

Figure 5.13: Vehicle File – REESS Tab.

The resistive battery model relies on specific parameters and curves, illustrated in Figure 5.14:

- Capacity of the battery pack, evaluated at 50% SOC.
- Minimum and maximum state of charge.
- Maximum current for charging and discharging curve over the state of charge.
- Battery pack open-circuit voltage curve.
- Internal resistance profile.

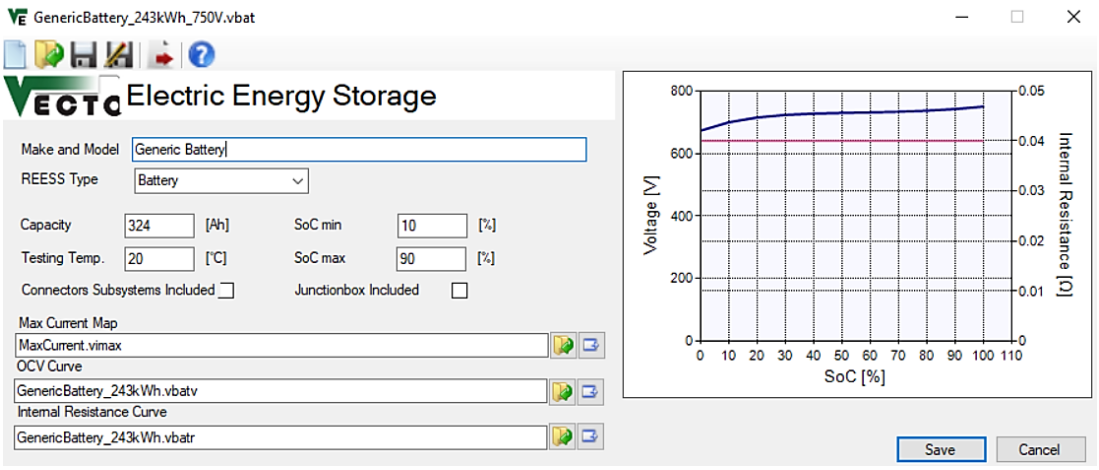

Figure 5.14: REESS Editor.

Gearbox File (.vgbx)

The Gearbox File serves to define all parameters related to the gearbox (Figure 5.15), encompassing gear and axle ratios, as well as transmission loss maps. The choice of gearbox

type depends on the vehicle type and can be selected from a drop-down menu. Options include manual transmission, automated manual transmission, and automatic transmission with various configurations tailored for pure electric vehicles. For each combination of vehicle and transmission type, VECTO incorporates a default gearshift strategy. However, in Engineering mode users have the flexibility to customize certain parameters, such as the gearshift lines, to align with specific preferences and requirements.

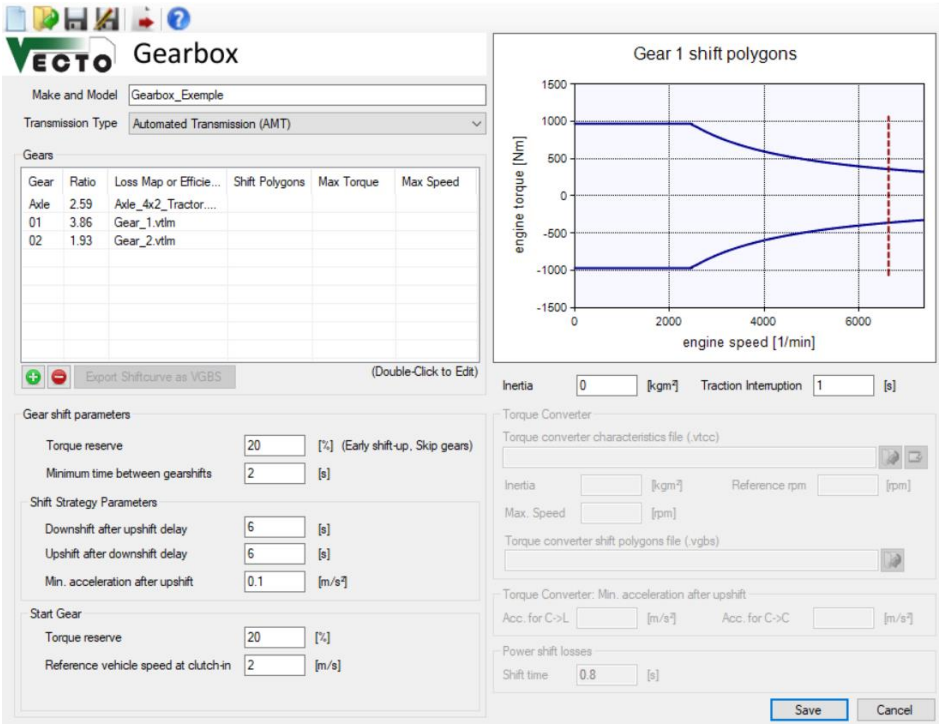

Figure 5.15: Gearbox and gearshift Tab.

Auxiliaries Tab

The Auxiliaries Tab, shown in Figure 5.16, is used to configure the vehicle's auxiliary systems. They are defined as components that are not part of the drivetrain and are associated with a non-negligible power demand. In Declaration Mode, a predefined set of auxiliaries and their power demands are established. Users need to choose the technology for each of them from a designated list, and the power consumption is automatically assigned based on the vehicle category and the selected driving cycle. The following technologies are considered, and no other auxiliary types can be added:

- Pneumatic system
- Engine cooling fan
- Steering pump
- Electric system
- Air Conditioning system (HVAC)
- Power take-off

In Engineering Mode, users have the flexibility to either specify the auxiliary power demand in the driving cycle over distance (or time) or set it as a constant overall load, without selecting predefined technologies. For an electric powertrain, they are all electrical, and the load contribution of the engine cooling fan and PTO is not considered. VECTO assumes that the power requirements for these auxiliaries remain constant throughout the entirety of the driving cycle. Their supply comes directly from the high-voltage DC-link necessitating the employment of a step-down converter to mediate and adjust the voltage to suitable levels for these components.

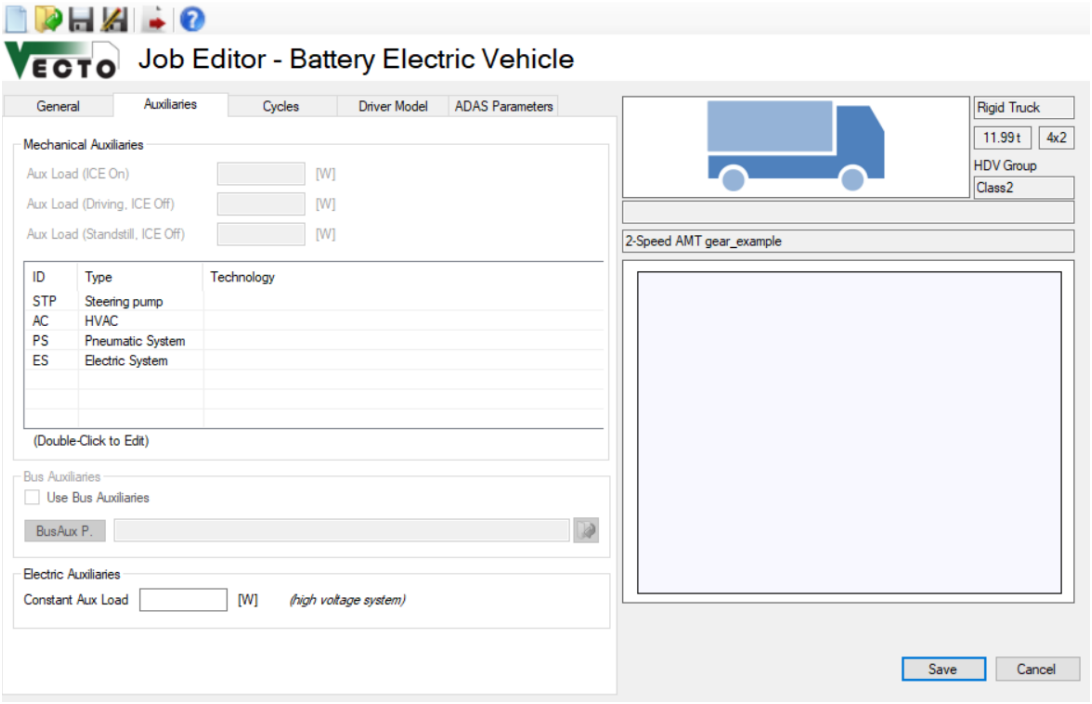

Figure 5.16: Auxiliaries Tab.

5.2.3 Model Output

In Declaration mode, VECTO generates two reports according to the technical annex for vehicle certification, containing a description of the simulated vehicle and the simulation results. Although they are of crucial importance for manufacturers, they are not particularly relevant for the purposes of this study, therefore the focus will be directed towards the additional output files that the software provides at the end of the simulation. In both modes, VECTO generates two .csv files.

The first file, referred to as the "summary file" (.vsum), encompasses information related to the total energy consumption of each powertrain component at the end of the mission profile. It also includes results for fuel consumption, CO_2 emissions, and other cycle-averaged metrics pertaining to vehicle operation and driving dynamics. This file consists of as many rows as

there are simulated driving cycle-payload combinations. The second file, known as the “modal file” (.vmod), contains second-by-second results produced during the simulation.
While the former helps to define the vehicle's energy balance and allows for swift assessments of the average performance of the vehicle and its components, the latter permits the continuous monitoring of specific components and vehicle performance throughout the entire duration of the driving mission. In addition, this detailed data is instrumental in creating graphical representations for in-depth analysis.

5.3 FCS certification procedure

The experimental procedure for the certification of fuel cell systems has recently been outlined in a technical annex [40], which will be integrated into Regulation (EU) 2017/2400 soon, compensating for an important gap in the legislation of new technologies. The primary objectives include validating the performance and capabilities declared by the manufacturer of the FCS and measuring hydrogen fuel consumption under well-defined operating conditions. This method ensures the generation of validated and reproducible data, essential qualities for obtaining reliable results in software outputs. Indeed, the certified map obtained at the end of the procedure will become the input for VECTO in modelling FC-HDVs.

The certification test procedure aims to record static data on a stabilized FCS at a specified number of operation points, with a minimum requirement of 12. Each operating point (OP) is defined by its target for the electrical FCS output power. These OPs need not be chosen to be equidistant but should facilitate good interpolation of the fuel consumption profile across the entire certification test range, specified by the manufacturer to cover the whole range of operations in real contexts. For instance, in regions with a non-linear relationship, a smaller step size between set-points is recommended, as illustrated by the example consumption curve in Figure 5.17.

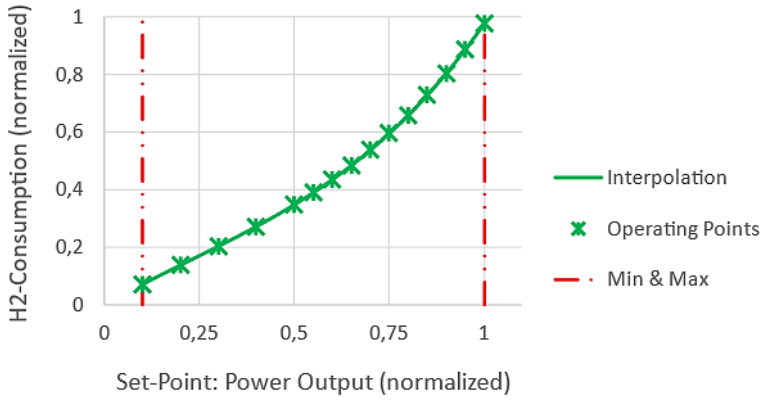

Figure 5.17: FCS consumption map example with test operating points.

Before the actual test at designated operating points, a conditioning phase is undertaken. The system operates for a minimum of 60 minutes at a conditioning set-point, ranging between 40%

and 60% of the maximum operating point, and defined by the manufacturer. Throughout certification, the FCS operates under standard conditions documented by the manufacturer, within a test lab meeting defined environmental standards and subject to continuous monitoring. Following this preliminary phase, the test begins. The series progresses from the minimum OP to the maximum power operation and then returns in descending order. The transition between set-points occurs with a moderate slope, typically specified by the manufacturer. Figure 5.18 schematically depicts the entire test sequence.

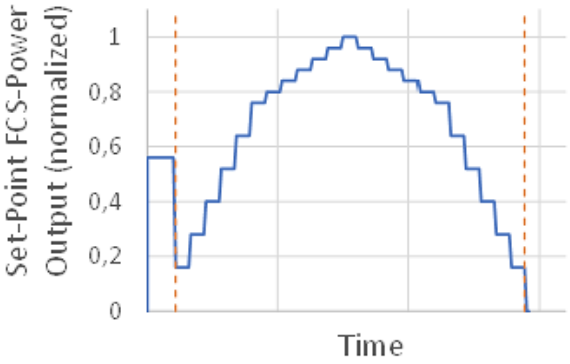

Figure 5.18: FCS test procedure outline.

For each operating point, the system is allowed to reach stable conditions before data processing commences, employing a "dwell" or "hold time". Variable dwell time or fixed dwell time approaches can be followed. In the former, a minimum hold time is defined, and to determine the system degree of steadiness two stability indicators are calculated in real-time through a moving time window. Stability is achieved if both indicators remain below a specific threshold value for a designated threshold period. Otherwise, a constant hold time is assumed, with stability assessed through the post-processing of recorded data. Opting for predefined dwell times extends the test duration, nevertheless, it is the preferred approach when prioritizing the reproducibility of test results. Once the FCS stabilizes at the operating point, the measured values of electric power and hydrogen flow rate are recorded. Data are sampled at a constant frequency of 10 Hz for a fixed duration. During this phase, the electrical power delivered by the FCS and the hydrogen flow rate required by the current OP are evaluated with the arithmetic mean of the recorded values, as follows:

$$P_{FCS,\,avg} = \frac{1}{n}\sum_{k=1}^{n} P_{FCS,\,k} \;\; [kW], \tag{Eq. 5.2}$$

$$\dot{m}_{\mathrm{H_2},avg} = \frac{1}{n}\sum_{k=1}^{n} \dot{m}_{H_2,k} \;\; [g/h], \tag{Eq. 5.3}$$

where:

- $P_{FCS,\,avg}$ and $\dot{m}_{\mathrm{H}_2,avg}$ are the arithmetic mean of the electrical power output and fuel flow metered.
- $P_{FCS,\,k}$ and $\dot{m}_{H_2,k}$ are the recorded value of electrical power output and fuel flow.
- n is the number of recorded values during the averaging period.

Finally, each operating point below the maximum is characterised with both values $P_{FCS,\,avg}$ and $\dot{m}_{\mathrm{H}_2,avg}$ calculated as the arithmetic mean of the averaged values from the ascending and descending part of the performance map measurement. At the conclusion of the procedure, a report is compiled, encompassing an Information Document, as mandated by regulations, input parameters for the simulation tool, recorder files, and documents pertinent to the conducted tests.

5.4 VECTO FCVs operation strategy

The following section outlines the control strategy implemented by VECTO when simulating a Fuel Cell-dominant hybrid vehicle, adhering to the guidelines provided in the VECTO User manual.

5.4.1 General approach overview

The operating strategy was designed to fulfil the requirements of maintaining the fuel cell system in a steady state as much as possible and close to its operating point of maximum efficiency, while ensuring the proper functioning of the battery to prevent its premature reduction in performance. Stationary operation for FCS is preferred to avoid efficiency losses associated with the FC operating in unfavourable areas of the map and to enhance the durability of the system. Indeed, frequent start-up/shutdown cycles, transient load variations, and extreme power operation can lead to various stack degradation phenomena, including carbon support corrosion and catalyst and electrolyte membrane degradation [41].

Fuel cell vehicles undergo a two-step simulation process:

1. Pre-simulation Run

The initial step aims to establish a reference electric power trend across the entire cycle. During this phase, the vehicle is simulated as a pure electric vehicle (PEV) in Charge Depleting mode. The battery system is modified to include the real vehicle battery and a second battery representing the fuel cell power, with a discharging power equal to the FCS maximum power and a charging power of 0 W, being it a one-way device. It is assumed that both batteries have infinite capacity to prevent SOC limits from being breached. This initial simulation yields the total electric power demand for vehicle propulsion throughout the driving cycle. After extensive post-processing of the results, this data is utilized to determine the actual fuel cell power demand.

2. Simulation of the Actual Fuel Cell Vehicle

In the second step, the real fuel cell vehicle is simulated using the power trace derived from the first step. This involves determining the power output of the FCS and battery along the entire cycle, thus as a function of the distance travelled.

The FCS power at a specific distance is determined by averaging the total reference electric power over a certain distance-based average window. To meet the general approach requirements, VECTO strives to use the largest possible window size without implying a violation of the battery SOC limits, specified in the REESS model, during the entire cycle. Indeed, the selected window width is primarily influenced by the battery size (capacity), with smaller batteries resulting in less steady FCS functioning. A challenge lies in optimizing this window size to ensure accurate simulation results while respecting the constraints imposed by the battery's characteristics. The methodology employed for this purpose is presented in the following subsection. The differences between the instantaneous reference electric power demand and the FCS power are covered by the battery, which functions as an energy buffer. In scenarios where the power demand for propulsion exceeds the output from the FCS, the battery discharges. Conversely, if the fuel cell system supplies more power than is needed for traction, the excess power is used to charge the battery.

During the mission, VECTO keeps track of the current SOC. The simulation tool calculates the initial State of Charge, adapting it to the mission's particulars to optimize the utilization of the battery as a buffer, without exceeding the limits, and achieve the Charge Sustaining mode operation.

Internal battery losses and other phenomena, such as FCS power limitations and variable auxiliary power, result in a disparity between the State of Charge value at the cycle's beginning and its value at the end. A correction is necessary to achieve an effective Charge Sustaining balance and to estimate the proper fuel consumption. This is addressed in a post-processing phase:

- If the final SOC is smaller than the initial SOC ($\Delta E_{REESS} < 0$), additional H_2 consumption is taken into consideration.
- If the final SOC is greater than the initial SOC ($\Delta E_{REESS} > 0$), a subtraction of hydrogen must be made from the overall fuel consumption.

The hydrogen mass required for ΔSOC correction is calculated using the following equation:

$$\Delta m_{H_2,corr}\,[g] = k_{FCS,line}\left[\frac{g}{kWh}\right] * \Delta E_{REESS}\,[kWh].$$

(Eq. 5.4)

Here, $k_{FCS,line}$ represents the gradient of the linear regression line derived from actual FCS operating points ($\dot{m}_{H2}(P_{FCS})$) throughout the driving cycle, and ΔE_{REESS} is the difference in energy stored in the REESS between start and end of the simulation run.

5.4.2 Average window algorithm

The power that FCS must provide at a certain distance s is calculated for a window size s_w, symmetrically centred around s and using the electric power demand $P_{el}(s)$ determined in the pre-simulation. The maximum window size is limited to the cycle length s_{cycle}. At the beginning and at the end of the cycle the window expands over the actual cycle, therefore for continuity of calculation, the $P_{el}(s)$ trend is also shifted on the left (at the beginning) and the right (at the end) of the actual cycle by s_{cycle} (Figure 5.19).

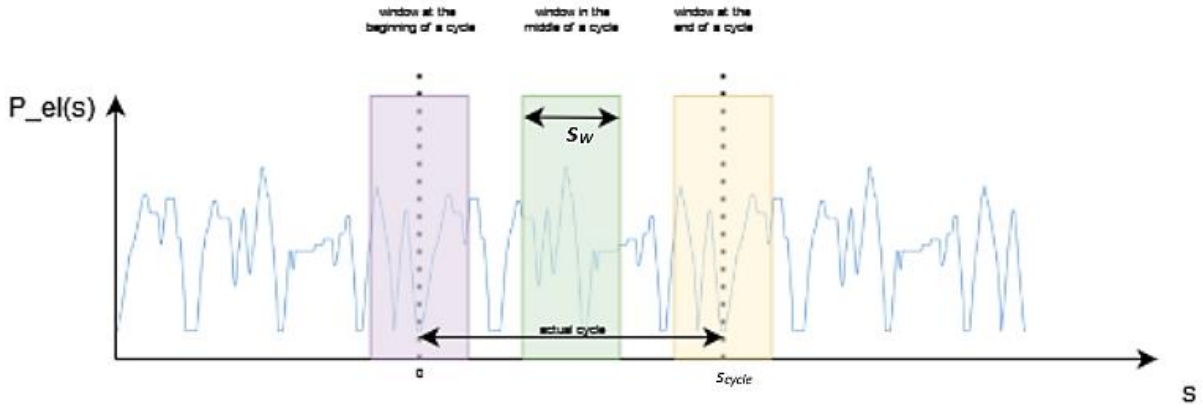

Figure 5.19: Composition of the reference electric power trend before averaging.

For a given window size s_w and power trend $P_{el}(s)$, the FC power at distance s is the average $P_{el}(s)$ within the window, as schematized in Figure 5.20:

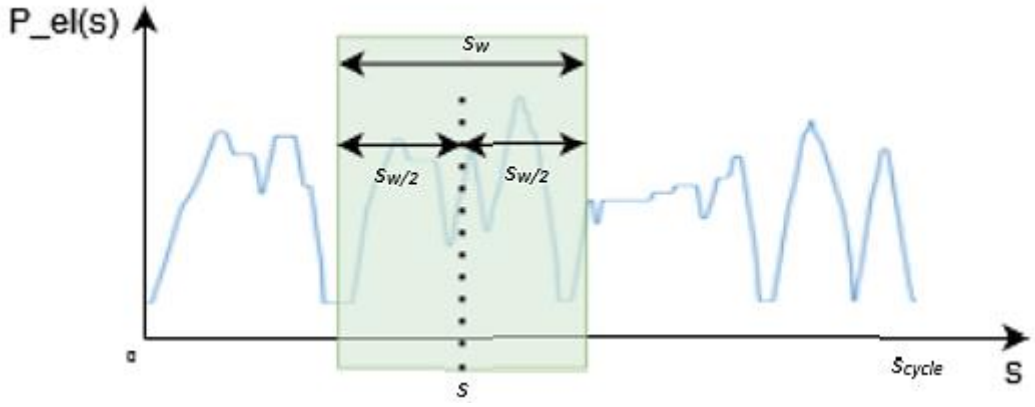

Figure 5.20: Reference power averaging at distance s for a given window size s_w.

The determination of the window size s_w follows the algorithm outlined in Figure 5.21. The process initiates with the largest possible size of s_{cycle}.

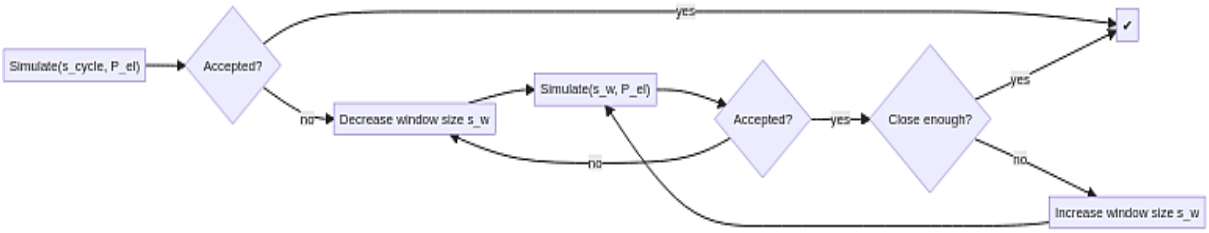

Figure 5.21: Algorithm for determining averaging window size.

The “condition of acceptance” is connected to the SOC limits violation. If the initially selected window size results in the calculation of a battery output power that leads to the violation of SOC limits, it is reduced. The algorithm iteratively checks compliance with constraints, employing a "rolling average" approach until an acceptable size is identified. If, at any point, the window size becomes smaller than 5 m, the simulation of the FCHV is aborted. This termination indicates that the battery capacity is insufficient for the task, and SOC limits are constantly being violated.

5.4.3 Power distribution algorithm for Composite-FCS

In the case of multiple FCS, the previously outlined power trace for a single FCS pertains to the overall power that the Composite-FCS must supply. When employing parallel strings (up to two), the total power is efficiently distributed among them through a calculation algorithm implemented by VECTO, as detailed below. Instead, within a string, power is always equally distributed between the switched-on FCSs.

For each $P_{CFCS}(s)$ value at a given distance s in the driving cycle, coefficients “a” (Share of FCS string 1) and “b” (Share of FCS string 2) are assessed. These parameters, complementary and ranging from 0 to 1, indicate the percentage of total power delivered by the respective strings. Their determination is crucial to ensure optimal power allocation aimed at minimising fuel consumption. The total fuel consumption (FC_{tot}) minimisation algorithm is based on the Equation 5.5:

$$FC_{tot}(P_{CFCS}(s)) = FC_1(a * P_{CFCS}(s)) + FC_2(b * P_{CFCS}(s)).$$

(Eq. 5.5)

Here, FC_1 and FC_2 represent the hydrogen consumption of strings 1 and 2, respectively, as functions of their power output fractions. To find the optimal power distribution VECTO evaluates all feasible combinations of “a” and “b” based on the total power to be delivered by the CFCS at distance a s, selecting the coefficients that minimize total fuel consumption. Figure 5.22 illustrates an example of this calculation. In cases where the requested power for a string is below the optimal efficiency point of a single FCS, a virtual "time splitting" occurs. This entails operating the FCS at its best efficiency point for a fraction of the time corresponding to

the requested energy during the time step. For the remaining duration, the FCS is considered switched off [39].

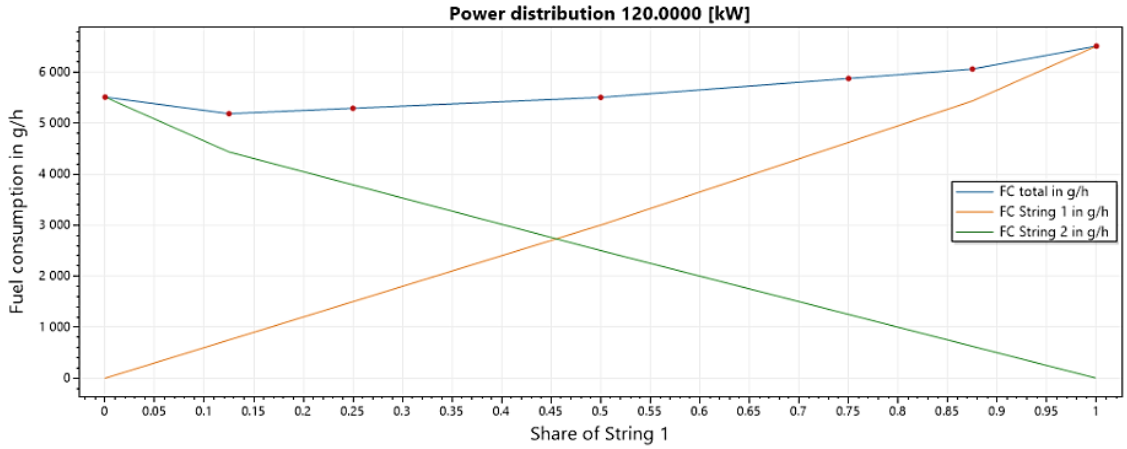

Figure 5.22: Example of optimal power allocation - Fuel consumption trends as a function of the share coefficient "a".

6. Generic HD vehicle model for long-haul applications

A VECTO fuel cell HDV model for long-haul freight transport applications has been created. This model serves as a "generic" representation, implying that it does not directly mirror any specific physical vehicle. However, each parameter or component is characterized and dimensioned to be representative and consistent with what real FC-HDVs employ for a comparable application. As VECTO was created as a certification tool for the performance of heavy vehicles placed on the European market, and intended for manufacturers, modelling a vehicle requires a substantial number of input data. Some of these are required in specific and less common forms, while others are difficult to acquire because they are neither declared by the manufacturers for confidentiality reasons nor described in other studies, which generally use a different modelling approach. Therefore, for model construction, it was decided not to conduct a market and literature analysis to identify representative average technical characteristics of available fuel cell vehicles but rather to find a literature study containing detailed information on a generic FC heavy vehicle already established and aligned with the goals of this work, in order to replicate it in VECTO. It was furthermore important that the vehicle model from this "reference study" was simulated under reproducible conditions, and that clear and useful results were reported for model validation purposes. In instances where the reference study did not provide all the necessary data required by the simulation tool, supplementary information was sought from scientific literature, generic VECTO models and regulatory directions. The ultimate aim of this activity was to develop a vehicle model that not only aligns with the specific case study at hand but also stands validated through comparisons with physical quantities that have been certified in the reference study. Subsequently, the fuel cell powertrain delineated in this context was isolated and employed as the basis for further analysis, which will be presented in the subsequent chapter.

For long-haul applications, vehicles are typically designed to cover distances of more than 100,000 km per year, with an average daily mileage of fewer than 500 km (Figure 6.1) [42].

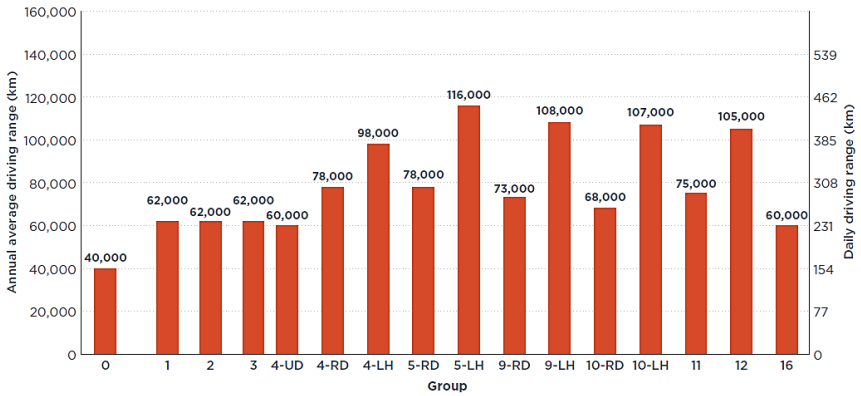

Figure 6.1: Average annual and daily driving range per HDV group.

Within the regulatory framework, several vehicle groups, including 4, 5, 9, 10, and 12, are capable of fulfilling these extensive travel demands. Therefore, before proceeding with the creation of the model, it was necessary to identify one of them as representative of this category. The choice fell on the most prevalent tractor-trailer configuration, characterized by a 4×2 axle setup and a maximum gross vehicle weight of 40 tonnes, categorizing it within group 5. As depicted in Figure 6.2 [43], illustrating the distribution of new conventional HDV registrations and associated CO_2 emissions in the European Union in 2016, this class of vehicle not only dominates sales but also contributes significantly to greenhouse gas emissions in the road freight transport sector. Although this data originates from a study conducted several years ago, subsequent research, such as [42] and [32], corroborates that the dominance of group 5 vehicles in long-haul applications has remained consistent, confirming the group 5 vehicle as the most suitable case study for long-haul applications.

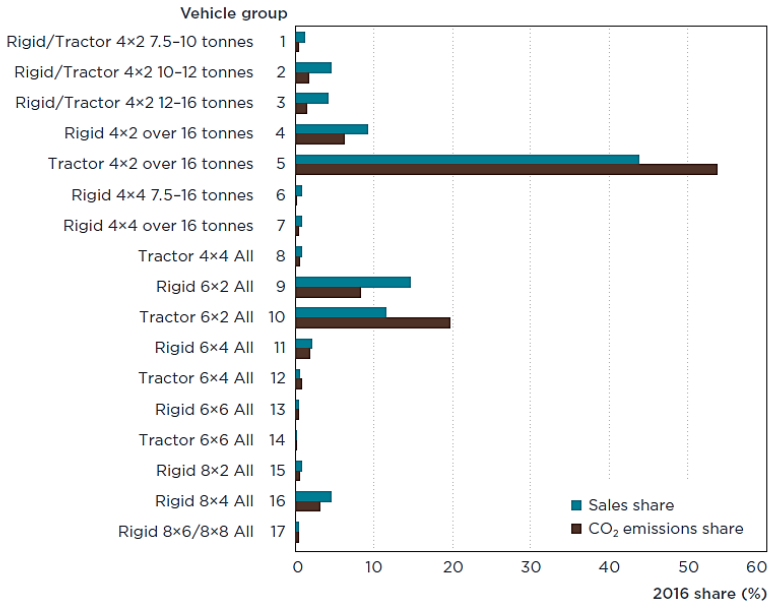

Figure 6.2: Distribution of HDV registration and CO_2 emissions in the EU in 2016.

6.1 VECTO model creation

The study “Fuel cell electric tractor-trailers: Technology overview and fuel economy” [6], published by the International Council on Clean Transportation (ICCT) in July 2022, was identified from the literature review and selected as a reference. This research aligns with the outlined requirements, focusing on the analysis of tractor-trailers, which are recognized as the most energy-intensive HDV segment in Europe. The paper extensively delves into the current state of FC technology within heavy-duty applications. However, its distinctive contribution lies in the presentation of a generic group 5 vehicle simulation conducted, using the commercial Simcenter Amesim software, to quantify its energy efficiency and fuel consumption within typical VECTO usage profiles. The employed software operates in a similar way to VECTO,

simulating the longitudinal dynamics of the vehicle and the operational behaviour of the different subsystems, including the fuel cell unit, battery, electric motor, and gearbox. Noteworthy differences exist, however, encompassing the power-split control algorithm, driver model, and the modelling of aerodynamic and rolling resistance [17]. In the ICCT's model, the power distribution between the battery and the fuel cell is determined by a Rule-Based control strategy. This strategy utilizes the battery state of charge and the electric motor power demand as state variables, while also ensuring that the REESS operates in Change Sustaining mode throughout the driving cycle. The generic vehicle parameters and component characteristics of the ICCT's FC-HDV model were meticulously curated by reviewing existing literature for established information and recent developments. Consultations with experts in the field further contributed to refining this dataset.

Table 6.1 compiles the principal characteristics of the vehicle and its subsystems as defined in the ICCT model. These parameters served as the foundation for generating the necessary VECTO inputs for model development. The subsequent subsections will provide a comprehensive overview of how they were integrated into the software.

Table 6.1: Main physical characteristics of the subsystems within the ICCT vehicle model.

Subsystem	Parameter	Value
Vehicle	Tractor mass [kg]	7665
	Trailer mass [kg]	7400
	RRC [-]	0.005
	C_d [-]	0.5
Electric Machine (PMS-EM)	Max. cont. power [kW]	350
	Max. cont. torque [Nm]	4000
	Max. speed [rpm]	2500
Battery (NMC Li-Ion)	Nominal energy [kWh]	72
	Nominal voltage [V]	660
	Nominal capacity [Ah]	109
Fuel Cell System (PEM)	Maximum power [kW]	180
	Maximum efficiency [-]	0.6
Transmission (AT)	1^{st} gear ratio [-]	5
	2^{nd} gear ratio [-]	1.02

	Gearbox efficiency [-]	0.985
	Axle gear ratio [-]	2
	Axle efficiency [-]	0.97

Vehicle General Tab

The "Vehicle category" specifications from Table 6.1 were directly incorporated into the VECTO model as the "Corrected actual curb mass vehicle", "Curb mass extra trailer/body" and "RRC_{ISO}" parameters, respectively. In pursuit of the ICCT study's aim to scrutinize the performance of an FC articulated truck under conditions mirroring those of VECTO, the aerodynamic resistance simulation mode from the European tool was replicated in Simcenter Amesim considering the influence of crosswind in the calculations. As a result, crosswind correction was enabled in the VECTO model. Concerning the Axles/Wheels board configuration, the tractor tyre marking outlined in [43] was adopted. Conversely, the standard marking specified by European regulations was applied to the trailer tyres. The corresponding Fz_{ISO} value was determined based on the wheel load index and the tyre manufacturers' datasheets. Defined wheel dimensions, VECTO provides wheel inertia standard values and for the drive wheel also the dynamic rolling radius parameter. Finally, the relative axle loads were sourced from official annexes of the simulation tool, depending on the driving cycle and vehicle group. Figure 6.3 reports the "General Tab" in the VECTO Vehicle File, containing the aforementioned inputs.

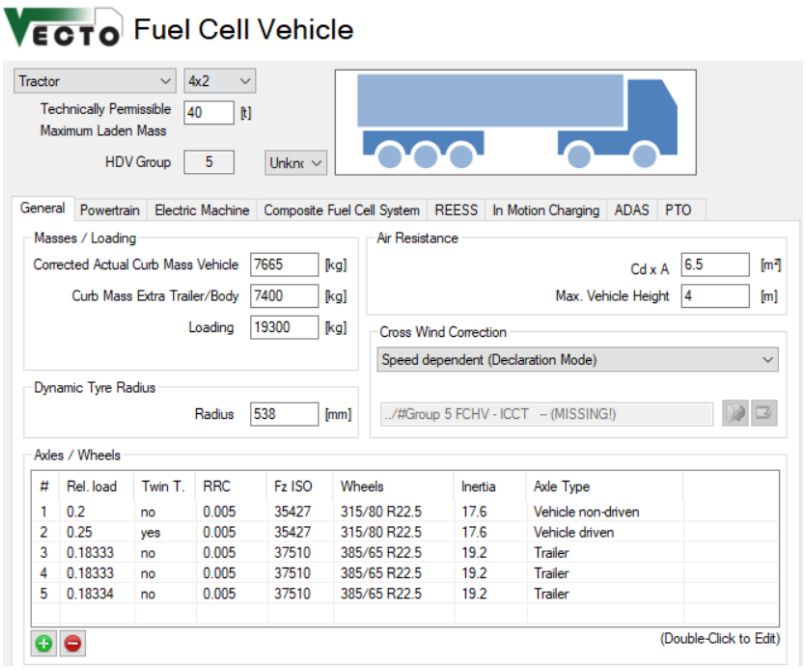

Figure 6.3: Vehicle General Tab.

Electric machine Tab

To initiate the modelling of the electric motor, the generic PMS-EM model available in VECTO served as the foundation. Modifications were made based on the information provided in the reference study, while generic default values were retained for unspecified inputs. In alignment with the conventions of the generic EM model, it was assumed that the electric motor was positioned upstream of the transmission, a configuration denoted as the "E2" position, and characterized by a direct connection, as illustrated in Figure 6.4.

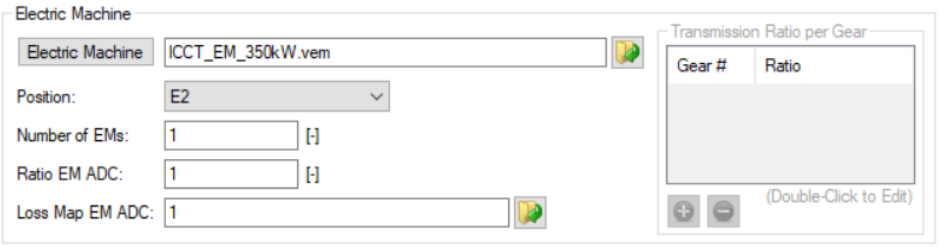

Figure 6.4: Electric Machine Tab.

Regarding the EM maps:

- The drag torque curve was established by rescaling the generic electric motor's drag curve to align with the specific motor characteristics employed in the system.
- The maximum drive/generation torque curve was manually derived based on the motor characteristics detailed in Table 6.1.
- The EM consumption map was developed using a generic template available in the official VECTO annex. The methodology followed the approach outlined in Regulation 2017/2400, which involves denormalizing a standardized grid of operating points based on specific EM characteristics, such as power and rated speed.

Figure 6.5 comprehensively illustrates all the parameters and characteristic maps of the adopted electric motor.

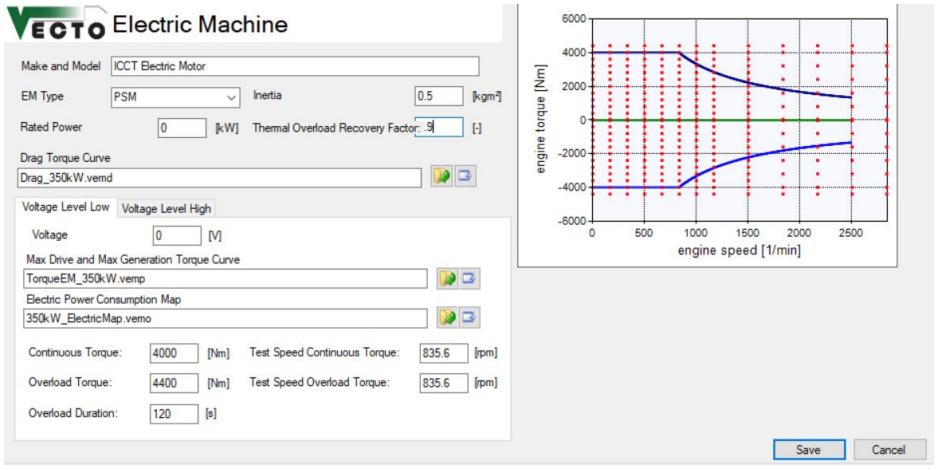

Figure 6.5: Electric Motor model input data.

Fuel cell system Tab

In the reference study, the PEM-FC system is modelled employing a generic FCS efficiency curve, reported in Figure 6.6. This curve is represented as a function of the load, which is normalized against the system's peak power capability. It is important to note that this efficiency curve was not obtained through empirical testing but rather was constructed to mirror actual performance trends. A peak efficiency of 60% was assumed for the FCS, a figure considered to be within the realm of feasibility for contemporary fuel cell technology as cited by [44].

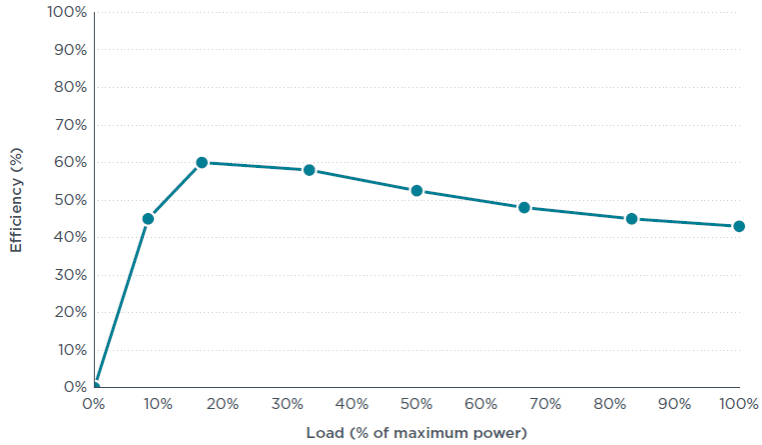

Figure 6.6: General FCS efficiency curve.

To adapt this model for use in VECTO, the curve was denormalised to reflect a maximum power output of 180 kW. Further, by applying the definition of FCS efficiency (Eq. 2.5) to selected sampled points, the hydrogen flux curve over the system's power output was derived, resulting in Figure 6.7. For this calculation, a hydrogen lower calorific value of $H_i = 119.96\ MJ/kg$ [44] was assumed.

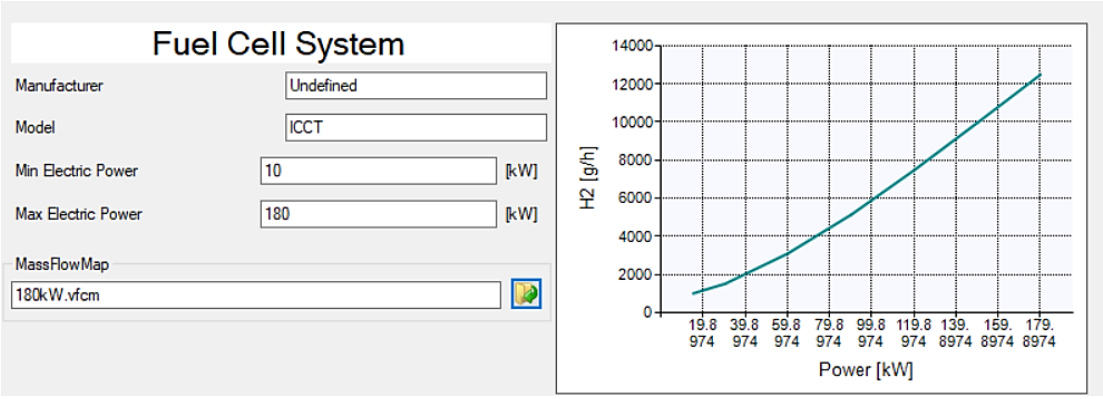

Figure 6.7: Fuel cell system Tab.

REESS Tab

For the battery model inputs, a VECTO generic battery of 80 kWh served as the initial reference. Given the absence of information from the reference paper and the relatively limited impact of these parameters on overall vehicle performance, the decision was made to keep the generic curves for internal resistance and maximum charge/discharge current unchanged. However, in consideration of the battery characteristics outlined in Table 6.1, the SOC-dependent open circuit voltage trend was rescaled to accurately reflect the specific battery attributes (660 V nominal voltage at 50% SOC). Figure 6.8 depicts the adopted battery configuration.

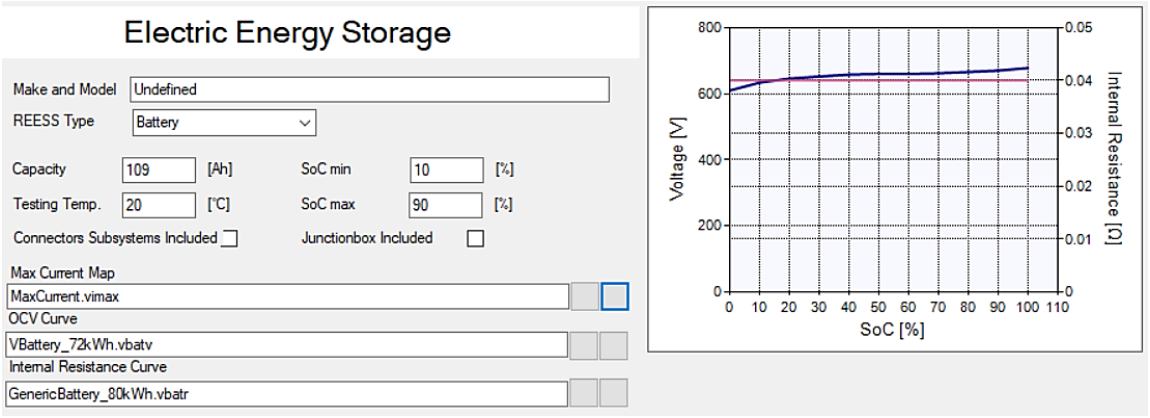

Figure 6.8: Battery model input data.

Gearbox Tab

The inputs for the gearbox model were straightforwardly defined, as illustrated in Figure 6.9. Aligning with market and literature analysis, an automatic gearbox was selected. Consequently, the transmission and axle ratios, along with the efficiency values, were specified. It was assumed that each gear maintains a constant efficiency, equal to the average gearbox efficiency value provided in Table 6.1. In terms of the gearshift strategy, the default strategy implemented by VECTO for the chosen gearbox type was adopted, and none of the associated parameters were altered.

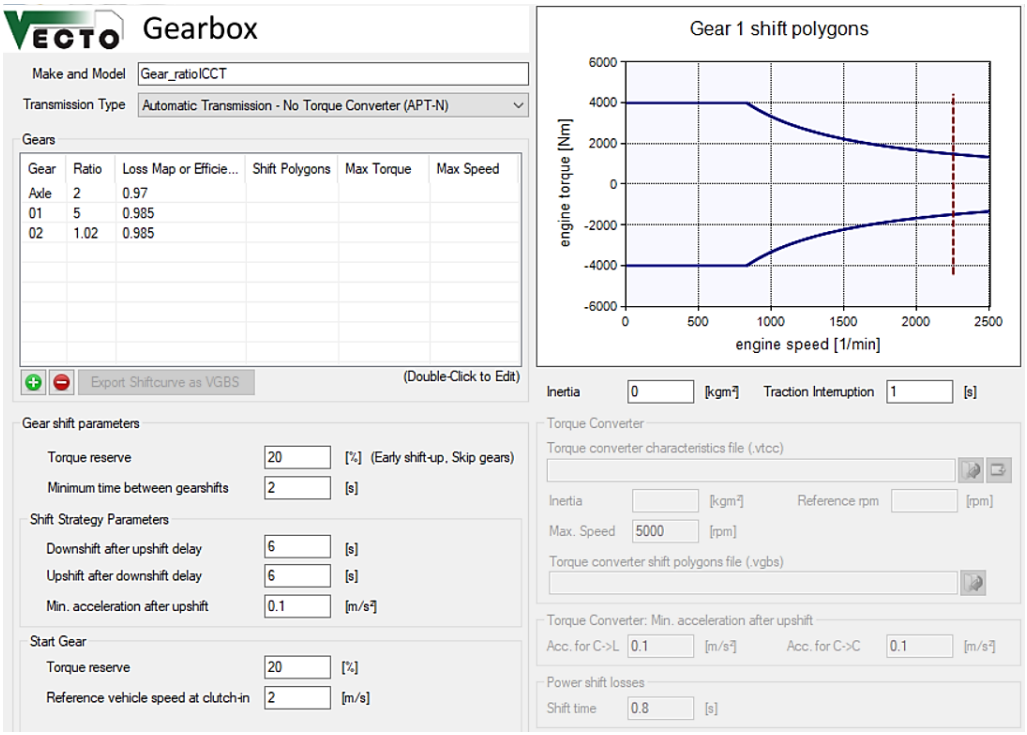

Figure 6.9: Gearbox and gearshift input data.

Auxiliaries

Concerning the vehicle's auxiliary systems, the reference study assesses electrical power consumption arising from the thermal management model of the battery and the driver's cabin. However, this approach is not congruent with modelling in VECTO. Consequently, a decision was made to compute the total electrical load of the auxiliaries by emulating the approach employed by the software in Declaration Mode. For each considered auxiliary, standard electrical consumption was identified based on the technology adopted, the vehicle group, and the driving cycle, using official annexes. The specific values are outlined in Table 6.2. In the VECTO Auxiliaries Dialogue, only the total electrical load is specified, maintaining a constant value throughout the driving cycle. The most widely used technology for each auxiliary in group 5 vehicles, as documented in [32], was assumed. Additionally, power consumptions were determined with the consideration that the vehicle will be simulated on “Long Haul” and “Regional Delivery” driving cycles.

Table 6.2: VECTO auxiliaries power consumption.

Auxiliary	Technology	Power consumption [W]
Electric system	Standard technology	1714.2857
Air Conditioning system (HVAC)	Default	350
Pneumatic system	Large Supply + elec. driven	1000
Steering pump	Full electric steering gear	12
Total electric Aux. load	-	3076.2857

Driver and ADAS Tab

Ultimately, the VECTO model was rounded out by defining parameters for the driver model and the vehicle's Advanced Driver Assistance Systems (ADAS). In both cases, the default values proposed by the software were retained, as depicted in Figure 6.10.

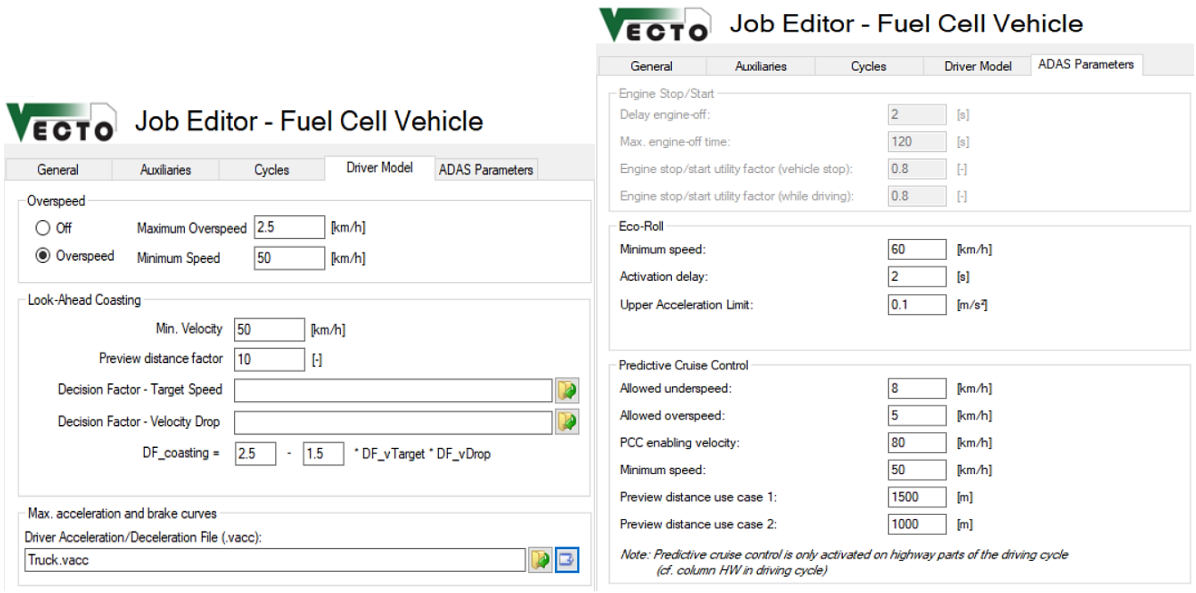

Figure 6.10: Driver model and ADAS parameters.

6.2 Vehicle model validation

The comprehensive vehicle model was simulated for the same mission profiles (driving cycle and payload) and environmental conditions as delineated in the ICCT study. For this purpose, the software was configured with an air density of 1.225 kg/m^3, corresponding to an ambient temperature of 15°C (as outlined in the study) and a pressure of 1 atm. The weight of the vehicle significantly influences the total energy required to complete a driving cycle, and thus its energy performance. Therefore, it is essential to consider different mission profiles to obtain a solid validation of the model. Various simulation cases were devised to analyse the effect of payload, thus assessing the overall hydrogen consumption for each of them. Then, these values were compared with those given in the reference paper to validate the vehicle model. Simulations were executed in Engineering Mode using VECTO version 0.11.1.3228, along the "Long Haul" and "Regional Delivery" driving cycles. In analogy to the reference study, the former was performed with a low, a reference (both defined by VECTO regulations), and a maximum payload. Conversely, the second driving cycle exclusively featured the reference payload (Table 6.3). The maximum payload depends on the remaining mass available, considering the maximum gross vehicle weight (MGVW) imposed by regulations, as well as the tractor and trailer masses. For a conventional group 5, the maximum vehicle mass is 40 tonnes. However, Regulation EU 2019/1242 permits an increase in this limit by a maximum of 2 tonnes to account for the higher powertrain weight of zero-emission vehicles. Consequently, an MGVW of 42 tonnes was assumed.

Table 6.3: Vehicle load conditions.

Driving cycle	Payload condition	Value [kg]
Long Haul	Low	2900
	Reference	19300
	Maximum	26935
Regional Delivery	Reference	12900

Before delving into the presentation of simulation results, it is necessary to briefly address the treatment of the input parameter "C_dA" in VECTO, which pertains to the aerodynamic resistance of the vehicle. In the model of the reference study, only the drag coefficient value is provided, overlooking the essential parameter of the vehicle's frontal area. Furthermore, given that VECTO necessitates the product of both values as input and considering that the experimental procedure, defined by VECTO-related regulation, involves the estimation of the overall parameter rather than its individual factors, a decision was made to treat the C_dA parameter as a degree of freedom to be calibrated in order to obtain an acceptable level of error

in fuel consumption under all the conditions analysed. In addition, the calibration allows to compensate for differences in simulation approaches and results between Simcenter Amesim and VECTO. Therefore, a C_dA value of 6.5 m^2 was selected. In light of information gathered from the literature, particularly in [32], this value appears to align with the vehicle class under consideration. Furthermore, as indicated in Table 6.4, it ensures a relative error of less than 5% between reference fuel consumption (FC) and fuel consumption calculated using the VECTO model across all analysed vehicle operating conditions. In conclusion, given that the observed level of discrepancy falls within acceptable bounds, the VECTO vehicle model is deemed to be validated, allowing its employment in further analysis.

Table 6.4: VECTO fuel consumption results and relative error.

Driving cycle	**Payload condition**	**Reference FC** [kg/100km]	**VECTO FC** [kg/100km]	**Relative error** [%]
Long Haul	Low	6.87	6.567	4.41
	Reference	9.04	8.998	0.45
	Maximum	10.62	10.280	3.20
Regional Delivery	Reference	9.15	8.723	4.67

7. Evaluation of FC powertrain for long haul applications

The VECTO model of the generic group 5 vehicle, representative of long-haul freight applications, has been developed and validated. Now, the study proceeds with the proposition of integrating the previously devised FC-hybrid powertrain into a wide range of long-haul freight vehicles within groups 4, 5, 9, and 10. For this purpose, the report titled "CO_2 Emissions of the European Heavy-Duty Vehicle Fleet: Analysis of the 2019-2020 reference year data" [32], published by the JRC in 2022, is utilized as a fundamental reference.

This study analyses the robustness of the reference CO_2 emissions, against which the reduction targets of Regulation (EU) 2019/1242 are benchmarked, focusing mainly on the contribution of class 4 and 9 rigid trucks and class 5 and 10 trailer trucks. To achieve this, the research leverages VECTO output files of the European HDV fleet simulated during a reference period (from October 1^{st,} 2019 to June 30^{th,} 2020) by the vehicle manufacturers. For vehicles belonging to groups 4,5,9 and 10 alone, 123,979 vehicle data were analysed, all of which were powered by an internal combustion engine. Furthermore, the report uses this dataset for an in-depth assessment of the HDV fleet, investigating its composition and the characteristics of main vehicle components. Based on this activity, reference vehicle properties for each group are generated to allow the representation and modelling of the European heavy-duty vehicle fleet in the reference period. This last contribution is particularly valuable for the research conducted in this thesis. The composition of the fleet is depicted in Figure 7.1, while Table 7.1 details the sales-weighted average properties of components and the most common auxiliary technologies.

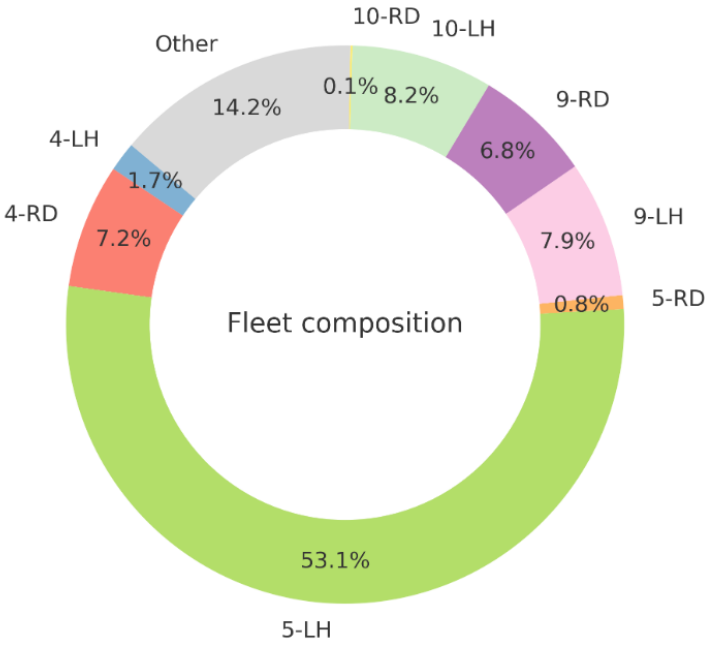

Figure 7.1: European fleet composition during the reference period.

Table 7.1: Average and most common vehicle properties per subgroup.

Subgroups:	4 - RD	4 - LH	5 - RD	5 - LH	9 - RD	9 - LH	10 - RD	10 - LH
$C_d A$ [m^2]	5.45	5.16	6.62	5.63	5.47	5.15	6.50	5.68
Curb mass [kg]	6328	7675	7093	7747	8245	9009	8041	8638
Dynamic tyre radius [m]	0.4922	0.4922	0.5223	0.4922	0.5223	0.4922	0.4922	0.4922
RRC axle 1	0.0057	0.0052	0.0056	0.0052	0.0057	0.0054	0.0057	0.0055
RRC axle 2	0.0064	0.0058	0.0062	0.0057	0.0064	0.0061	0.0064	0.0057
RRC axle 3	-	-	-	-	0.0057	0.0054	0.0062	0.0060
Steering pump	Fixed displ.	Variable displ. mech. contr.	Fixed displ.	Variable displ. mech. contr.	Fixed displ.	Variable displ. mech. contr.	Fixed displ.	Variable displ. mech. contr.
HVAC system	Default	Default	Default	Default	Default	Default	Default	Default
Electric system	Std. Tech.	Std. Tech.	Std. Tech.	Std. Tech.	Std. Tech.	Std. Tech.	Std. Tech.	Std. Tech.
Pneumatic system	Large Supply + ESS + AMS	Large Supply + ESS + AMS	Large Supply + ESS + AMS	Medium Supply 2-stage + ESS + AMS	Large Supply + ESS + AMS	Large Supply + ESS + AMS	Large Supply + mech. clutch + AMS	Large Supply + mech. clutch + AMS

In the report, each vehicle group is segmented into two subgroups considering the type of vehicle cabin and the rated engine power, as shown in Figure 7.2 and mentioned in Regulation (EU) 2019/1242. This subdivision allows to better capture the vehicle's specific technical characteristics than groups by factoring in the variability of their usage within the same HDV category and factors such as driving patterns, annual mileage, and payload. Vehicles featuring a sleeper cabin, designed with a sleeping compartment adjacent to the driver's area, are predominantly classified under the Long Haul (LH) subgroup, indicating their suitability for multi-day intercity travel without daily return to the truck's home. Conversely, vehicles equipped with a day cabin, which lacks such a compartment, fall into the Regional Delivery (RD) subgroup, signalling their alignment with shorter daily trips in regional or suburban contexts with a return to base operation at the end. Moreover, vehicles with higher engine power are deemed more appropriate for sustained long-distance travel, meriting their classification within the LH subgroup. The data presented in Table 7.1 reveal that the LH configuration across all examined vehicle groups exhibits superior optimization in terms of aerodynamics and tyre efficiency. However, they are characterized by a significantly higher curb mass due to the

equipment needed to travel long distances. Similarly, vehicles equipped with three axles, as categorized in groups 9 and 10, exhibit a greater mass relative to their counterparts with two axles, found in groups 4 and 5.

Vehicle group	Cabin type	Engine power [kW]	Subgroup
4	All	< 170	4-UD
	Day cab	≥ 170	4-RD
	Sleeper cab	≥ 170 and < 265	
	Sleeper cab	≥ 265	4-LH
5	Day cab	All	5-RD
	Sleeper cab	< 265	
	Sleeper cab	≥ 265	5-LH
9	Day cab	All	9-RD
	Sleeper cab	All	9-LH
10	Day cab	All	10-RD
	Sleeper cab	All	10-LH

Figure 7.2: Vehicle subgroups.

For the subsequent analysis, the previously developed generic fuel cell powertrain, encompassing the battery, FCS, EM, and transmission VECTO models, is integrated into the representative heavy-duty vehicles as delineated by the JRC report. This integration aims to create realistic VECTO fuel cell vehicle models for each of the regulated subgroups for long-range applications. The assumption underlying this approach posits that the data presented in Table 7.1, originally pertaining to conventional internal combustion engine vehicles, hold sufficient relevance and applicability to represent fuel cell vehicles. This presumption ensures the integrity and consistency of the input data employed in the construction of models, aligning with the rigorous standards and findings of the JRC's research activity.

This chapter aims to evaluate the energy performance of different hybrid fuel cell vehicles tailored for long haul freight applications, evaluated by modelling them in VECTO. Initially, the analysis focused on assessing the vehicles' performance across various use cases, building upon a foundational architecture as previously described. This initial framework established a benchmark for understanding the energy behaviour of hybrid fuel cell vehicles that exhibit common features with the European HDV fleet. Subsequently, a further analysis explored potential strategies for improving the fuel efficiency of fleet vehicles. This process has involved changes to the vehicle's degree of hybridisation, through a variation of the FCS size and the battery pack capacity.

Prior to delving into these analyses, a brief presentation of the vehicle simulation conditions is provided. Following this, the outcomes of VECTO simulations, pertaining to a vehicle that exemplifies the entire category of long-haul freight vehicles, are detailed and discussed. The objective of this latter paragraph is to provide an overview of how the VECTO software is applied in simulating a fuel cell hybrid powertrain, alongside clarifying the operational principles of this innovative technology. Furthermore, the steps performed to calculate the metrics needed to assess the energy performance of the entire HDV fleet are reported and explained.

7.1 Declaration Mode vehicles configuration

The simulation of all vehicles encompassed the execution of both "Long Haul" and "Regional Delivery" driving cycles, under conditions of low and reference payloads, resulting in a set of four mission profiles. In a driving cycle, the "low payload" is employed to represent the missions undertaken by the vehicle when it is in a near-empty state, whereas "reference payload" denotes a standard typical value used to characterize the vehicle during medium-high load missions. VECTO simulations were carried out in Engineering Mode, even if tailored to mirror the envisaged conditions for Declaration Mode simulations in order to ensure the derivation of results that are both valid and compliant with regulatory requirements. This adjustment was imperative, given that Declaration Mode has not yet been enabled for FC vehicles. Tables 7.2 and 7.3 show the vehicle configurations and loading conditions according to the group and driving cycle. In accordance with regulatory mandates, rigid trucks (belonging to groups 4 and 9) are simulated over the "Long Haul" cycle considering the presence of an additional towed trailer. This inclusion not only increases the total mass of the vehicle assembly but also elevates the aerodynamic drag area, a standard increment being 1.5 m².

Table 7.2: Vehicle configuration according to Regulation (EU) 2017/2400 for each group and driving cycle.

	Driving cycle and vehicle configuration	
HDV group	**Long Haul**	**Regional Delivery**
4	Rigid + Trailer (T2)	Rigid
5	Tractor + Semi-Trailer (ST1)	Tractor + Semi-Trailer (ST1)
9	Rigid + Trailer (T2)	Rigid
10	Tractor + Semi-Trailer (ST1)	Tractor + Semi-Trailer (ST1)

Table 7.3: Vehicle payload according to Regulation (EU) 2017/2400 for each group and driving cycle.

Payload (kg)	**Long Haul**		**Regional Delivery**	
HDV group	*Low*	*Reference*	*Low*	*Reference*
4	1,900	14,000	900	4,400
5	2,600	19,300	2,600	12,900
9	2,600	19,300	1,400	7,100
10	2,600	19,300	2,600	12,900

The evaluation of auxiliary consumption necessitates manual calculation, adhering to the Declaration Mode approach. Taking up the methodology employed in Chapter 6 and leveraging the insights from the report [32], the predominant technology within each specific subgroup was identified. Subsequently, in alignment with the stipulations outlined in the official VECTO annexes, a standard electricity consumption value was attributed to the selected technology.

7.2 FC powertrain operation for a representative vehicle in long haul applications

To delve deeper into the functioning of a typical HD-FC powertrain and the VECTO software, this section dissects the operational dynamics, hydrogen fuel consumption, total energy usage, and the associated losses across the various components of the group 5 FC articulated truck in an LH configuration. This particular subgroup was chosen for its prevalence and representativeness in European long-haul freight applications, as illustrated in Figure 7.1. Furthermore, this paragraph elucidates the method of processing VECTO simulation outputs to derive essential metrics of interest. This will allow subsequent chapters to examine the results and their implications in a focused manner, without having to resort to repetitive explanations. For the sake of compactness and clarity of graphical depictions, the "cycle – LOAD" combinations examined are denoted as "LongHaul – REF", "LongHaul – LOW", "RegionalDelivery – REF" and "RegionalDelivery – LOW". Furthermore, to prevent repetition and ensure a streamlined presentation, only essential graphs that contribute to a full understanding and insights will be included. Graphs related to other mission profiles that do not offer additional valuable information will be omitted.

Figure 7.3 shows the actual vehicle speed trend over time, juxtaposed against the target speed profile delineated by the selected driving cycle. The graphical depictions provided herein reflect only the conditions under reference payload, given the negligible variance in the speed profile at lower loads. Conversely, the main characteristics pertinent to driving cycle performance, as

derived from the “vsum” VECTO results file, are collected in Table 7.4 for each mission profile. In both cases, there is a remarkable congruence between the actual and target speeds, with few minor deviations. This highlights the ability of the simulated vehicle to comply with the prescribed driving cycle, suggesting a good response of the power sources and the electric motor to road and load conditions, and more generally, a satisfactory operation of the FC hybrid powertrain model designed in the Chapter 6.

Notably, during segments of the cycle characterized by a uniform speed, the vehicle exhibits frequent minor accelerations, engendering a discrepancy between the target and actual speeds. This phenomenon stems from a feature within the driver model termed "Overspeed," engineered to mimic the behaviour of an average real-life driver. This function becomes operative when the vehicle inadvertently accelerates due to a downward slope. Upon reaching the speed threshold (target speed augmented by a maximum overspeed allowance of 2.5 km/h), mechanical brakes are engaged to inhibit further acceleration, thereby rectifying the deviation.

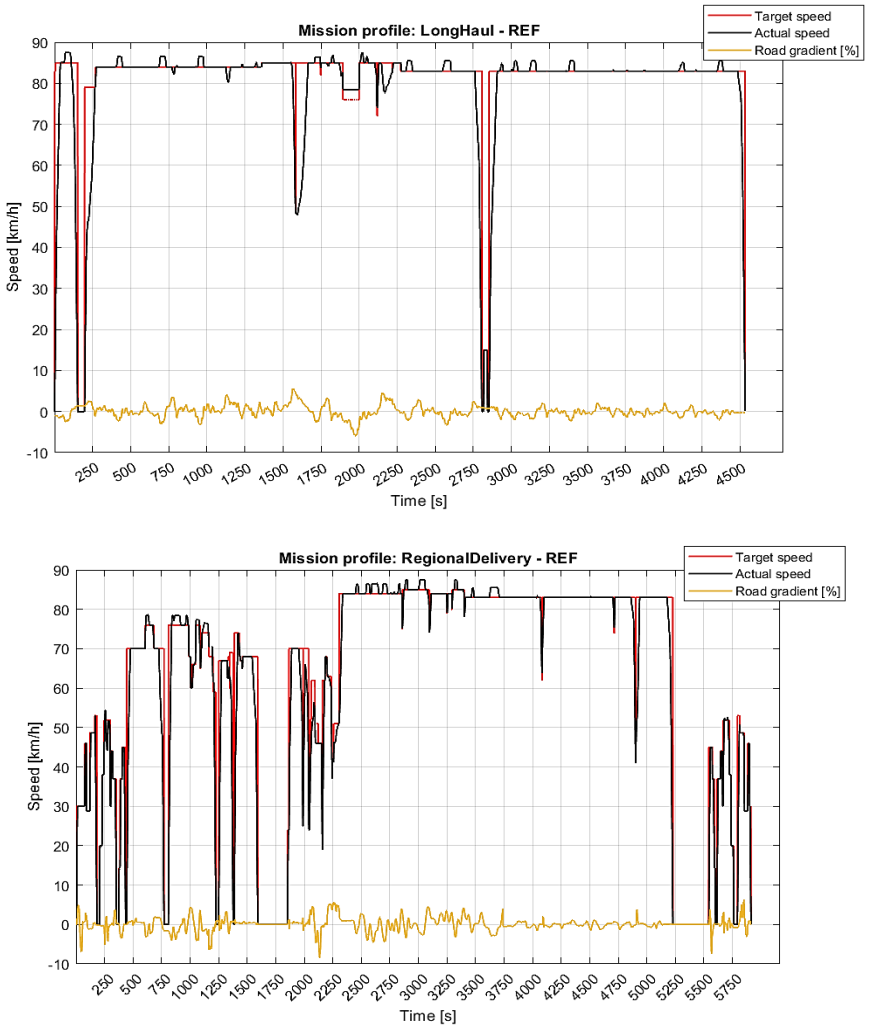

Figure 7.3: Time-based target speed, actual speed, and road gradient for Long Haul and Regional Delivery driving cycle with reference payload.

Table 7.4: Simulated driving cycle metrics.

Group 5-LH	**Long H. - REF**	**Long H. - LOW**	**Reg. Del. - REF**	**Reg. Del. - LOW**
Time [s]	4535.5	4501.7	5917.1	5891.7
Distance [km]	100.185	100.185	100	100
Avg. speed [km/h]	79.52	80.12	60.84	61.10
Avg. acceleration [m/s^2]	0.2	0.61	0.44	0.66
Avg. power at wheels [kW]	86.07	68.13	56.42	47.66
Acceleration TS [%]	5.07	3.28	9.13	7.57
Deceleration TS [%]	3.84	3.66	8.23	8.86
Cruise TS [%]	89.62	91.57	70.04	70.91
Stop TS [%]	1.48	1.49	12.61	12.66
Braking TS [%]	2.21	2.16	5.12	4.74

The data gathered in Table 7.4 reveals that despite the driving cycles sharing a similar spatial extent of approximately 100 km, their respective travel times diverge significantly due to variations in average speed and duration of stops, reflecting the distinct characteristics of the two cycles. This disparity is further clarified through the examination of the time shares (TS) across various kinematic modes of the vehicle. Notably, the Long Haul (LH) driving cycle predominantly features periods of constant speed cruising, interspersed with minimal instances of deceleration, acceleration, and stop. Conversely, the Regional Delivery (RD) cycle exhibits a pronounced increase in the duration of these phases, highlighting the dynamic nature of this cycle. Furthermore, it is observed that an increase in the transported mass imposes an additional burden on the powertrain for both LH and RD cycles, as evidenced by the higher average power output at the wheels. This increment in load results in slightly lower vehicle kinematic performance and a slightly longer cycle. However, the impact of load variations on time shares is minimal and predominantly associated with the enhanced dynamic capabilities of the vehicle under lighter load conditions, leading to more agile performance.

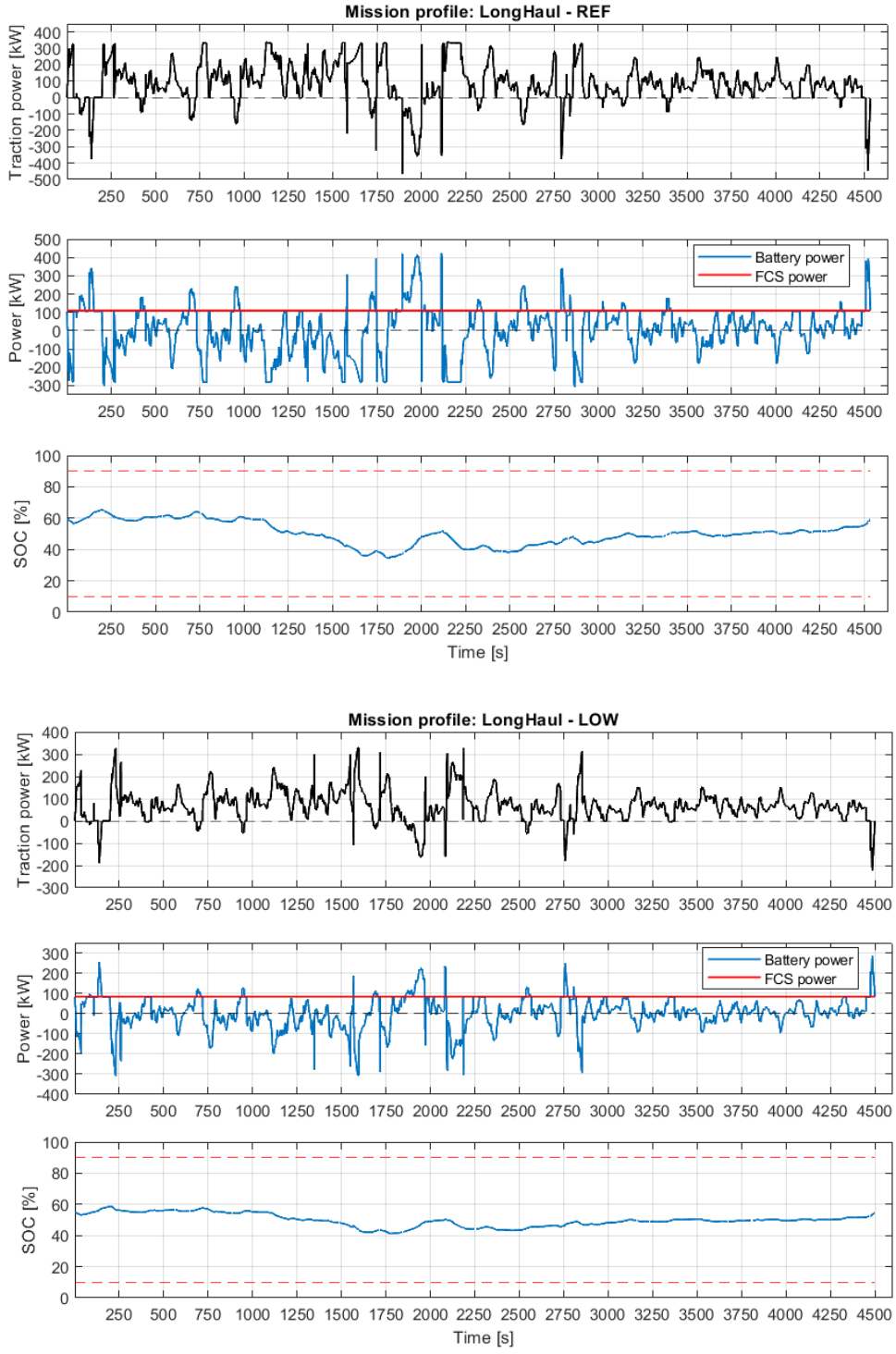

Figure 7.4: Vehicle's traction power, energy sources power, and SOC over time for Long Haul driving cycle with reference and low payload.

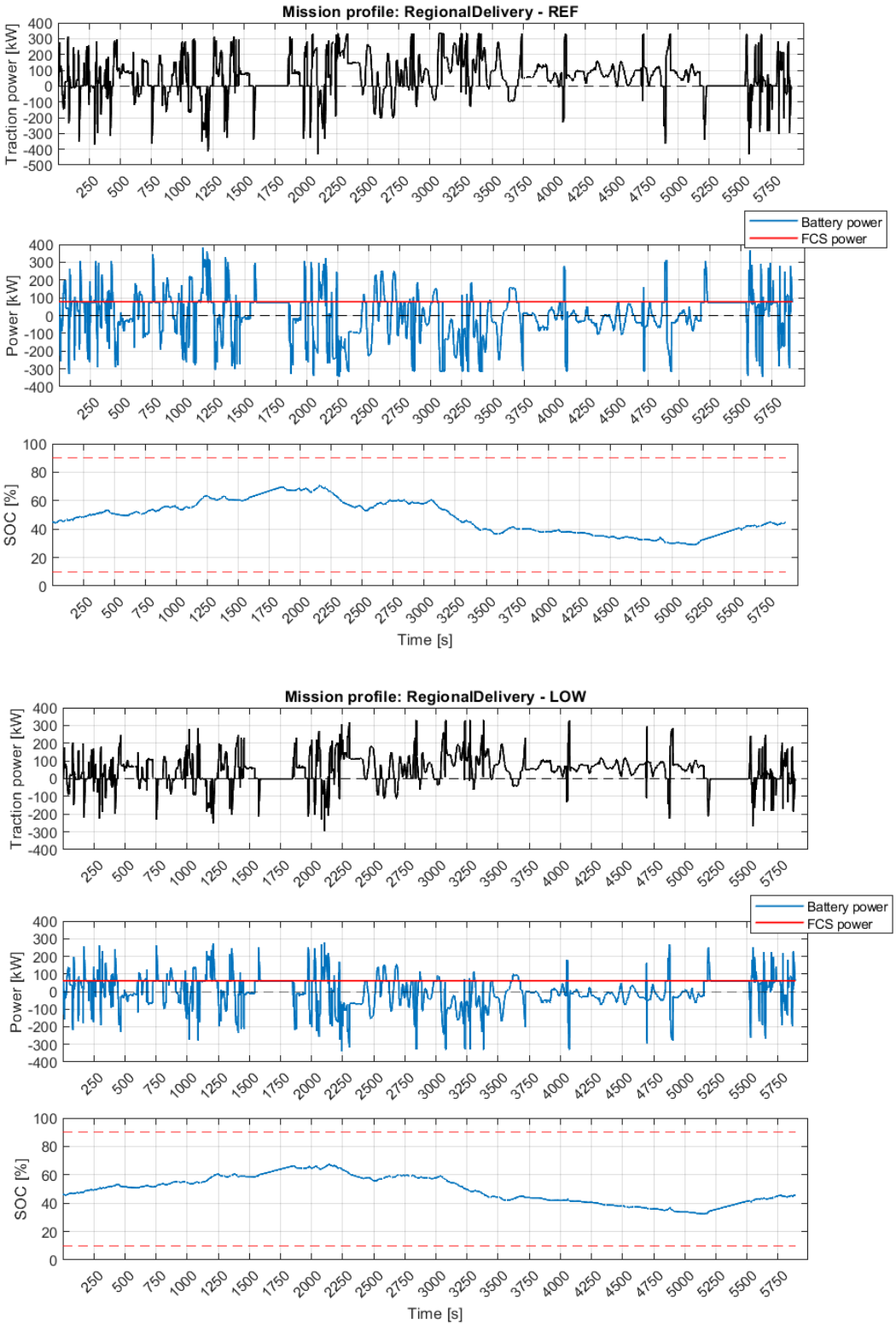

Figure 7.5: Vehicle's traction power, energy sources power, and SOC over time for Regional Delivery driving cycle with reference and low payload.

Figures 7.4 and 7.5 present the temporal evolution of the power dynamics for all the mission profiles assessed, showcasing the vehicle's traction power requirements alongside the energy

supplied by the power sources to meet these demands, as well as the battery SOC profiles. In all cases, the VECTO operation strategy ensures a steady fuel cell system operation, covering the constant average power demand of the cycle, while the battery serves as an “energy buffer” by compensating for the differences between the instantaneous power demand imposed by the driving cycle and that delivered by the FCS. This operational approach ensures that the highly dynamic trend in traction power is followed by the battery, rather than the FCS, allowing the power sources to operate most appropriately for their technical characteristics. The effectiveness of this power distribution strategy is attributed to the correct sizing of the battery employed, which boasts a capacity adequate for all considered missions. It allows a sufficiently large reference power averaging window to be assumed in the operating strategy, which results in a constant power delivery from the FCS, and maintaining the SOC profile largely within the operational bounds (denoted by a red dotted line in the SOC graphs). Moreover, it is important to note the distinct conventions VECTO employs for representing traction and battery power: traction power is positive during vehicle propulsion and negative when it is dragged, whereas battery power is positive during energy intake (typically during regeneration phases) and negative when discharging to provide traction. Therefore, these two profiles appear mirrored with respect to the x-axis, with different scales due to the power contribution provided by the FCS and the losses along the powertrain. The battery SOC trajectory is derived from the energy profile, calculated by integrating the power curve over time. The power split identification strategy executed by VECTO allows the Charge Sustaining mode to be effectively achieved. This accurate result comes from the pre-simulation performed by VECTO, which allows the overall energy flows associated with the vehicle battery to be quantified in advance of the actual simulation, and from the identification of the most appropriate initial SOC value.

A detail of the synergetic operation of FCS and the battery is depicted in Figure 7.6, displaying the electric power output from the sources as scatter plots at each simulation instant, correlated with the power at the wheels.

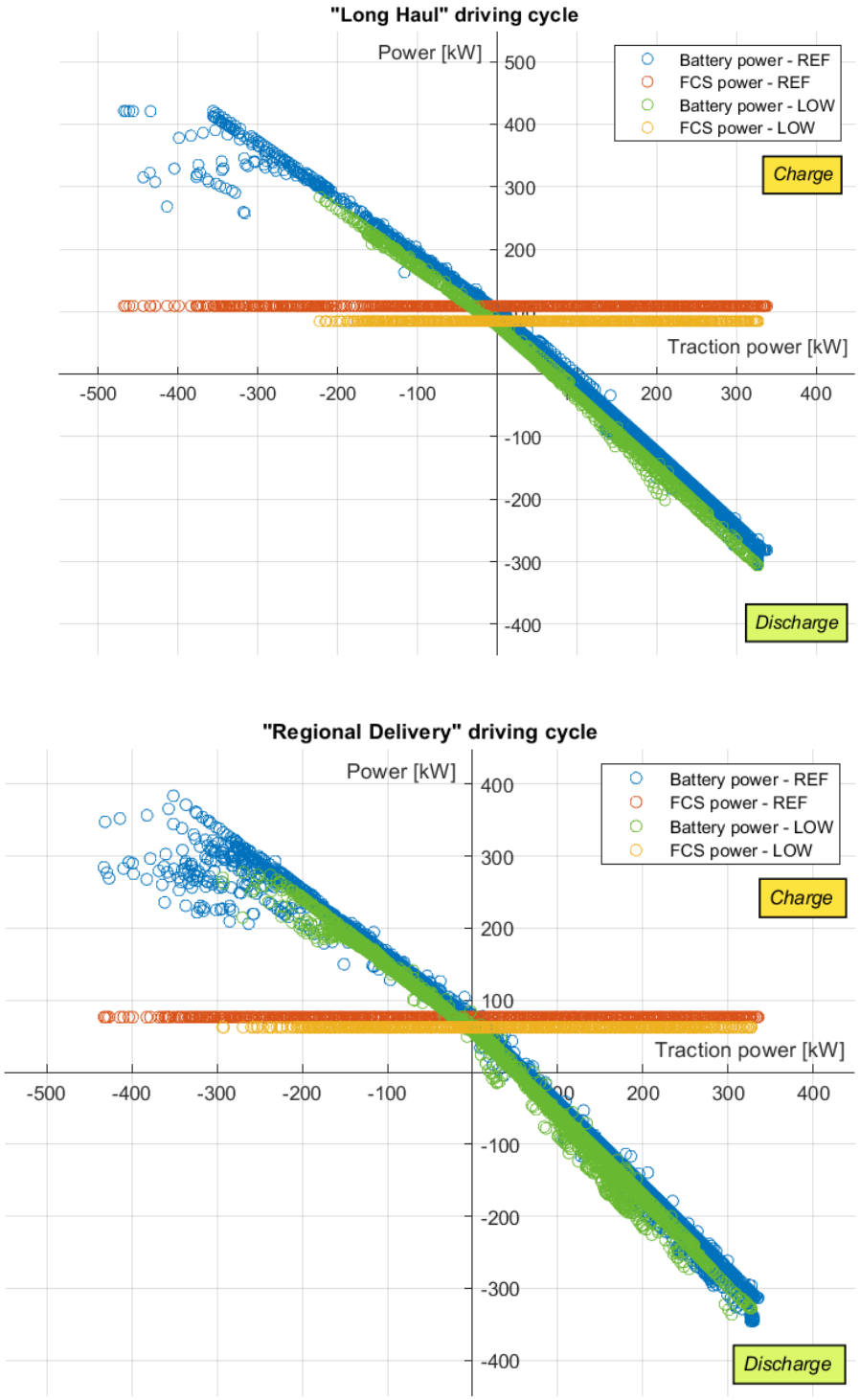

Figure 7.6: Energy source power as a function of traction power for Long Haul and Regional Delivery driving cycle, with reference and low payload.

These graphs allow for the discernment of different battery operating conditions depending on the vehicle's state of motion:

- Stationary vehicle ($P_{trac} = 0$): the entirety of the power output from the FCS is allocated towards recharging the battery ($P_{batt} > 0$), as evidenced by the intersection of the two curves at the y-axis.
- Low traction power ($P_{trac} > 0$): in scenarios where traction power is minimal, the surplus power from the FCS, not requisitioned for traction, is redirected to replenish the battery.
- High traction power ($P_{trac} \gg 0$): under conditions of elevated power requirements, both the FCS and the battery concurrently supply power.
- Vehicle dragged ($P_{trac} < 0$): during instances where the vehicle is coasting, the battery engages in energy recuperation, harnessing power from both the FCS and the road, through kinetic energy regeneration.

The FCS characteristic of delivering a constant output power across all vehicular power demands, coupled with the battery compensatory function, leads to a linear trajectory of the battery operational curve, with a slight scattering of points in the regeneration zone attributable to rapid decreases in road incline or intensive braking events. Comparing the operation in the individual mission profiles, it can be noted that as the vehicle load decreases, the domain of the curves narrows, and they shift slightly downwards. The domain does not change so much on the positive x-axis side, since the reduction in vehicle mass is exploited to achieve better vehicle dynamic performance, as can be seen from the average acceleration values visible in Table 7.4, but it changes on the negative x-axis side since because a reduction in mass leads to a proportional reduction in the vehicle kinetic energy that can be regenerated.
The constancy of the FCS output also implies a steady hydrogen flow rate, facilitating the straightforward computation of hydrogen mass utilized throughout the driving cycle by integrating the instantaneous flow rate, provided in the "vmod" file of the VECTO outputs, over time. Figure 7.7 shows the trend over time of the cumulative hydrogen mass consumed during the whole driving cycle. Since the flow rate is constant in all cases, the mass increases linearly with time.

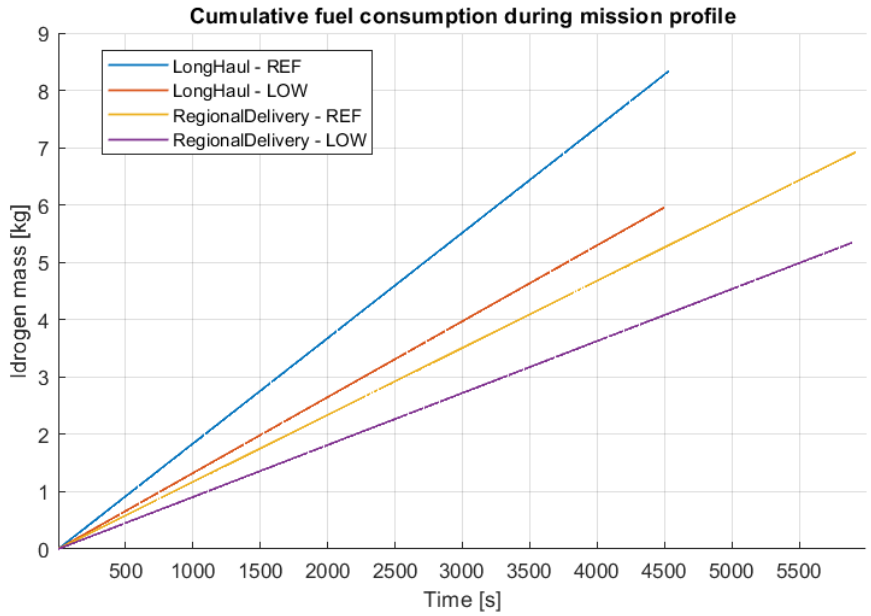

Figure 7.7: Cumulative hydrogen consumption trend.

The hydrogen mass thus obtained is then adjusted to account for the "virtual" fuel consumption associated with the charge sustaining balance of the battery. In all analysed scenarios, there is a negative variation between battery energy at the end and at the beginning of the mission, hence an additional mass of hydrogen must be assessed. The comprehensive fuel consumption metrics are provided in Table 7.5, covering all mission profiles.

Table 7.5: Group 5-LH vehicle fuel consumption values.

Group 5 - LH	**Long H. - REF**	**Long H. - LOW**	**Reg. Del. - REF**	**Reg. Del. - LOW**
FC not corrected [g]	8338.41	5959.47	6916.73	5340.81
Add. mass [g]	12.65	4.87	10.68	5.33
FC corrected [g]	8351.06	5964.34	6927.41	5346.14
FC [kg/100km]	8.3356	5.9533	6.9274	5.3461

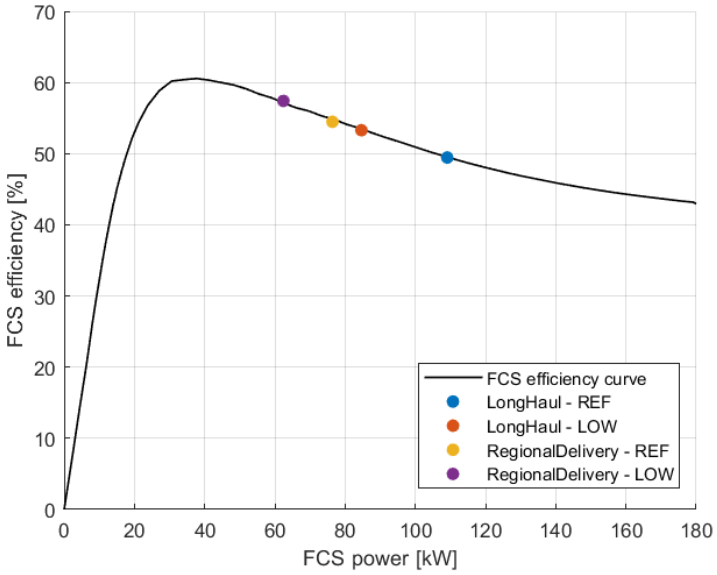

Figure 7.8: FCS efficiency curve and operating points.

Figure 7.8 shows the FCS operating points for each mission profile, plotted against its efficiency curve. This representation, in accordance with the characteristics of the guide cycles presented in Table 7.4, reveals that the LH cycle under reference payload is the most demanding condition for the FCS, pushing its operational point to a less favourable position relative to its peak efficiency. Conversely, by reducing the load and switching to a Regional Delivery driving cycle the operational points gradually approach the zone of maximum efficiency. This trend aligns with the intended goals of the VECTO operation strategy, aiming to optimize FCS efficiency within the constraints of the driving cycles. Table 7.6 compiles the average efficiency figures for the FCS (calculated according to Equation 2.5) alongside those for other principal components of the powertrain, as well as the aggregate tank-to-wheel (TTW) efficiency for each mission profile. Notably, the derived TTW efficiencies corroborate with the benchmark average efficiency of approximately 45% for hybrid fuel cell HDVs, as documented in the literature [45].

Table 7.6: Average efficiencies of the main group 5-LH vehicle subsystems and TTW efficiency.

Avg. Efficiency [%]	**Long H. - REF**	**Long H. - LOW**	**Reg. Del. - REF**	**Reg. Del. - LOW**
FCS	49.46	53.29	54.48	57.40
EM	89.44	89.92	89.58	90.23
Gearbox	98.50	98.50	98.49	98.49
Axle	97	97	97	97
TTW	38.97	42.86	40.18	43.79

The tank-to-wheel efficiency quantifies the energy conversion efficiency from the onboard chemical energy storage to mechanical energy at the wheels, encapsulating the entire energy transformation chain within the vehicle. This efficiency metric was derived using Equation 7.1, adhering to the methodology presented in [10]:

$$\eta_{TTW} = \frac{E_{traction}}{E_{H_2,corr}}.$$

(Eq. 7.1)

Where:

- $E_{traction}$ $[kWh]$ is the total traction energy, computed as the sum of the energy expended to overcome aerodynamic drag, rolling resistance, and the incline resistance throughout the driving cycle. These energy components are retrievable from the "vsum" output file of VECTO simulations.
- $E_{H_2,corr}[kWh]$ represents the energy associated with the fuel consumed over the driving cycle, corrected to account for variations in the battery stored energy from the start to the end of the mission. The fuel energy is calculated using Equation 7.2, assuming a constant hydrogen lower calorific value, where the corrected mass was obtained by adding to the actual mass consumed by the FCS, the virtual mass associated with the ΔE_{REESS}, according to Equation 5.4:

$$E_{H_2,corr} = \int_T \dot{m_{H_2}} * H_i * dt = m_{H_2,corr} * H_i.$$

(Eq. 7.2)

The final step entails examining how the total energy output from the fuel cell system is utilized and allocated among the main vehicle subsystems and driving resistances. VECTO, through its comprehensive vehicle energy balance assessment during a driving mission, quantifies these contributions and records them in the "vsum" output file. These allocations are represented in Figure 7.9, where pie charts illustrate the proportional energy consumption shares dedicated to each aspect of the vehicle operation. These graphs aid in understanding the energy dynamics within the vehicle, while also highlighting key areas where vehicle characteristics might be optimized to achieve the greatest benefits.

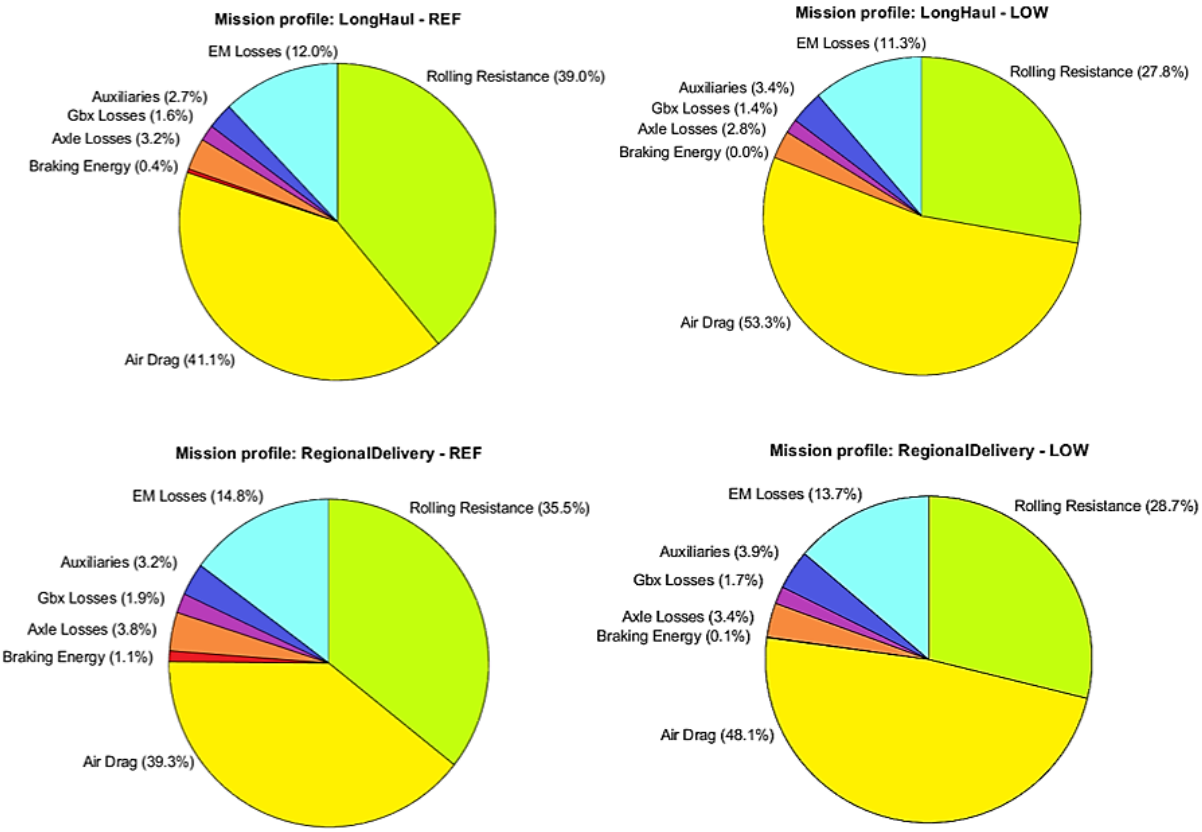

Figure 7.9: Energy consumption shares for each cycle-loading combination.

In all examined mission profiles, the predominant energy expenditure is attributed to overcoming road resistances, namely air drag and rolling resistance. This component constitutes over 80% of the total energy supplied for the LH cycle and 70% for the RD. Analysis of both driving cycles reveals that transitioning from reference to low payload significantly reduces the energy required to counter rolling resistance, attributable to the decrease in mass and total RRC value. Conversely, the energy fraction dedicated to aerodynamic resistance rises due to increased average vehicle speeds and the quadratic relationship between speed and air resistance. A considerable amount of energy is also dissipated through losses in the electric motor, which together with gearbox and axle losses contribute to a total driveline consumption share of 16.8% and 15.5% for Long Haul with reference and low payload, respectively, and of 20.5% and 18.8% for Regional Delivery missions. Regarding the relative consumption of auxiliaries, while higher in power in the LH cycle, the weight on energy consumption in the Regional Delivery cycle is greater for all load conditions, due to both the significantly longer travel time and the lower total energy expenditure. Finally, as far as the energy lost due to mechanical braking is concerned, these are identified as marginal, underscoring the effectiveness and importance of regenerative braking. Specifically, for the Long Haul driving cycle, the contribution of mechanical braking is minimal due to the quasi-stationary characteristics of the cycle, while it becomes slightly larger with the RD cycle due to the frequent acceleration and deceleration transients. The necessity to supplement regenerative

braking with mechanical braking escalates with heavier payloads, to avoid excessive strain on the electric motor and battery.

7.3 Energy performance analysis of the reference HDV fleet

The current section evaluates the energy performance of FC-hybrid vehicles simulated with VECTO in the representative reference configurations of the European long haul HDV fleet. The purpose of this activity is not only to show realistic indications of the hydrogen consumption characteristic of the different classes of heavy vehicles in the standard use cases but also to create a baseline against which possible improvements in terms of FC and powertrain efficiency can be observed through a change in architecture.

Fuel consumption values were calculated following the procedure described in the previous subsection, starting from the hydrogen flow rate required by the FCS to deliver the fraction of electric power calculated by VECTO. In all 32 use cases analysed, the software succeeds in making the FCS operate in a stationary manner, identifying an average power value over the cycle sufficient to satisfy both the dynamic performance of the vehicle and the charge sustaining management of the battery. This result is allowed by the capacity of the battery employed, which proves to be sufficient to manage the differences between the power required for traction and the power supplied by the FCS, without dangerously approaching the limits of the SOC. This approach allows a direct correlation between the amount of driving cycle effort due to vehicle drags and losses, the power delivered by the FCS and thus the required hydrogen consumption.
The constant output power values of the FCS for each group and mission profile are shown through bar graphs in Figure 7.10, while Figure 7.11 shows the corresponding FCS efficiency values.

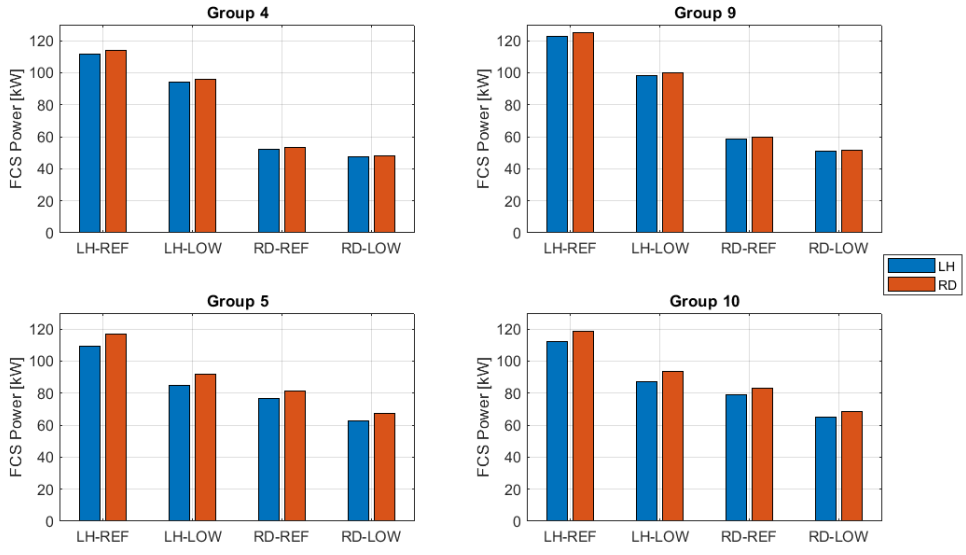

Figure 7.10: FCS constant output power for each use case.

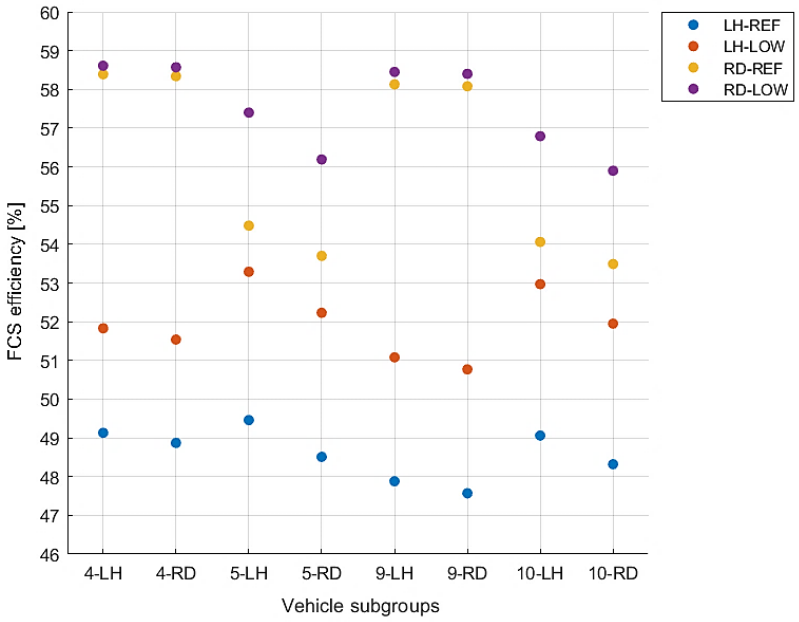

Figure 7.11: FCS efficiency for each use case.

Across all subgroups, transitioning from the most demanding scenario, represented by the Long Haul driving cycle with a reference payload, to the less intensive scenario of Regional Delivery with a low payload, results in a decrease in the power output required from the FCS, allowing it to operate closer to its peak efficiency. However, a comparison between the two vehicle subgroups reveals that the RD configuration consistently demands more power from the FCS across all mission profiles compared to the LH configuration. Consequently, for identical use cases, the FCS's efficiency in the RD configuration is consistently slightly lower. This discrepancy primarily stems from the intrinsic differences in vehicle characteristics between the two subgroups: despite a lower mass, the RD vehicles exhibit higher aerodynamic drag coefficients and less efficient tyres, factors that significantly influence the energy needed to complete the driving cycles.

A similar trend is observed in TTW efficiency, suggesting that there is a strong correlation between the two. Table 7.7 presents the TTW efficiency metrics for each vehicle subgroup and their respective use cases.

Table 7.7: Tank to wheel efficiency values for each vehicle subgroup and use case.

TTW efficiency [%]		**Long H. - REF**	**Long H. - LOW**	**Reg. Del. - REF**	**Reg. Del. - LOW**
Group 4	***LH***	39.5	42.2	44.3	44.8
	RD	39.5	42.2	44.8	45.3
Group 9	***LH***	38.2	41.6	43.5	44.5
	RD	38.2	41.6	44.1	45.2
Group 5	***LH***	39.0	42.9	40.2	43.8
	RD	38.8	42.6	40.4	43.6
Group 10	***LH***	38.7	42.6	39.8	43.2
	RD	38.5	42.2	40.0	43.1

As illustrated in Figure 7.12, a diminution in cycle intensity corresponds to enhanced TTW efficiency. This improvement stems mainly from the increased efficiency of the FCS, facilitated by the decrease in the average power output required. Additionally, both the enhancements in the efficiency of the vehicle's subsystems, especially the electric motor, and the decrease in ΔSOC together with the related corrective mass contribute to this trend. This tendency is particularly noticeable in rigid trucks; transitioning from the “LongHaul-REF” to the “RegionalDelivery-LOW” mission profile leads to a reduced traction energy requirement, largely because the RD cycle is undertaken without an extra trailer thus facilitating the increasingly efficient operation of the powertrain. Furthermore, the RD cycle exhibits superior TTW efficiency compared to the corresponding LH missions also due to the more frequent application of regenerative braking, because of the transient nature of the cycle itself. This is evidenced by a higher time share of deceleration phases. The role of regenerative braking becomes even more relevant in low-load conditions, allowing for the recuperation of kinetic energy without overloading the components and therefore having to resort to mechanical braking, as observed in Figure 7.20.

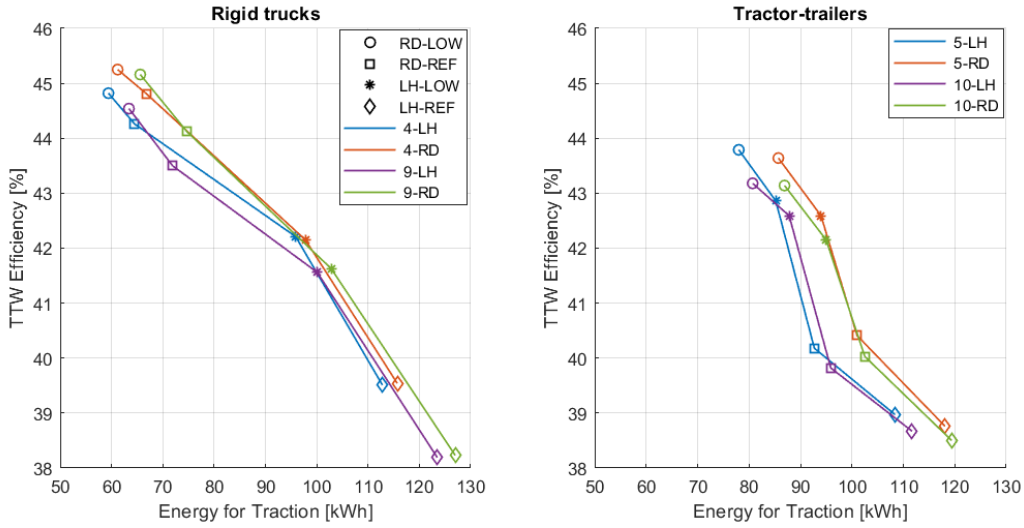

Figure 7.12: TTW efficiency in relation to traction energy demand, for rigid and articulated trucks.

Table 7.8 presents the hydrogen consumption values for rigid trucks within groups 4 and 9, alongside tractor-trailers in groups 5 and 10, delineated across both LH and RD design configurations, hence covering the entirety of the use cases examined in this study. Simultaneously, Figure 7.13 graphically represents these metrics through bar diagrams, organized by mission profile for each subgroup.

Table 7.8: Fuel consumption values for LH freight vehicles with the reference hybrid architecture.

FC [kg/100km]		**Long H. - REF**	**Long H. - LOW**	**Reg. Del. - REF**	**Reg. Del. - LOW**
Group 4	***LH***	8.55	6.81	4.37	3.98
	RD	8.77	6.95	4.47	4.06
Group 9	***LH***	9.69	7.21	4.96	4.27
	RD	9.95	7.40	5.08	4.36
Group 5	***LH***	8.34	5.95	6.93	5.35
	RD	9.13	6.61	7.50	5.89
Group 10	***LH***	8.65	6.18	7.22	5.61
	RD	9.29	6.75	7.68	6.05

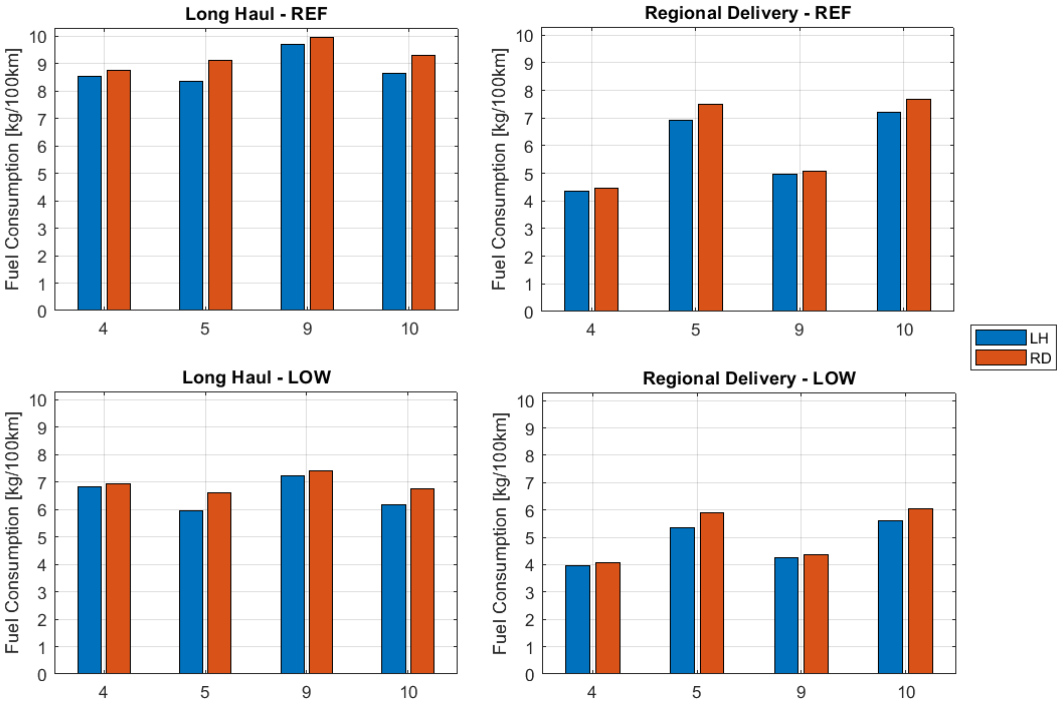

Figure 7.13: Fuel consumption bar graphs.

The analysis of the fuel consumption data reveals distinct trends and characteristics that are closely tied to various vehicle configurations and their respective mission profiles. The most pronounced distinction observed across all groups is between Long Haul and Regional Delivery driving cycles. Vehicles engaged in LH missions, with the same load state, consistently exhibit higher fuel consumption when compared to those operating under the Regional Delivery profile. This disparity is primarily attributed to the nature of Long Haul missions, which involve running a stretch of highway at a high and mostly constant speed requiring on average more power for traction, a factor that inherently leads to higher fuel consumption.
Furthermore, vehicles in RD subgroups exhibit higher hydrogen consumption across all considered use cases. This result can be attributed to the fact that this vehicle configuration is not optimised from an aerodynamic and rolling resistance point of view, as it is representative of those vehicles mainly used in daily missions within a regional context. These inefficient properties eclipse the effect of the mass reduction characteristic of RD configurations when compared to their LH counterparts, resulting in a significant increase in energy expenditure. The analysis progresses to an evaluation of fuel consumption and TTW efficiency across the distinct mission profiles, enabling a thorough comparative and quantitative assessment of various use cases and vehicle types.

1. Comparison between LH and RD vehicle configurations)

In this initial comparative analysis, variations in hydrogen consumption for a designated mission profile are assessed, contrasting the performance of a vehicle configured for Long Haul

operations against its configuration for Regional Delivery assignments. This comparison sheds light on the impact that specific vehicle configurations have on hydrogen usage, in order to understand how they could be optimised to achieve greater fuel economy and lower environmental footprint in varying operational contexts. Figure 7.14 graphically displays the results of this comparison across all evaluated mission profiles, showing the percentage increase in fuel consumption attributable to the adoption of an RD configuration.

- Long Haul driving cycle

Within the domain of rigid trucks, specifically for the "Long Haul" driving cycle, it is observed that the vehicles in the second subgroup, characterized by less optimized features, exhibit a marginal increase in fuel consumption, ranging between 2.2% and 2.7%. On the other hand, the impact on tractor-trailers is markedly higher, with fuel consumption escalating by approximately 7% to 11%.
The differential in energy requirements for traction due to suboptimal properties necessitates FCS to operate at varied efficiency levels. For rigid trucks, switching from an LH to an RD subgroup results in a minor decrease in FCS efficiency, approximately 0.3%, for both groups and payload categories. In contrast, tractor-trailers exhibit a more significant drop in FCS efficiency when making the same transition, with reductions of 0.95% in group 5 and 0.74% in group 10 at reference payload, and even larger declines of 1.06% and 1.02%, respectively, at low payload.
This variation in efficiency dynamics between vehicle configurations does not lead to any significant change in TTW efficiency between the rigid truck setups, whereas tractor-trailers show a decrease, with the maximum difference reaching -0.4%.

- Regional Delivery driving cycle

The analysis of the Regional Delivery driving cycle mirrors the findings from the Long Haul cycle, where tractor-trailers experience a greater percentage increase in consumption compared to rigid trucks under both load conditions. Specifically, for rigid trucks, the increase is around 2%. Conversely, tractor-trailers show a wider fluctuation in consumption, with increases spanning from 6% to a peak of about 10%.

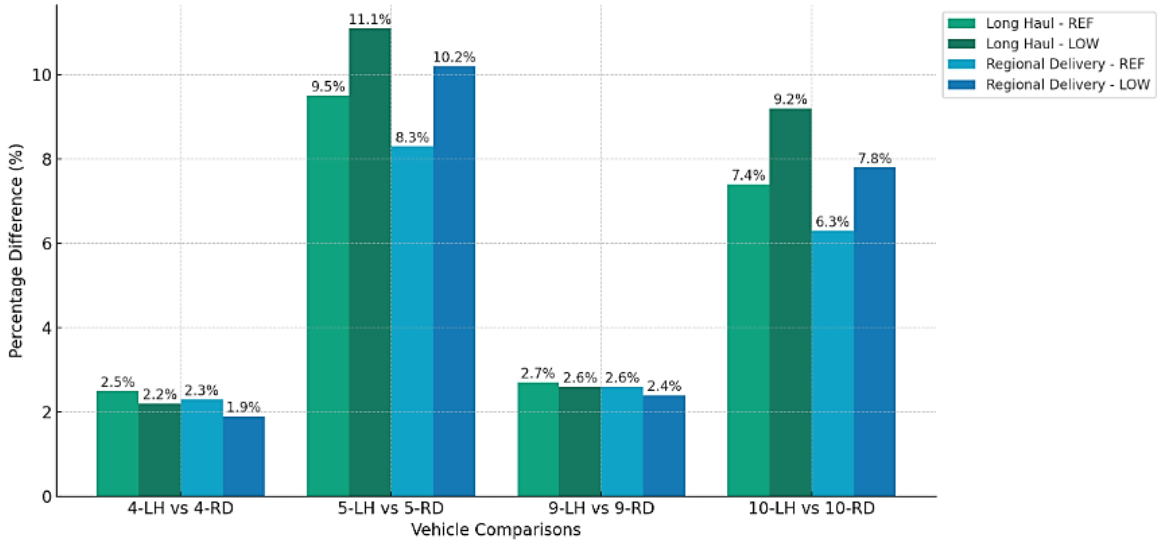

Figure 7.14: Percentage increase in fuel consumption between RD and LH configuration for both Long Haul and Regional Delivery driving cycles.

2. Comparison between rigid trucks and tractor-trailers)

Now, it is assessed whether it is more advantageous to carry out a certain mission profile by employing a rigid truck or a tractor-trailer. In this case, comparisons are made between vehicles with the same axle configuration and the same subgroup. The objective is to discern the potential benefits tied to the choice of vehicle type under comparable conditions.

- Long Haul driving cycle

When comparing fuel consumption by looking at the different performance between rigid trucks and tractor-trailers, it becomes evident that during the Long Haul driving cycle performed under the operative conditions specified by regulation (EU) 2017/2400, rigid trucks consume significantly more than the respective tractor-trailer configurations with the same axle arrangement, as depicted in Figure 7.15. Additionally, rigid trucks generally demonstrate lower TTW efficiency, with reductions ranging from -0.3% to -1%, with the exception of comparisons involving group 5.

Specifically, in the "LongHaul-REF" scenario, the 4x2 rigid truck belonging to the 4-LH subgroup consumes 2.6% more hydrogen than the 4x2 tractor-trailer in the 5-LH subgroup, even though it carries a lower mass load. This discrepancy becomes even more pronounced with 6x2 configurations, where the fuel consumption increase escalates to 12% for the comparison between the 9-LH and 10-LH subgroups and 7.1% for the comparison between the 9-RD and 10-RD subgroups.

Under the "LongHaul-LOW" mission profile, these differences widen further. The hydrogen consumption for 4x2 vehicles varies significantly, with a 14.3% increase in the comparison between the 4-LH and 5-LH subgroups, and a 5.2% rise when comparing the 4-RD and 5-RD subgroups. In the case of 6x2 vehicles, the escalation in hydrogen consumption is significant as

well, ranging from 9.6% in the comparison between the 9-RD and 10-RD subgroups, to a higher 16.7% when comparing the 9-LH to the 10-LH subgroup.

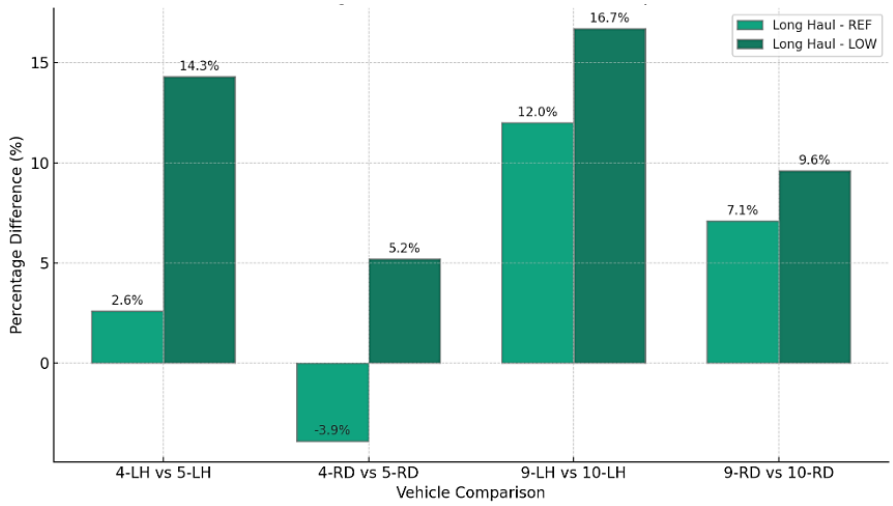

Figure 7.15: Percentage difference in fuel consumption of rigid trucks compared to tractor-trailers along the Long Haul driving cycle.

This is largely due to the regulatory requirement for simulating rigid trucks with an additional towed trailer, which markedly impacts the power needed for traction and adversely affects the vehicle's performance characteristics, making it less efficient. Specifically, this additional trailer contributes to a notable increase in total mass by 7.5 tons and the vehicle's drag coefficient (C_dA) by 1.5 m², along with an implicit rise in the rolling resistance coefficient, further aggravated by the increased mass and additional axles.
An exception to this trend emerges in the "LongHaul-REF" scenario where the tractor-trailer from the 5-RD subgroup shows a 3.9% higher fuel consumption than the 4-RD rigid truck, together with a lower TTW efficiency of 0.8%.
In this instance, the tractor-trailer presents a particularly high C_dA and total RRC values, which are comparable to those of the 4-RD configuration with the addition of a trailer. In addition, there is an important disparity in the total vehicle mass, primarily due to the divergent reference payload values employed for each configuration, as detailed in Table 7.3.

- Regional Delivery driving cycle

Rigid trucks, adhering to their fundamental configuration without an additional trailer, exhibit notable advantages for this type of usage, as shown in Figure 7.16. The comparison of the 4-LH rigid truck and the articulated truck of sub-group 5-LH shows that driving the cycle with the former results in 58.35% and 34.3% lower hydrogen consumption, with reference and low payload respectively. Instead, trucks in the 9-LH subgroup see 45.6% and 31.4% lower consumption than those in the 10-LH subgroup.
When examining RD configurations, the differences in consumption become even more pronounced.

Operating a 5-RD tractor-trailer under reference and low payload conditions leads to a surge in hydrogen consumption by 67.7% and 45.3%, respectively, in comparison to a 4-RD rigid truck. Similarly, when a 10-RD tractor trailer is employed under analogous conditions, the increase in hydrogen consumption is observed to be 51.3% and 38.6%, respectively, relative to a 9-RD rigid truck.

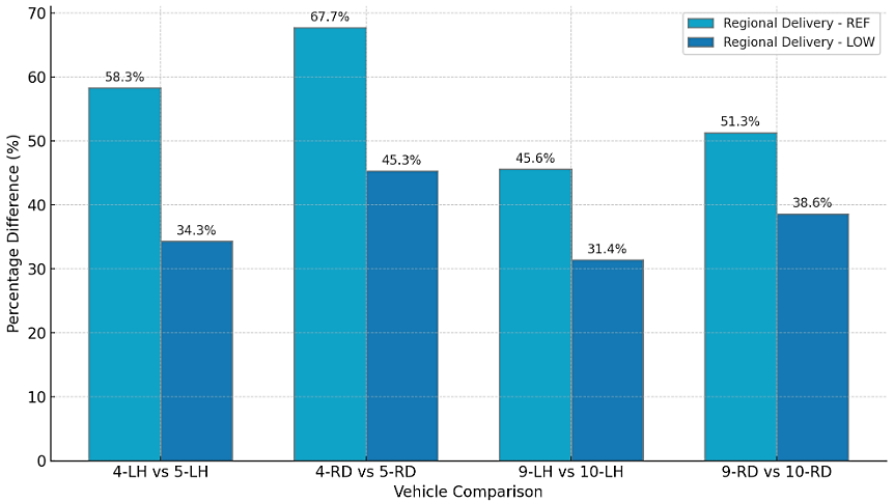

Figure 7.16: Percentage increase in fuel consumption of tractor-trailers compared to rigid trucks along the Regional Delivery driving cycle.

The very large differences in consumptions are a direct consequence of the vehicle setups, whose divergence of properties becomes even more pronounced when considering vehicles of the RD subgroup. The primary factors contributing to these differences include the significant disparity in vehicle mass, with rigid trucks being between 33% and 53% lighter than their tractor-trailer counterparts, largely due to the different payload capacities mandated by regulatory standards. Additionally, rigid trucks benefit from a lower drag coefficient, which can be up to 18% less than that of tractor-trailers. These factors result in significantly higher TTW efficiency for rigid trucks, which ranges from an improvement of +1% to as much as +4.4%.

3. Comparison between axle configurations)

In conclusion, the study examines the influence of axle configuration on hydrogen consumption by comparing outcomes from mission profiles performed with vehicles of the same subgroup category, but different in their axle setups.

- Long Haul driving cycle

The analysis within the categories of rigid trucks and tractor-trailers, focusing on the variation of axle configurations, reveals notable distinctions based on vehicle properties, as detailed in Table 7.1. The primary variances in vehicle features are observed in the curb mass and the rolling resistance coefficient of the axles. Specifically, the 4x2 configuration is generally characterized by a lower curb mass, whereas the total RRC tends to be higher in the 6x2

configuration. The drag coefficient shows negligible differences in rigid trucks, but they are significant for tractor-trailers.

As illustrated in Figure 7.17, when analysing the "LongHaul-REF" scenario for rigid trucks in groups 4 and 9, transitioning to a 6x2 axle configuration results in a 13% increase in fuel consumption for both LH and RD subgroups. However, this increase moderates to approximately 6% under the "LongHaul-LOW" mission profile.

For tractor-trailers, when comparing the consumption between groups 5 and 10 under the LH "LongHaul-REF" condition, group 10 exhibits a 4% higher fuel consumption than group 5. This gap decreases to 2% in the RD subgroups. Equal magnitudes of increase are noted in scenarios involving a low payload.

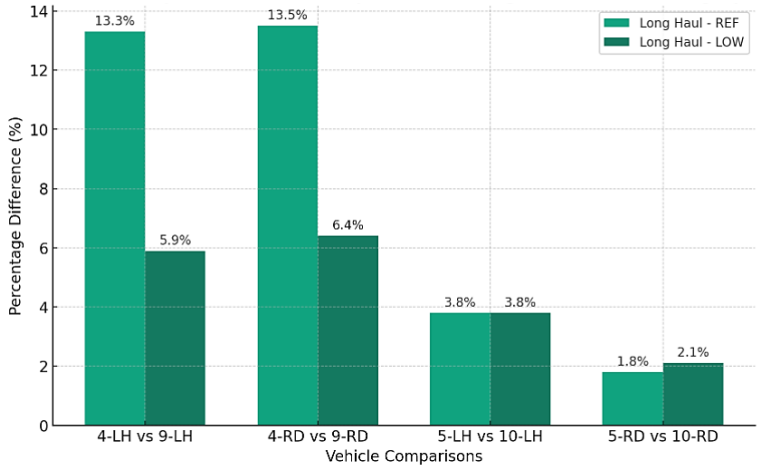

Figure 7.17: Fuel consumption percentage increase comparing 6x2 vehicle to 4x2 vehicle with Long Haul driving cycle.

- Regional Delivery driving cycle

Along the Regional Delivery driving cycle, findings align closely with observations from mission profiles involving long-haul missions. Vehicles equipped with a 6x2 axle configuration exhibit higher fuel consumption compared to their 4x2 counterparts, as illustrated in Figure 7.18. Within the realm of rigid trucks, under the "RegionalDelivery-REF" mission profile, there is an increase of about 13% in fuel consumption for both the LH and RD subgroups. Conversely, articulated trucks experience a more modest elevation in fuel usage, with approximately a 4% increase for the LH configuration and 2% for the RD setup. Furthermore, when examining the "RegionalDelivery-LOW" mission profile, the increment in fuel consumption is mitigated to 7% among rigid trucks. Articulated trucks, on the other hand, exhibit a 5% increase in the LH category and an approximately 3% rise in the RD subgroup.

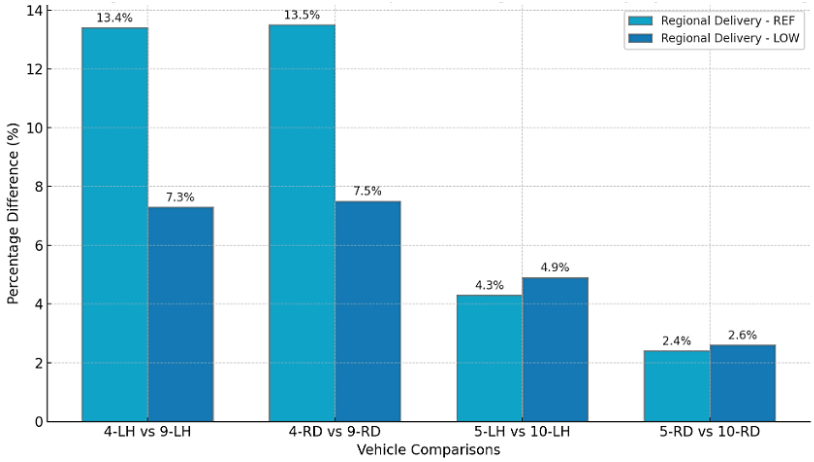

Figure 7.18: Fuel consumption percentage increase comparing 6x2 vehicles to 4x2 vehicles along the Regional Delivery driving cycle.

Based on the comparative analysis undertaken, several conclusions can be drawn regarding the deployment and optimisation of vehicles belonging to the average European HDV fleet:

1. Vehicles specifically engineered for regional and daily operations, categorized within the RD subgroups, exhibit substantially higher fuel consumption compared to configurations that, although less streamlined, are optimized for extended journeys.

2. For all use cases considered, when transitioning from LH to RD configuration, tractor-trailers consistently show a higher percentage increase in hydrogen consumption compared to rigid trucks. This underlines the more urgent need to optimise the aerodynamic characteristics and tyre efficiency of articulated trucks, rather than lorries, in order to enhance fuel economy and achieve a greater hydrogen savings margin.

3. The comparison between rigid trucks and tractor-trailers for the same mission profile suggests fuel consumption plays an important role in the choice of vehicle type to be used for a given task. Rigid trucks tend to be more efficient in regional delivery scenarios due to both their more compact design and the operational requirements, but less so in long haul missions. At the same time, tractor-trailers result to be more suitable for long haul transport in a highway context.

4. Axle configuration significantly influences fuel consumption, with the 6x2 setup generally leading to higher fuel usage compared to the 4x2 configuration. This effect is more pronounced in rigid trucks than in articulated trucks, as in the former there is an important increase in mass due to the different payload used in the same use case. In contrast, such a weight discrepancy is not observed in tractor-trailers as they use the same payloads, meaning the difference in fuel consumption between these configurations can be solely attributed to the different vehicle characteristics. Furthermore, 4x2 vehicles outperform their 6x2 counterparts in terms of TTW

efficiency across all mission types, with an average improvement of about 0.7% for rigid trucks and 0.4% for articulated trucks.

Finally, an evaluation of the energy distribution across the principal subsystems constituting the various vehicles under consideration, as well as the driving resistances encountered in each mission profile, is conducted. Figure 7.19 reports the cumulative energy shares with a bar graph for each use case.

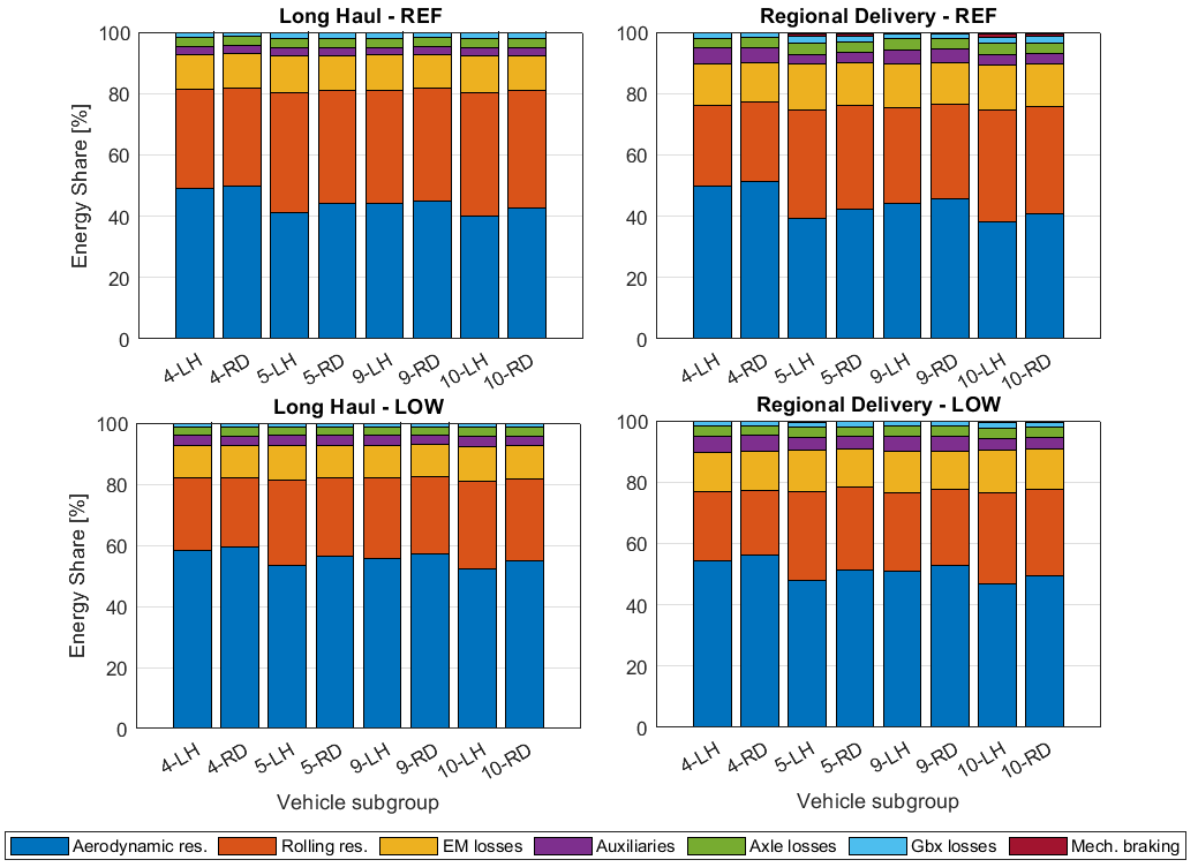

Figure 7.19: Energy distribution among vehicle subgroups.

The distribution of energy allocation varies slightly depending on the type of vehicle and the mission profile. Specifically, vehicles belonging to the RD subgroups, tend to prioritize less on aerodynamic optimization. This results in increased aerodynamic drag compared to their long-haul counterparts. On the other hand, despite their tires being less efficient than those of the LH subgroups, these vehicles demonstrate a reduced expenditure on rolling resistance, attributable to their considerably lower mass. Furthermore, during driving cycles involving low payloads, a decrease in rolling resistance is observed, whereas the proportion of energy consumed by aerodynamic drag escalates due to higher velocities. However, across all scenarios, the energy allocated for traction predominates, accounting for roughly 75% to 82% of the total energy expenditure.

Regarding other energy contributions, losses in the electric motor are notably substantial, accounting for 10% to 15% of the total energy usage. In contrast, auxiliary consumptions are relatively minor, contributing between 2% and 5%, with axle losses ranging from 3% to 4%, and gearbox losses falling below 2%.
Mechanical braking plays a minimal role in energy dissipation. Typically, it is negligible, but if present it contributes at most 1% of the total energy consumption. This latter scenario is most common under heavy load conditions or during regional delivery missions characterized by frequent decelerations. These findings highlight the crucial role of regenerative braking systems in these vehicles, which, supported by large battery capacities, effectively recover most of the available energy, and only in rare circumstances require the intervention of mechanical brakes.

7.4 Hybridisation analysis

In this assessment, the reference powertrain was modified in order to identify potential changes that could lead to improvements in the energy performance of the vehicles analysed so far. The focus was on changing the level of hybridisation of the vehicles, investigating the impact of various factors, including battery capacity, fuel cell system power, payload, and driving cycles, on hydrogen consumption. For this purpose, a simulation matrix was developed, encompassing a broad range of component specifications to ensure a thorough examination of potential scenarios. The study particularly highlighted the effects of adjusting the sizes of the battery pack and the FCS, involving changes to the REESS capacity and the peak power output of the FCS, respectively. These powertrain attributes were selected due to their substantial influence on the vehicle's operational strategy and the management of onboard energy. The capacity of the battery directly impacts the algorithm used by VECTO to calculate the FCS's power output, whereas modifications to the FCS's maximum power output allow to change its efficiency characteristic and thus the position on it of the system's operating points during the driving cycle.
In addition, considering that the previous analysis was conducted assuming the use of the same powertrain across all analysed vehicles, this step enabled the determination of the most suitable hybrid powertrain configuration for each vehicle within the fleet, tailored to specific missions. This approach also allows the identification of relevant insights in order to facilitate the initial estimation of the required energy capacities and their respective proportion, during a preliminary powertrain design phase. These deductions are based on the analysis of the variations in hydrogen consumption resulting from the adoption of different powertrain configurations, compared to the results of the reference model equipped with a 180 kW FCS and a 72 kWh accumulator.
To investigate different degrees of hybridization, the study was expanded to include case studies with both smaller and larger sizes for the REESS and FCS than those initially considered. As a result, this research allowed for the exploration of eight additional hybrid-FC powertrain configurations for each vehicle, in addition to the reference setup, across the eight vehicles in the European fleet.

Overall, the following sizes were adopted:

- Battery sizes: 36, 72 and 108 kWh.
- FCS sizes: 140, 180 and 220 kW.

Given the baseline battery pack capacity of 72 kWh, typically achieved by connecting multiple units in parallel (a strategy employed by manufacturers like Hyundai [23]), a decision was made to decrease the capacity by utilizing a single 36 kWh unit and to increase it by integrating three 36 kWh cells connected in parallel, resulting in a total of 108 kWh. In terms of the fuel cell system, the choice was to equip the vehicles with an FCS capable of meeting at least the average power demand of the most demanding mission considered, leading to the selection of a minimum size of 140 kW. The larger size was determined to provide a symmetrical variation relative to the reference size. These configurations yield a hybridization ratio in line with those observed in both existing FC-dominant hybrid vehicles and those documented in the literature. For the creation of the new vehicle models in VECTO, it was necessary not only to adjust the models of the aforementioned components but also to correct the curb mass of the vehicle. The change in battery pack capacity was related to the change in mass by applying Equation 7.3, where 6.5 kg/kWh, the official value used in the VECTO environment, was taken as the weight multiplier:

$$\Delta m_{curb,batt} = 6.5 * \left(E_{bat} - E_{batt,ref}\right).$$

(Eq. 7.3)

Instead, Equation 7.4 was used for the curb mass adjustments attributed to changes in the size of the fuel cell system. This equation uses a fuel cell specific weight multiplier derived from existing literature and set at 3 kg/kW [51]:

$$\Delta m_{curb,FCS} = 3 * \left(P_{max,FCS} - P_{max,FCS_{ref}}\right).$$

(Eq. 7.4)

Table 7.9 shows the total curb mass corrections for each hybrid powertrain configuration considered:

Table 7.9: Total curb mass corrections for each powertrain setup.

		Battery sizes		
	Δm_{curb} [kg]	**36 kWh**	**72 kWh**	**108 kWh**
FCS sizes	**140 kW**	-354	-120	+114
	180 kW	-234	0	+234
	220 kW	-114	+120	+354

For the 36 kWh battery model, the parameters of the 72 kWh VECTO model were reworked, considering the latter as consisting of two packs in parallel. Instead, the same approach was followed for the creation of the map as for the original FCS, thus also assuming a maximum system efficiency of 60% and scaling the curve according to the maximum power value.

Figures 7.20 and 7.21 illustrate, through bar charts, the percentage changes in fuel consumption, for rigid trucks and tractor-trailers categorized under the LH subgroups, respectively. For the sake of compactness, the diagrams for the RD subgroups are omitted, as their graphical representation does not reveal any appreciable differences from what will be shown. A negative percentage signifies a reduction in fuel consumption, reflecting enhanced energy efficiency. A complete detail of the variations in fuel consumption across all cases analysed is provided in Appendix A, where the relevant tables are presented together with the TTW efficiency metrics.

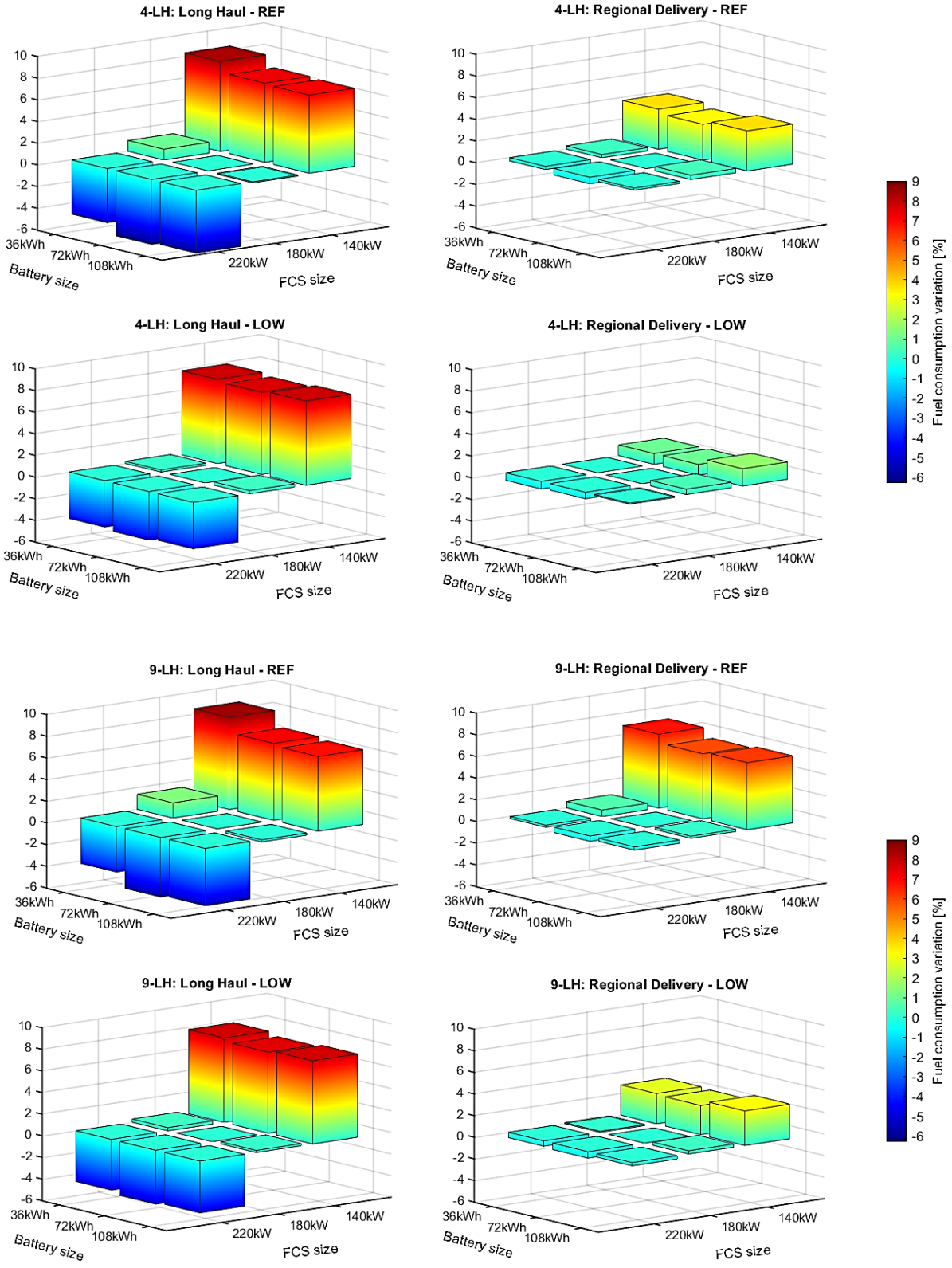

Figure 7.20: Fuel consumption variation for LH rigid trucks.

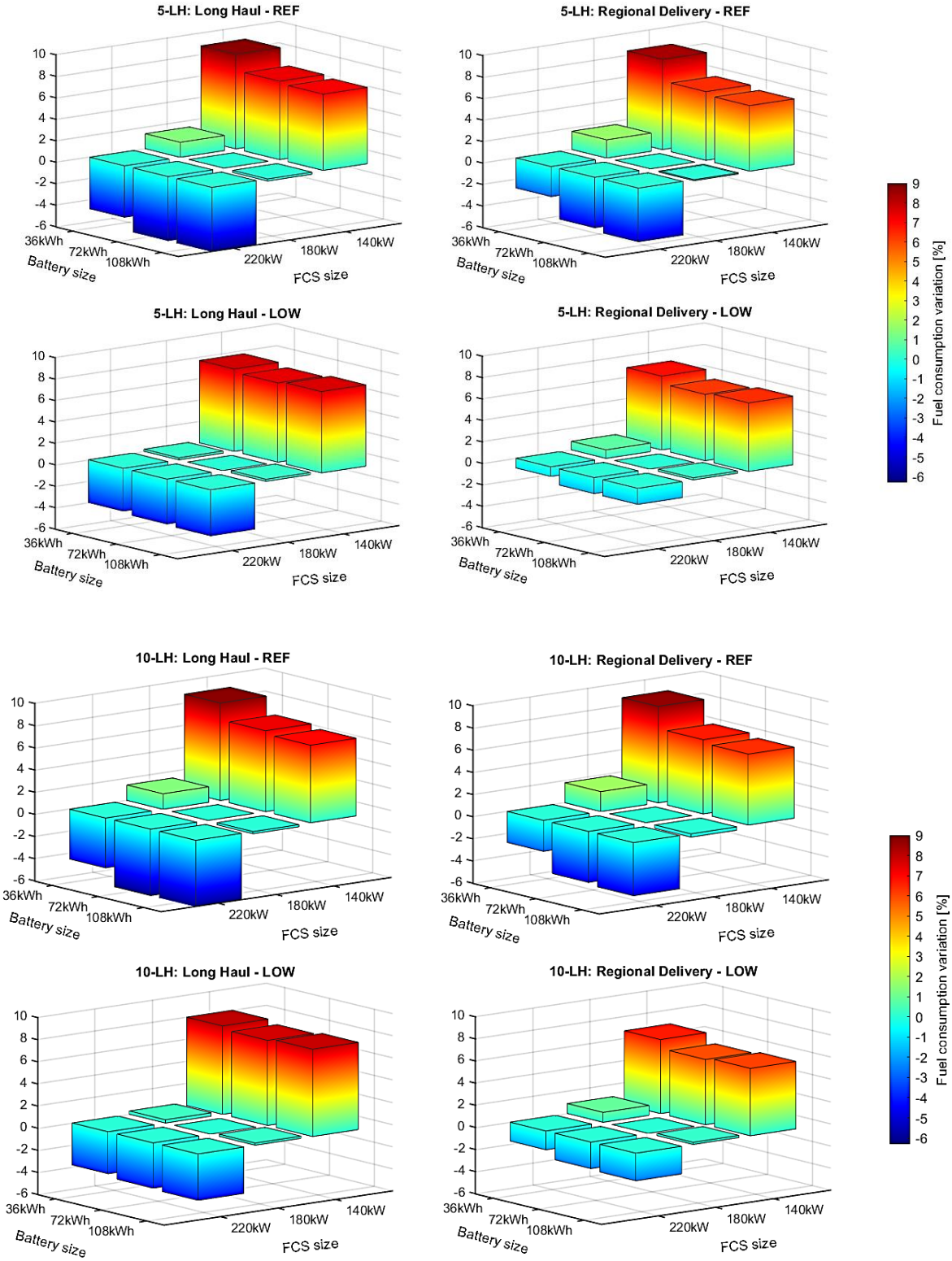

Figure 7.21: Fuel consumption variation for LH tractor-trailers.

The analysis of the presented graphs yields insightful observations regarding the operational dynamics of the VECTO tool. A strong correlation is observed between fuel consumption and the dimensions of the FCS adopted, which starkly contrasts with the minor influence exerted by the battery pack's capacity. In fact, examining the fuel consumption variations across scenarios with identical FCS size (180 kW, for instance) but differing battery capacities (from 36kWh to 108kWh) highlights a marginal fluctuation in overall consumption among all vehicles and mission profiles, ranging from a decrease of -0.2% to an increase of +2%. On the other hand, when looking at cases with a constant battery pack size (72kWh, for example), varying the FCS power (from 140kW to 220kW) exhibits a significantly broader spectrum of consumption changes, spanning from a reduction of -6.1% to an augmentation of +7.7%. Furthermore, the comparative analysis between distinct vehicles, specifically within the rigid trucks and tractor-trailers categories, reveals neither substantial differences nor particular trends in the effects brought about by the different hybridisation. Therefore, it is possible to base observations directly on the comparison between rigid truck and tractor-trailer branches under various operating conditions.

In particular, the employment of a smaller FCS has been observed to significantly elevate fuel consumption across all mission profiles. Conversely, it is possible to reduce consumption by adapting a larger FCS than the reference one. This phenomenon is clarified by Figure 7.22, which exemplifies this effect for a vehicle within the 4-LH subgroup. The figure demonstrates that increasing the maximum power of the FCS allows the efficiency characteristic of the system to be scaled up, placing the operating points imposed by the driving cycle in locations on the curve with higher efficiency. This is also reflected in the current trend of manufacturers to oversize the fuel cell system in HDVs, compatible with costs and available volume, in order to reduce hydrogen consumption [10].

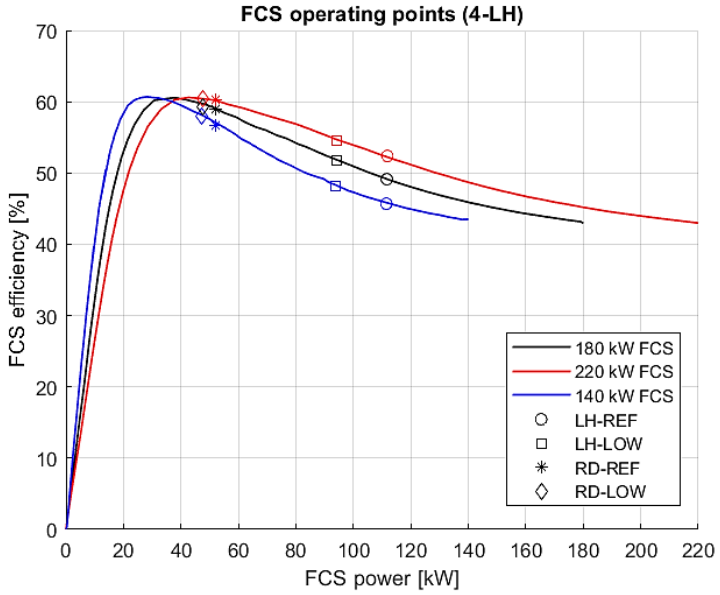

Figure 7.22: FCS efficiency curves and operating points for the 4-LH vehicle with 72 kWh REESS.

On the other hand, in the various scenarios analysed, it has been noted that employing a larger REESS, despite contributing to an increase in the vehicle's mass, tends to enhance fuel savings. In VECTO, the battery plays the role of a compensator between the power demand of the driving cycle and that provided by the FCS. Therefore, the power it must deliver or absorb depends on both the driving cycle load and the power of the FCS. The capacity of the battery is decisive in the algorithm that is implemented by VECTO to determine the power trend of the FCS through an iterative averaging process. An increasing battery size ultimately results in a constant power operation of the FCS and a progressively decreasing modulus, at least until the opposite effect induced by increasing curb mass prevails. This approach allows the battery to assume a more significant role in vehicle propulsion throughout the driving cycle, thereby reducing the reliance on the FCS. Furthermore, a larger battery capacity facilitates a higher proportion of energy recapture during braking phases, enhancing the overall efficiency of the powertrain.

The analysis of the case studies results reveals that the adoption of a 140 kW FCS invariably leads to a marked increase in fuel consumption across all vehicle types and battery configurations, which is progressively more marked as the power demand by the driving cycle, and therefore the power delivered by the FCS, increases.

In fact, taking into account the configuration equipped with a 36 kWh battery, the most important increases occur with the “Long Haul-REF” mission profile, being close to +8% for rigid trucks and +9% for tractor-trailers. These increments progressively drop towards lighter driving cycles such as the “Regional Delivery-LOW”.
In addition, in the context of tractor-trailers, it is observed that a 36 kWh battery is not sufficient to guarantee constant power operation of the FCS during RD driving cycles with both low and reference payload, unlike rigid trucks in the same vehicle configuration. This happens due to the high dynamism of the driving cycle, which requires equally dynamic operation of the power sources, and the particularly heavy load (higher than that characterising rigid trucks). This leads the FCS to operate at time-varying operating points and sometimes far from maximum efficiency, thereby resulting in a deterioration of the average energy performance.
The effect is mitigated slightly by using batteries with a larger capacity. Indeed, switching to a larger 72 kWh battery reduces these increases by between 0.2% and 2% depending on use cases. This enhancement is particularly pronounced in tractor-trailers because it allows VECTO to guarantee FCS operation at constant power.
However, expanding the battery capacity further to 108 kWh yields negligible benefits. While a minor improvement is observed in the “Long Haul-REF” cycle, the augmented mass attributed to larger batteries predominates in other mission profiles, leading to a resurgence in consumption levels.
The configurations incorporating a 140 kW FCS experience a notable decline in powertrain efficiency, which is proportional to the intensity of the mission profile. In the less efficient case with the smallest battery, a reduction in TTW efficiency of around 3% in the “Long Haul-REF” driving cycle is commonly observed for all vehicles, which narrows to -2% for the “Regional

Delivery-LOW" cycles. As the capacity of the REESS is enhanced, these efficiency losses are slightly mitigated.

In the simulation outcomes for the powertrain equipped with the 180 kW FCS, it is possible to observe the effect of purely varying the battery size compared to the reference case. A reduction in battery capacity from 72 kWh to 36 kWh results in a slight increase in consumption despite a reduction in the vehicle curb mass. This result is primarily due to VECTO's computational mechanism, which slightly elevates the FCS's power output (by approximately 1% in the most demanding conditions) when operating with a smaller REESS. This adjustment leads to a less efficient functioning of the FCS, and also to a lower TTW efficiency across all vehicles, with the most significant drop of around -1%.
For the LH mission profiles, the variation in consumption remains stable across all different vehicles, marking a 1.3% increase in the LH-REF scenario and a 0.3% rise in the LH-LOW scenario. However, a pronounced disparity in consumption rates between rigid trucks and tractor-trailers emerges during the RD cycles. Indeed, even in this case, VECTO determines a non-constant FCS operation in order not to violate the SOC limits, as is shown as an example in Figure 7.23 for the 5-LH vehicle.
This modulation exacerbates hydrogen consumption in tractor-trailers by +2% during "Regional Delivery-REF" missions and by approximately +1% during "Regional Delivery-LOW" missions compared to the reference powertrain setup. Conversely, rigid trucks exhibit a negligible consumption increase, remaining well below +1% for both load scenarios. The variation in TTW efficiency mirrors these consumption trends, although in a narrower range between -0.2% and -0.9%.

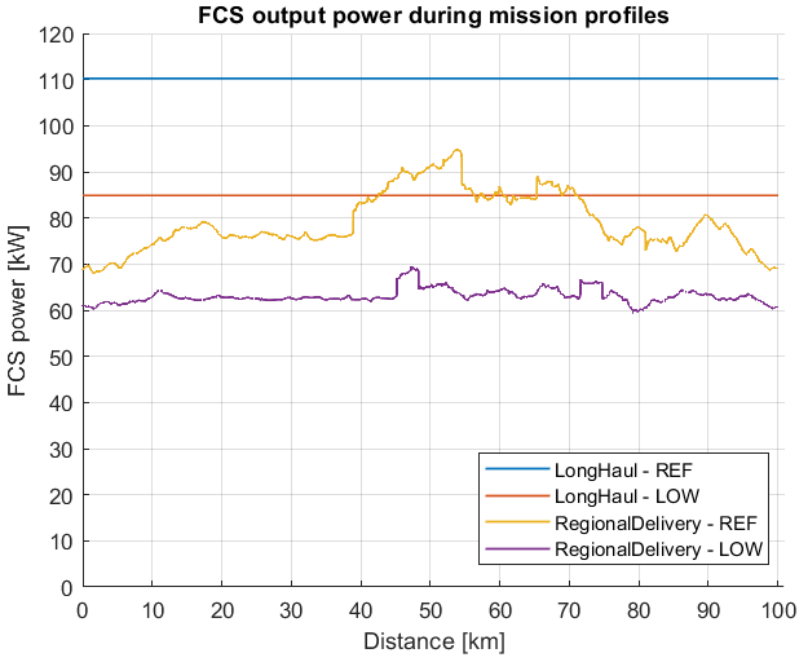

Figure 7.23: FCS power trend for the 5-LH vehicle with 36 kWh battery across all mission profiles.

Integrating a 108 kWh battery with a 180 kW FCS yields negligible deviations from the energy efficiency benchmarks set by the reference powertrain with a 72 kWh battery. In the most demanding “Long Haul-REF” mission profile, a marginal benefit in fuel saving, of approximately -0.2%, is observed across the entire vehicle fleet. This slight enhancement is attributed to the larger battery's ability to accommodate peak power demands more effectively, thereby reducing reliance on the FCS.
Similarly, tractor-trailers experience a modest efficiency gain of up to -0.3% during the “Regional Delivery-REF” scenario, where the load on the power sources is also high. However, under less severe driving conditions this effect is not achieved. On the contrary, an increase in consumption of between +0.2% and +0.5% is observed, caused by the higher power demand at the FCS, and the latter generated by the greater vehicle mass.
Thus, it can be deduced that during operations characterized by lower loads, the additional hydrogen consumption necessitated by the increased vehicle weight overshadows the advantages conferred by the enhanced availability of stored energy in the battery. Therefore, in the case of equipment with a medium-sized FCS, a careful assessment of what will be the most frequent conditions of vehicle use must be made when sizing the battery: the use of a larger battery may be suitable in vehicles intended for long-haul routes (classifiable in the LH subgroups) and for tractor trailers in the RD subgroup, given the latter's greater demand for energy, while it is less effective and appropriate in rigid trucks. The employment of a medium-sized FCS, such as the 180 kW, could allow for a battery downsizing of rigid trucks with minimal adverse effects. This is particularly evident given the marginal consumption increase observed with a 36 kWh REESS across all mission profiles, especially for HDVs within group 4.

The most interesting hybrid powertrain configurations for the intended purposes are obtained, as mentioned previously, by employing an FCS with a higher maximum power than the reference power, in this case 220 kW.
This setup yields the most significant hydrogen savings during high-load mission profiles, such as the “Long Haul-REF” and “Regional Delivery-REF” for tractor-trailers. The advantage in these scenarios is attributed to the pronounced divergence between the characteristic curves of the FCS at higher power outputs, as illustrated in Figure 7.22. Such conditions favour a notable enhancement in the FCS's efficiency, which in turn beneficially impacts the TTW efficiency.
An important reduction in hydrogen consumption is observed already with the 36 kWh battery, in a range between -4% and -5% across mission profiles with Long Haul driving cycle. This improvement is consistent for both rigid trucks and tractor-trailers under all load conditions. Correspondingly, the TTW efficiency, in comparison to the reference powertrain setup, registers an increase of approximately +2%.
However, during Regional Delivery cycles, the extent of fuel savings and vehicle efficiency enhancement for rigid trucks diminishes to below -1%. In contrast, the efficiency gains remain substantial for tractor-trailers, with hydrogen consumption reductions of around -3%.
The margin on fuel economy improves significantly by switching from the 36 kWh battery to the 72 kWh battery. Rigid trucks experience a notable improvement in fuel savings, achieving

-6% in the “Long Haul-REF” profile, -5% in the “Long Haul-LOW” scenario, and -0.6% in RD driving cycles.
Tractor-trailers also benefit from this battery upgrade in Long Haul cycles, with fuel savings reaching approximately -6% and -4% in the reference and low load conditions, respectively. With the Regional Delivery driving cycle, it goes up to -5% and -4% in the reference and low payload missions, respectively. Consistently, this transition also results in a slight increase in TTW efficiency.
Finally, enhancing battery capacity beyond the benchmark 72 kWh in rigid trucks does not yield further reductions in hydrogen consumption. Specifically, when equipped with a 108 kWh REESS, the variations in consumption are less pronounced than those observed with a 72 kWh battery. In such scenarios, there is an appreciable rise, approximately +2% in the heaviest case, in the power demand from the FCS for traction, compared to the 220 kW-72 kWh powertrain configuration. This suggests that the additional vehicle mass from the larger battery may lead to a less efficient operation of the powertrain. In contrast, tractor-trailers exhibit marginal enhancements, with hydrogen savings increasing further by up to +0.3%, indicating a differential response to increased battery capacity within different vehicle types.

The VECTO simulations of vehicles have yielded several key insights into the interaction between hybrid powertrain components and their impact on fuel consumption and efficiency, according to the tool’s operational strategy. These findings can inform strategic decisions regarding the configuration of heavy-duty vehicles to optimize performance and sustainability. The following summary encapsulates the major conclusions drawn from the simulation results:

1. A proper sizing of the FCS is essential for the reduction of hydrogen consumption, as it exerts the most significant impact, surpassing the relevance of battery pack dimensions for optimising energy performance. This highlights the pivotal role of the FCS within the hybrid powertrain configuration.

2. Reducing the size of the FCS, even when compensated by larger battery capacities, does not emerge as a viable strategy for decreasing fuel consumption.

3. Oversizing the FCS emerges as an effective strategy to reduce hydrogen consumption, with its greatest benefits occur in scenarios involving high-load mission profiles. Therefore, this approach is particularly suitable for vehicles within the LH subgroups, notably tractor-trailers, where the employment of an FCS boasting a robust maximum power output aligns seamlessly with their operational demands. On the other hand, for rigid trucks primarily engaged in daily missions within a regional framework (therefore classifiable in the RD subgroups), in the face of limited improvements in energy performance, opting for a more modestly sized FCS, exemplified by a 180 kW unit among the cases scrutinized, remains a viable and efficient choice.

4. Incorporating a high-power FCS alongside a large-capacity REESS, exemplified by a 108 kWh unit, proves to be an advantageous strategy for tractor-trailers across all

operational scenarios. This combination not only elevates efficiency but also amplifies fuel savings relative to the configurations equipped with a medium-sized REESS.
However, this setup does not produce similar benefits for rigid trucks, where the increase in vehicle mass attributable to the large-capacity REESS limits the potential for fuel savings. In these cases, a medium-capacity battery emerges as the most effective option, showing the most significant improvements.
This phenomenon highlights a critical trade-off between the added mass from larger battery capacities and the resulting powertrain efficiency: in some contexts, the addition of electrification components, intended to improve energy availability and support more efficient FCS operation, may act as a counterproductive factor, adding a "dead weight" and thus diminishing the expected benefits in terms of reduced fuel consumption due to the increase in overall vehicle mass.

5. The optimal battery size for consumption reduction varies significantly across vehicle types and mission profiles. Therefore, it becomes crucial to conduct a meticulous evaluation of the specific application, expected usage patterns and energy requirements of the HDVs to determine the most appropriate battery size.

In conclusion, this study underscores the importance of a tailored approach to hybrid powertrain configuration design for HDVs. By carefully considering the specific requirements of different vehicle types and their operational contexts, manufacturers can significantly improve fuel efficiency and optimize the overall performance of their fleets, aligning with the broader objectives of minimizing environmental impact in the heavy transport sector.

8. Conclusions

This study situates itself within the broader research landscape that explores the application of fuel cells within the domain of long haul heavy-duty vehicles, with a view to its future decarbonisation.
First, a summary of the technology trends for fuel cell systems and powertrain architecture was presented. In addition, to define the newly emerging industrial context of this research and to provide references on the technical characteristics of real vehicles, an overview of the recent market for zero-emission vehicles, alongside a focus on the main FC vehicles intended for commercialisation in the European market was reported. The research carried out in this study made a significant contribution to the understanding of energy performance and operational effectiveness of this new vehicle category. Through it, the main heavy vehicle configurations, in accordance with current regulations, and representative of the average European heavy-duty vehicle fleet were examined, offering a comprehensive view of the potential of these vehicles across a broad range of mission scenarios.
Furthermore, the investigation made it possible to explore and illustrate the innovative methodology employed by the VECTO software for the simulation of fuel cell hybrid vehicles, highlighting its peculiarities and advantages.

The activities carried out had the following outcomes:

a) The applicability of the innovative VECTO methodology to FC-HDVs was proved.

b) A comprehensive set of VECTO models for FC heavy-duty vehicles was developed, encompassing the entire spectrum of configurations subject to CO_2 emission reduction mandates. This effort was in rigorous alignment with the simulation protocols delineated in the European Regulation (EU) 2017/2400, ensuring strict adherence to legislative standards.

c) A robust baseline for hydrogen and energy consumption within the HDV fleet was established, with the aim of supporting the development of further studies relating to the modelling of these vehicles according to the regulations of the European Community and enhancing powertrain efficiency. The simulation energy audit suggested a high potential for future energy savings through further improvements in FCS technology, vehicle aerodynamics, and reduction of rolling resistance.

d) An analysis of hybridization shed light on the influence of varied onboard power source configurations on the hydrogen consumption and overall energy efficiency of fleet vehicles. This exploration enabled the formulation of preliminary design insights for powertrains that align with VECTO's operational framework. Furthermore, it provided a basis for drawing findings into the optimal hybrid configurations for specific fleet vehicles, tailored to meet designated operational objectives.

Delving into every possible strategy to enhance efficiency and minimize consumption is essential, given that even marginal improvements can significantly contribute to climate change mitigation efforts. Further research could explore the potential of integrating supercapacitors alongside batteries in the hybrid fuel cell powertrain within the VECTO framework, investigating their operating strategy and their contribution to vehicle energy dynamics. Due to their remarkable specific power characteristics, these components could be promising for application in heavy vehicles engaged in dynamic missions, such as those found in urban and suburban contexts. Moreover, to refine and augment the efficacy of the analyses conducted in this study, ways of integrating the VECTO software with automatic optimisation algorithms could be investigated.

In conclusion, in light of the research and analysis presented in this thesis, it is evident that the transition towards sustainable road freight is not only necessary but also increasingly feasible thanks to advancements in clean technologies, and especially the efforts of government institutions. The utilization of VECTO in this research marks a significant methodological advancement in evaluating the energy performance of FC-HDVs. Through its application, this study has led to results that have provided a more accurate and comprehensive understanding of the potential and challenges associated with the adoption of hydrogen fuel cell technology in long-haul freight operations, contributing to research efforts towards the realisation of more sustainable and environmentally friendly transport.

Appendix A

- Fuel consumption variations and TTW efficiency values with 140 kW FCS:

	Fuel consumption variations				TTW efficiency values			
Battery: 36 kWh	LH-REF	LH-LOW	RD-REF	RD-LOW	LH-REF	LH-LOW	RD-REF	RD-LOW
4-LH	8.33%	7.79%	3.67%	0.98%	36.3%	39.0%	42.4%	44.0%
4-RD	8.14%	7.63%	4.02%	1.30%	36.4%	38.9%	42.7%	44.3%
9-LH	8.50%	7.85%	6.84%	2.82%	35.1%	38.3%	40.4%	43.0%
9-RD	8.27%	7.73%	7.26%	3.31%	35.2%	38.4%	40.8%	43.3%
5-LH	8.84%	7.68%	8.38%	6.93%	35.8%	39.8%	37.1%	41.0%
5-RD	8.55%	7.89%	8.83%	6.36%	35.6%	39.3%	37.0%	40.8%
10-LH	8.77%	8.00%	8.70%	6.75%	35.4%	39.2%	36.4%	40.2%
10-RD	6.22%	6.78%	9.26%	6.38%	36.1%	39.3%	36.5%	40.3%

	Fuel consumption variations				TTW efficiency values			
Battery: 72 kWh	LH-REF	LH-LOW	RD-REF	RD-LOW	LH-REF	LH-LOW	RD-REF	RD-LOW
4-LH	7.29%	7.57%	3.34%	1.03%	36.8%	39.2%	42.7%	44.2%
4-RD	7.25%	7.54%	3.82%	1.52%	36.8%	39.1%	43.0%	44.5%
9-LH	7.09%	7.47%	5.98%	2.74%	35.6%	38.6%	40.9%	43.2%
9-RD	6.95%	7.44%	6.55%	3.26%	35.7%	38.7%	41.3%	43.6%
5-LH	7.31%	7.39%	6.41%	6.18%	36.3%	39.9%	37.8%	41.2%
5-RD	7.20%	7.71%	7.13%	5.60%	36.1%	39.5%	37.7%	41.2%
10-LH	7.28%	7.67%	6.73%	5.87%	36.0%	39.5%	37.2%	40.7%
10-RD	7.19%	7.60%	7.25%	5.44%	35.9%	39.1%	37.3%	40.8%

	Fuel consumption variations				TTW efficiency values			
Battery: 108 kWh	LH-REF	LH-LOW	RD-REF	RD-LOW	LH-REF	LH-LOW	RD-REF	RD-LOW
4-LH	7.21%	7.83%	3.70%	1.58%	36.9%	39.2%	42.8%	44.3%
4-RD	7.23%	7.84%	4.21%	2.03%	36.9%	39.2%	43.1%	44.5%
9-LH	6.87%	7.69%	6.24%	3.17%	35.8%	38.7%	41.1%	43.3%
9-RD	6.77%	7.69%	6.74%	3.73%	35.8%	38.7%	41.4%	43.7%
5-LH	7.10%	7.64%	6.15%	6.39%	36.4%	39.8%	37.9%	41.2%
5-RD	7.04%	8.03%	6.80%	5.72%	36.3%	39.5%	37.9%	41.4%
10-LH	7.03%	7.93%	6.40%	6.09%	36.2%	39.5%	37.5%	40.8%
10-RD	7.03%	7.84%	7.00%	5.61%	36.0%	39.2%	37.5%	40.9%

- Fuel consumption variations and TTW efficiency values with 180 kW FCS:

	Fuel consumption variations				**TTW efficiency values**			
Battery: 36 kWh	LH-REF	LH-LOW	RD-REF	RD-LOW	LH-REF	LH-LOW	RD-REF	RD-LOW
4-LH	1.00%	0.22%	0.31%	0.03%	39.01%	41.97%	43.89%	44.81%
4-RD	0.85%	0.11%	0.17%	0.01%	39.10%	41.95%	44.49%	45.24%
9-LH	1.41%	0.34%	0.36%	0.12%	37.56%	41.28%	43.01%	44.23%
9-RD	1.31%	0.26%	0.28%	0.06%	37.64%	41.37%	43.58%	44.86%
5-LH	1.43%	0.24%	1.73%	0.78%	38.42%	42.76%	39.49%	43.45%
5-RD	1.25%	0.18%	1.84%	0.57%	38.17%	42.36%	39.55%	43.20%
10-LH	1.45%	0.29%	1.84%	0.86%	38.00%	42.30%	38.96%	42.62%
10-RD	1.27%	0.27%	2.00%	0.65%	37.91%	41.88%	39.12%	42.66%

	Fuel consumption variations				**TTW efficiency values**			
Battery: 108 kWh	LH-REF	LH-LOW	RD-REF	RD-LOW	LH-REF	LH-LOW	RD-REF	RD-LOW
4-LH	-0.1%	0.25%	0.39%	0.52%	39.65%	42.25%	44.32%	44.84%
4-RD	-0.1%	0.30%	0.35%	0.49%	39.66%	42.18%	44.91%	45.31%
9-LH	-0.19%	0.20%	0.19%	0.33%	38.35%	41.63%	43.64%	44.65%
9-RD	-0.16%	0.24%	0.20%	0.39%	38.38%	41.67%	44.25%	45.25%
5-LH	-0.21%	0.23%	-0.14%	0.20%	39.05%	42.77%	40.23%	43.70%
5-RD	-0.17%	0.29%	-0.23%	0.13%	38.92%	42.63%	40.63%	43.77%
10-LH	-0.23%	0.21%	-0.30%	0.21%	38.86%	42.67%	40.07%	43.28%
10-RD	-0.19%	0.28%	-0.20%	0.14%	38.67%	42.20%	40.24%	43.26%

- Fuel consumption variations and TTW efficiency values with 220 kW FCS:

	Fuel consumption variations				**TTW efficiency values**			
Battery: 36 kWh	LH-REF	LH-LOW	RD-REF	RD-LOW	LH-REF	LH-LOW	RD-REF	RD-LOW
4-LH	-5.00%	-4.28%	-0.27%	-0.68%	41.5%	44.0%	44.3%	45.0%
4-RD	-4.98%	-4.55%	-0.41%	-0.76%	41.6%	44.1%	44.9%	45.5%
9-LH	-4.16%	-4.67%	-0.18%	-0.45%	39.8%	43.5%	43.6%	44.6%
9-RD	-4.27%	-4.94%	-0.17%	-0.48%	39.9%	43.7%	44.2%	45.3%
5-LH	-4.75%	-3.97%	-2.78%	-2.67%	40.9%	44.6%	41.3%	44.2%
5-RD	-4.42%	-4.03%	-2.84%	-2.72%	40.5%	44.3%	41.5%	44.8%
10-LH	-4.51%	-3.76%	-2.77%	-2.74%	40.4%	44.2%	40.9%	43.9%
10-RD	-4.27%	-4.12%	-2.75%	-3.03%	40.2%	43.9%	41.1%	44.4%

	Fuel consumption variations				**TTW efficiency values**			
Battery: 72 kWh	LH-REF	LH-LOW	RD-REF	RD-LOW	LH-REF	LH-LOW	RD-REF	RD-LOW
4-LH	-6.01%	-4.48%	-0.58%	-0.64%	42.1%	44.3%	44.6%	45.3%
4-RD	-5.85%	-4.65%	-0.55%	-0.62%	42.1%	44.3%	45.2%	45.7%
9-LH	-5.49%	-4.97%	-0.57%	-0.62%	40.5%	43.8%	43.8%	45.0%
9-RD	-5.46%	-5.17%	-0.56%	-0.58%	40.5%	44.0%	44.4%	45.6%
5-LH	-6.06%	-4.25%	-4.73%	-3.69%	41.5%	44.8%	42.2%	44.5%
5-RD	-5.66%	-4.18%	-4.43%	-3.37%	41.1%	44.5%	42.4%	45.3%
10-LH	-5.98%	-4.07%	-4.61%	-3.55%	41.2%	44.5%	41.8%	44.3%
10-RD	-5.55%	-4.38%	-4.29%	-3.75%	40.8%	44.2%	41.9%	44.9%

	Fuel consumption variations				**TTW efficiency values**			
Battery: 108 kWh	LH-REF	LH-LOW	RD-REF	RD-LOW	LH-REF	LH-LOW	RD-REF	RD-LOW
4-LH	-5.81%	-4.26%	-0.20%	-0.14%	41.8%	44.3%	44.1%	45.3%
4-RD	-5.57%	-4.39%	-0.21%	-0.14%	41.9%	44.3%	45.2%	45.4%
9-LH	-5.34%	-4.80%	-0.33%	-0.27%	40.3%	43.7%	44.0%	45.1%
9-RD	-5.33%	-4.97%	-0.31%	-0.18%	40.3%	44.0%	44.2%	45.4%
5-LH	-6.22%	-4.31%	-5.03%	-1.50%	41.6%	44.8%	42.3%	45.7%
5-RD	-5.84%	-4.33%	-4.61%	-3.62%	41.3%	44.6%	42.6%	45.4%
10-LH	-6.20%	-4.22%	-4.77%	-2.54%	41.4%	44.6%	42.0%	45.6%
10-RD	-5.75%	-4.42%	-4.53%	-3.82%	41.0%	44.2%	42.1%	45.1%

Bibliography

[1] European Environment Agency. “Carbon dioxide emissions from Europe's heavy-duty vehicles”. April 2018. Available: https://www.eea.europa.eu/publications/carbon-dioxide-emissions-from-europes.

[2] European Environment Agency (2023). “Trends and projections in Europe 2023”. EEA Report July 2023.

[3] European Environment Agency. “Greenhouse gas emissions from transport in the EU”. November 2022. Available: https://www.eea.europa.eu/signals-archived/signals-2022/infographics/greenhouse-gas-emissions-from-transport.

[4] Dicks, A.L., Rand, D.A.J., ”Fuel cell systems explained”, ISBN 9781118706978, Wiley, Third edition, 2018.

[5] U.S. Department of Energy. (2016). “Comparison of Fuel Cell Technologies: Fact Sheet”. Energy.Gov. https://www.energy.gov/eere/fuelcells/downloads/comparison-fuel-cell-technologies-fact-sheet, accessed on December 13th, 2023.

[6] Basma, H., & Rodríguez, F. (2022). “Fuel Cell Electric Tractor-Trailers: Technology Overview and Fuel Efficiency”. International Council on Clean Transportation.

[7] Doppler, C., Lindner-Rabl, B. “Fuel Cell Trucks: Thermal Challenges in Heat Exchanger Layout”. Energies 2023, 16, 4024. https://doi.org/10.3390/en16104024.

[8] Bethoux, O. (2020). “Hydrogen fuel cell road vehicles: State of the art and perspectives”. Energies, 13(21). MDPI. https://doi.org/10.3390/en13215843.

[9] CNHI (2020). “Truck Architecture and Hydrogen Storage”. https://joint-research-centre.ec.europa.eu/system/files/2020-11/cnh_20201028_-_truck_architecture_public.pdf, accessed on December 18th, 2023

[10] Pardhi, S., Chakraborty, S., Tran, D. D., El Baghdadi, M., Wilkins, S., & Hegazy, O. (2022). “A Review of Fuel Cell Powertrains for Long-Haul Heavy-Duty Vehicles: Technology, Hydrogen, Energy and Thermal Management Solutions”. In *Energies* (Vol. 15, Issue 24). MDPI. https://doi.org/10.3390/en15249557.

[11] Moreno-Blanco, J., Petitpas, G., Espinosa-Loza, F., Elizalde-Blancas, F., Martinez-Frias, J., & Aceves, S. M. (2018). “The Fill Density of Automotive Cryo-Compressed Hydrogen Vessels”. International Journal of Hydrogen Energy (Vol. 44, Issue 2), pages 1010–1020. https://doi.org/10.1016/j.ijhydene.2018.10.227.

[12] Belli, C., Chizzolini, P., “Conversione dell’energia”, page 629, Università degli studi di Pavia, 2009.

[13] Camacho, M. de las N., Jurburg, D., Tanco, M. (2022). “Hydrogen fuel cell heavy-duty trucks: Review of main research topics”. In *International Journal of Hydrogen Energy* (Vol. 47, Issue 68, pp. 29505–29525). Elsevier Ltd. https://doi.org/10.1016/j.ijhydene.2022.06.271.

[14] FCH JU & Roland Berger. (2020). "Fuel Cells Hydrogen Trucks—Heavy Duty's High Performance Green Solution". Study Summary. Available online: https://www.rolandberger.com/en/Insights/Publications/Fuel-Cells-Hydrogen-Trucks.html, accessed on December 14th, 2023.

[15] Forrest, K., Mac Kinnon, M., Tarroja, B., & Samuelsen, S. (2020). "Estimating the technical feasibility of fuel cell and battery electric vehicles for the medium and heavy-duty sectors in California". *Applied Energy*, *276*. https://doi.org/10.1016/j.apenergy.2020.115439.

[16] Ribberink, H., Wu, Y., Lombardi, K., & Yang, L. (2021). "Electrification opportunities in the medium- and heavy-duty vehicle segment in Canada". *World Electric Vehicle Journal*, *12*(2). https://doi.org/10.3390/wevj12020086.

[17] Basma, H., Beys, Y., & Rodríguez, F. (2021). "*Battery electric tractor-trailers in the European Union: A vehicle technology analysis"*. International Council on Clean Transportation.

[18] Lu, Y., Rong, X., Hu, Y. S., Chen, L., & Li, H. (2019). "Research and development of advanced battery materials in China". In *Energy Storage Materials* (Vol. 23, pages 144–153). Elsevier B.V. https://doi.org/10.1016/j.ensm.2019.05.019.

[19] Hu, J., Yan, K., Li, J., Liu, S., Hu, Z., Xu, L., & Ouyang, M. (2021). "Design and Performance Analysis of Multi-axle Independent-drive Heavy-duty Fuel Cell Vehicles". 2021 IEEE Vehicle Power and Propulsion Conference, VPPC 2021 - https://doi.org/10.1109/VPPC53923.2021.9699284.

[20] Smith, D., Graves, R., Ozpineci, B., Jones, P. T., Lustbader, J., Kelly, K., Walkowicz, K., Birky, A., Payne, G., Sigler, C., & Mosbacher, J. (2019). "Medium-and Heavy-Duty Vehicle Electrification An Assessment of Technology and Knowledge Gaps". Oak Ridge National Laboratory and National Renewable Energy Laboratory Report.

[21] Mulholland, E., & Rodríguez, F. (2023). "Zero-emission bus and truck market I n Europe: A 2022 update". International Council on Clean Transportation.

[22] Basma, H., & Rodríguez, F. (2021). "How manufacturers are positioned for zero-emission commercial trucks and buses in Europe". International Council on Clean Transportation.

[23] Hyundai Motor Company (2022). "*XCIENT Fuel Cell"*. Available online: https://trucknbus.hyundai.com/hydrogen/en, accessed on December 12th, 2023.

[24] Daimler Truck (2020), "Daimler Trucks presents technology strategy for electrification – world premiere of Mercedes-Benz fuel-cell concept truck." Press Information. Available online: https://www.daimlertruck.com/en/newsroom/pressrelease/daimler-trucks-presents-technology-strategy-for-electrification-world-premiere-of-mercedes-benz-fuel-cell-concept-truck-47453560, accessed on January 12th, 2024.

[25] IVECO (2019). "IVECO, FPT Industrial e Nikola Corporation presentano il Nikola TRE". Press Release. Available online: https://www.iveco.com/italy/scopri-iveco/Sala-stampa/Release-Pages/PressReleasePages/2019/515, accessed on January 12th, 2024.

[26] IVECO (2022). "IVECO and Nikola launch the Nikola Tre BEV battery electric heavy-duty truck with best-in-class range in the European markets at IAA 2022". Press Release. Available online: https://www.iveco.com/en-us/press-room/kit/Documents/IAA_2022/3_PR_IVECO_NikolaTRE_launch_at_IAA_2022.pdf , accessed on January 12th, 2024.

[27] FCH JU & Roland Berger. (2020). "Fuel Cells Hydrogen Trucks—Heavy Duty's High Performance Green Solution". Study Report. Available online: https://fuelcelltrucks.eu/wp-content/uploads/2021/03/roland_berger_fuel_cells_hydrogen_trucks.pdf, accessed on December 15th, 2023.

[28] Interreg NWE, "H2-Share: Reducing emissions for heavy-duty transport in NWE through hydrogen solutions", Available online: https://vb.nweurope.eu/projects/project-search/h2share-hydrogen-solutions-for-heavy-duty-transport/, accessed on January 15th, 2024.

[29] H2Haul. "H2Haul: Paving the Road for a Carbon-Neutral Europe". Available online: https://www.h2haul.eu/ , accessed on December 14th, 2023.

[30] European Parliament, "Commission Regulation (EU) 2017/2400 of 12 December 2017 implementing Regulation (EC) No 595/2009 of the European Parliament and of the Council as regards the determination of the CO_2 emissions and fuel consumption of heavy-duty vehicles," 2017. [Online].

[31] European Parliament, "Regulation (EU) 2019/1242 of the European Parliament and of the Council of 20 June 2019 setting CO_2 emission performance standards for new heavy-duty vehicles and amending Regulations (EC) No 595/2009 and (EU) 2018/956," 2018.

[32] Broekaert, S., Fontaras, G. "CO_2 Emissions of the European Heavy-Duty Vehicle Fleet: Analysis of the 2019-2020 Reference Year Data". EUR 31032 EN, Publications Office of the European Union, Luxembourg, 2022, ISBN 978-92-76-49854-4, doi:10.2760/764148, JRC127220.

[33] Mulholland, E., Rodríguez, F. (2023). "An analysis on the revision of Europe's heavy-duty CO_2 standards". International Council on Clean Transportation.

[34] European Commission, "Proposal for a Regulation of the European Parliament and of the Council Amending Regulation (EU) 2019/1242 as Regards Strengthening the CO_2 Emission Performance Standards for New Heavy-Duty Vehicles and Integrating Reporting Obligations, and Repealing Regulation (EU) 2018/956". Official Journal of the European Union, February 14, 2023, https://eur-lex.europa.eu/legalcontent/EN/TXT/?uri=COM%3A2023%3A88%3AFIN.

[35] Savvidis, D. "Vehicle Energy Consumption calculation TOol-VECTO". European Commission, DG Climate Action Unit C4: Road Transport.

[36] Bitsanis, E., Broekaert, S., Tansini, A., Savvidis, D., Fontaras, G., "Experimental Evaluation of VECTO Hybrid Electric Truck Simulations", SAE Technical Paper 2023-01-0485, 2023, doi:10.4271/2023-01-0485.

[37] Fontaras, G., Rexeis, M., Dilara, P., Hausberger, S., Anagnostopoulos, K. (2013). "The development of a simulation tool for monitoring heavy-duty vehicle CO_2 emissions and fuel consumption in Europe". SAE Technical Papers, 6. https://doi.org/10.4271/2013-24-0150.

[38] Zacharof, N., Fontaras, G., Grigoratos, T., Ciuffo, B., Savvidis, D., Delgado, O., Rodriguez, J. F. "Estimating the CO_2 Emissions Reduction Potential of Various Technologies in European Trucks Using VECTO Simulator". SAE Technical Paper, 2017-24-0018, 2017. https://doi.org/10.4271/2017-24-0018.

[39] European Commission, "VECTO user manual", 2023.

[40] European Commission," FCS-Certification Test Protocol", Draft version, 2022.

[41] Ferrara, A., Jakubek, S., Hametner, C. (2021). "Energy management of heavy-duty fuel cell vehicles in real-world driving scenarios: Robust design of strategies to maximize the hydrogen economy and system lifetime". Energy Conversion and Management, 232. https://doi.org/10.1016/j.enconman.2020.113795.

[42] Basma, H., Rodríguez, F. (2023). "The European heavy-duty vehicle market until 2040: Analysis of decarbonization pathways". International Council on Clean Transportation.

[43] Delgado, O., Rodríguez, F., Muncrief, R. (2017). "Fuel efficiency technology in European heavy-duty vehicles: baseline and potential for the 2020-2030 time frame". International Council on Clean Transportation.

[44] Di Pierro, G., Tansini, A., Fontaras, G., Bonato, C. "Experimental assessment of powertrain components and energy flow analysis of a Fuel Cell Electric Vehicle (FCEV)". SAE Technical Paper 2022-37-0011, 2022, doi:10.4271/2022-37-0011.

[45] Cunanan, C., Tran, M. K., Lee, Y., Kwok, S., Leung, V., Fowler, M. (2021). "A Review of Heavy-Duty Vehicle Powertrain Technologies: Diesel Engine Vehicles, Battery Electric Vehicles, and Hydrogen Fuel Cell Electric Vehicles". In Clean Technologies (Vol. 3, Issue 2, pp. 474–489). MDPI. https://doi.org/10.3390/cleantechnol3020028.

[46] Sutharssan, T., Montalvao, D., Chen, Y. K., Wang, W. C., Pisac, C., Elemara, H. (2017). "A review on prognostics and health monitoring of proton exchange membrane fuel cell". In Renewable and Sustainable Energy Reviews (Vol. 75, pp. 440–450). Elsevier Ltd.

[47] Olivaud, U., Cambriglia, L., Zanelli, A., Vankayala, S. N., De Araujo, P., Bontemps, N. "Integrated modelling of a fuel cell electric truck for energy management optimization". SIA Powertrain International Congress and Exhibition, Paris, France, June 14-15, 2023.

[48] Joint Research Centre, "VECTO Workshop, November 2018". Available online: https://climate.ec.europa.eu/document/download/c0b9671d-b48e-418f-9b1f-e265f6ec2ffb_en?filename=201811_overview_en.pdf&prefLang=it, accessed on December 16th, 2023.

[49] Rodríguez, F., Delgado, O., Muncrief, R. (2018). “Fuel consumption testing of tractor trailers in the European Union and the United States”. International Council on Clean Transportation.

[50] Transportonline. “Mercedes-Benz GenH2 Truck da record: 1.000 chilometri con un pieno di idrogeno liquido”. Available online: https://www.transportonline.com/notizia_57429_Mercedes-Benz-GenH2-Truck-da-record:-1.000-chilometri-con-un-pieno-di-idrogeno-liquido-.html.

[51] Anselma, P. G., Belingardi, G. (2022). “Fuel cell electrified propulsion systems for long-haul heavy-duty trucks: present and future cost-oriented sizing”. Applied Energy, 321. https://doi.org/10.1016/j.apenergy.2022.119354.